EVALUATION OF THE PERFORMANCE OF REFERENCE ELECTRODES EMBEDDED IN REINFORCED CONCRETE

Final Report

by

Milo Koretsky and Farid Abooameri
Department of Chemical Engineering
Oregon State University
Corvallis, Oregon 97331

and

John C. Westall
Department of Chemistry
Oregon State University
Corvallis, Oregon 97331

Prepared for

Oregon Department of Transportation
Salem, Oregon 97310

December 1994

1. Report No. FHWA OR-RD-95-08	2. Government Accession No.	3. Recipient's Catalog No.
4. Title and Subtitle EVALUATION OF THE PERFORMANCE OF REFERENCE ELECTRODES EMBEDDED IN REINFORCED CONCRETE		**5. Report Date** December 1994
		6. Performing Organization Code
7. Author(s) Milo Koretsky, Farid Abooameri, and John C. Westall		**8. Performing Organization Report No.**
9. Performing Organization Name and Address Research and Development Unit/Policy Section Transportation Development Branch Oregon Department of Transportation Transportation Building, Room 405 Salem, OR 97310		**10. Work Unit No. (TRAIS)**
		11. Contract or Grant No. SP&R #5294
12. Sponsoring Agency Name and Address Oregon Department of Transportation Research Unit 2950 State Street Salem, OR 97310 and U.S. Department of Transportation Federal Highway Administration Washington D.C. 97310		**13. Type of Report and Period Covered** Final Report
		14. Sponsoring Agency Code
15. Supplementary Notes		

16. Abstract

This study evaluates the suitability of graphite electrodes for imbedded reference cells in reinforced steel bridges which are cathodically protected with a sprayed zinc anode. It was assumed that a 100 (or 150) mV polarization decay criteria would be used. The work plan was divided into two parts: laboratory scale experimentation and computer simulation.

The response of graphite probes to a varying electric potential was compared to that of an Orion silver-silver chloride electrode. Additionally, commercial and laboratory fabricated electrodes were compared and the effect of electrode conditioning was assessed. The graphite electrodes appear to be a suitable choice for a rugged monitor of the 100mV polarization decay when the cathodic protection system is deactivated, especially when a 3 electrode configuration is used.

A finite difference code was developed to solve for the potential and current distributions in a simplified rectangular geometry. The model addressed cathodic protection of reinforced concrete using a sprayed zinc anode. Input parameters were based on available experimental data. A sensitivity analysis of the input parameters was performed. The effects of pore saturation, concrete cover and applied potential were studied. Oxygen transport significantly contributes to the polarization decay of the reinforcing steel. Additionally, the environmental conditions at the structure greatly affects the potential distribution and the polarization decay.

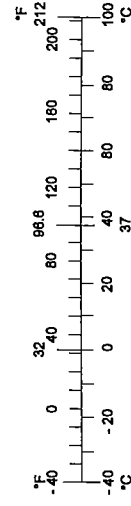| 17. Key Words Reference Cell, Corrosion, Cathodic Protection, Electrodes, Polarization Decay	18. Distribution Statement No restrictions. Available through the Oregon Department of Transportation (Research Unit).	
19. Security Classif. (of this report) Unclassified	20. Security Classif. (of this page) Unclassified	21. No. of Pages	22. Price

Form DOT F 1700.7 (8-72)   Reproduction of completed page authorized

d:\forms\technical.rpt

SI* (MODERN METRIC) CONVERSION FACTORS

APPROXIMATE CONVERSIONS TO SI UNITS

Symbol	When You Know	Multiply By	To Find	Symbol
	LENGTH			
in	inches	25.4	millimeters	mm
ft	feet	0.305	meters	m
yd	yards	0.914	meters	m
mi	miles	1.61	kilometers	km
	AREA			
in²	square inches	645.2	millimeters squared	mm²
ft²	square feet	0.093	meters squared	m²
yd²	square yards	0.836	meters squared	m²
ac	acres	0.405	hectares	ha
mi²	square miles	2.59	kilometers squared	km²
	VOLUME			
fl oz	fluid ounces	29.57	milliliters	mL
gal	gallons	3.785	liters	L
ft³	cubic feet	0.028	meters cubed	m³
yd³	cubic yards	0.765	meters cubed	m³

NOTE: Volumes greater than 1000 L shall be shown in m^3.

Symbol	When You Know	Multiply By	To Find	Symbol
	MASS			
oz	ounces	28.35	grams	g
lb	pounds	0.454	kilograms	kg
T	short tons (2000 lb)	0.907	megagrams	Mg
	TEMPERATURE (exact)			
°F	Fahrenheit temperature	5(F-32)/9	Celsius temperature	°C

APPROXIMATE CONVERSIONS FROM SI UNITS

Symbol	When You Know	Multiply By	To Find	Symbol
	LENGTH			
mm	millimeters	0.039	inches	in
m	meters	3.28	feet	ft
m	meters	1.09	yards	yd
km	kilometers	0.621	miles	mi
	AREA			
mm²	millimeters squared	0.0016	square inches	in²
m²	meters squared	10.764	square feet	ft²
ha	hectares	2.47	acres	ac
km²	kilometers squared	0.386	square miles	mi²
	VOLUME			
mL	milliliters	0.034	fluid ounces	fl oz
L	liters	0.264	gallons	gal
m³	meters cubed	35.315	cubic feet	ft³
m³	meters cubed	1.308	cubic yards	yd³
	MASS			
g	grams	0.035	ounces	oz
kg	kilograms	2.205	pounds	lb
Mg	megagrams	1.102	short tons (2000 lb)	T
	TEMPERATURE (exact)			
°C	Celsius temperature	1.8 + 32	Fahrenheit	°F

°F   -40   0   32 40   80   98.8 120   160   200 212
                                                                  °F
°C   -40   -20   0   20   37 40   80   100
                                                          °C

(4-7-94 jbp)

ACKNOWLEDGEMENTS

DISCLAIMER

This document is disseminated under the sponsorship of the Oregon Department of Transportation in the interest of information exchange. The State of Oregon assumes no liability of its contents or use thereof.

The contents of this report reflect the views of the authors who are solely responsible for the facts and accuracy of the material presented. The contents do not necessarily reflect the official views of the Oregon Department of Transportation .

This report does not constitute a standard, specification, or regulation.

EXECUTIVE SUMMARY

The objectives of this work were to evaluate the suitability of graphite electrodes as imbedded reference electrodes in reinforced concrete structures that are cathodically protected and to examine placement strategies for the electrodes. It was assumed that a sprayed zinc anode would be used, and that the electrodes would be used in the 100-mV polarization decay test and to evaluate adequacy of protection. The work plan was divided into two parts: computer simulation and laboratory experimentation.

Computer simulation of potential and current distributions in cathodic protection. A finite difference code was developed to solve for the potential and current distributions in a simplified rectangular geometry. Input parameters were based on available experimental data. A sensitivity analysis was performed to evaluate the effects of pore saturation, concrete cover and applied potential. The following recommendations resulted from this study:

- Potential mapping of reinforced concrete structures is an effective method of locating actively corroding reinforcing steel.

- Reference electrodes should be placed at locations with the most negative potential and as close to the centerline of the reinforcing steel as possible.

- Care should be taken to account for the environmental conditions. In dry environments (low pore saturation), placement of the reference electrode has a large affect; in wet environments, electrode placement is much less critical.

- In wet environments, the magnitude of the applied potential should be limited to prevent hydrogen evolution.

- Calculations of anode life should be based on the effective anode area (based on actual current density) rather than the total sprayed area. For thin concrete covers, lifetimes based on effective area could be 1/6 as long as lifetimes based on total area.

Experimental study of graphite reference electrodes. Reference electrodes mounted in a concrete block were evaluated under ambient laboratory conditions. The evaluation was based on a comparison of graphite electrodes to silver-silver chloride electrodes. Both commercially available and laboratory fabricated graphite electrodes were tested, as well as the effect of conditioning the graphite electrodes in $Ca(OH)_2$ solution. Conclusions were:

- Graphite electrodes appear to be suitable to monitor the 100-mV polarization decay.

- Graphite electrodes should be conditioned in saturated $Ca(OH)_2$ before installation.

**Evaluation of the Performance of Reference Electrodes Embedded
in Reinforced Concrete**

TABLE OF CONTENTS

APPENDICES

Evaluation of the Reference Electrodes Embedded
in Reinforced Concrete

LIST OF FIGURES

Evaluation of the Performance of Reference Electrodes Embedded in Reinforced Concrete

LIST OF TABLES

Evaluation of the Performance of Reference Electrodes Embedded in Reinforced Concrete

LIST OF SYMBOLS

a_m	activity of species m
b	Tafel slope (V/decade)
C_m	concentration of species m (mol/m^3)
D_m	diffusion coefficient of species m
E	half-cell potential (V)
E^{eq}	Equilibrium half-cell potential (V)
E^o	Standard half-cell potential (V)
E_{corr}	corrosion potential of iron (V)
E_{appl}	applied potential (V)
E_{ohm}	potential drop in bulk of concrete (V)
F	Faraday constant (96,485 C/mol of electrons)
H	Henry's law constant (m_{liq}^3/m_{gas}^3)
I	current (A)
i	net current density (A/m^2)
i^o	exchange current density (A/m^2)
i_{corr}	corrosion current density (A/m^2
i^L	limiting current density for oxygen reduction (A/m$_2$)
i^o	exchange current density (A/m^2)
J_m	molar flux of species m (mol/m^2's)
k_o	mass tranfer coefficient of oxygen
L	distance between iron and zinc (m)
n	number of electrons in a reaction
n	unit vector perpindicular to insulating surface
p_o	partial pressure of oxygen adjacent to rebar (atm)
PS	pore saturation
R	gas constant (8.314 J/mol K)
R_B	bulk resistance (ohm)
R_{mt}	mass transfer resistance at iron electrode (ohm)
R_{ct}	charge transfer resistance at iron electrode (ohm)
T	temperature
v	bulk velocity of fluid (m/s)
X	length of sprayed zinc (m)
Y	distance between iron and zinc (m)
z_m	integer charge of ion m
δ	thickness of water layer at iron electrode
ϕ	electric potential in concrete

κ conductivity of concrete $(ohm^{-1}m^{-1}$

ρ resistivity of concrete (ohm m)

∇ gradient operator

Subscripts

Fe,center	centerline of rebar
Fe,edge	edge of rebar
Fe	pertaining to the ferrous ion, Fe^{2+}, the iron electrode, or the iron oxidation reaction, $Fe \rightarrow Fe^{2+} + 2e^-$
O	pertaining to di-oxygen, O_2, or the oxygen reduction reaction, $O_2 + 2H_2O + 2e^- \rightarrow 4OH^-$
Zn	pertaining to the zinc ion, Zn^{2+}, the zinc electrode, or the zinc oxidation reaction, $Zn \rightarrow Zn^2 + 2e^-$.

Superscripts

air	pertaining to air, the mixture of gases composing the ambient atmosphere
liq	pertaining to the liquid phase at the iron surface
gas	pertaining to the gas phase
y=0	at the Zn surface
y=L	at the Fe surface

1.0 INTRODUCTION

1.1 CORROSION OF REINFORCING STEEL IN COASTAL BRIDGES

Corrosion of steel in reinforced concrete is a major concern to transportation agencies nationwide because of the expenses incurred for repair and replacement of structures. The estimated value to repair all the deficient bridges in the United States is about $90 billion[1]. One cause of the deficiency is corrosion of reinforcing steel in concrete. Cathodic protection (CP), as a remedy, has been applied to reinforced bridges since 1974[2]. In Oregon, an estimated savings of $250 million within 10 years will be realized by applying CP systems on 35 coastal bridges[3]. While the principle of cathodic protection is well established, engineering issues on how to optimize these systems remain unresolved. In this project, the performance of graphite reference electrodes in monitoring the effectiveness of cathodic protection systems is evaluated. Additionally, electrode placement strategy is examined through numerical modeling.

Corrosion is a natural electrochemical process whereby metals return to a lower energy (oxidized) state in the presence of an oxidant. A schematic of one of the corrosion processes of the reinforcing steel in coastal bridges is shown in Figure 1.1.
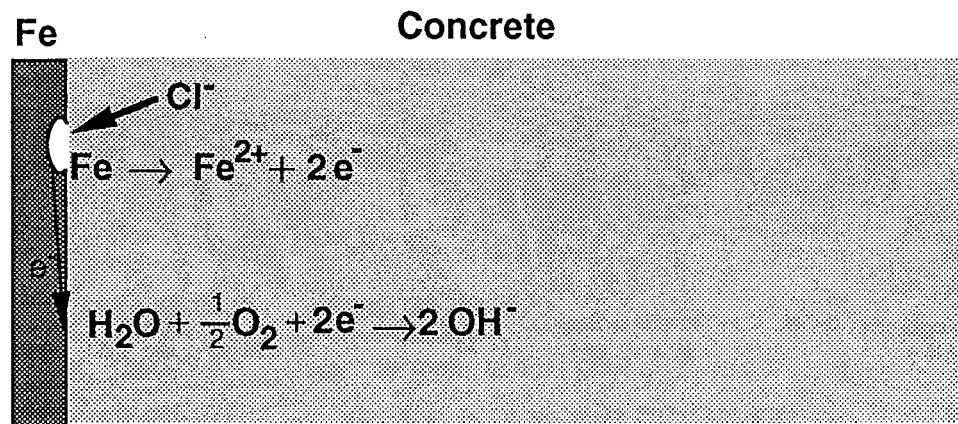
Figure 1.1 Corrosion in Reinforced Concrete

In the alkaline concrete, iron forms a chemically resistant oxide film (γ-Fe_2O_3) which isolates the underlying steel from naturally occurring oxidants. Consequently, the iron does not oxidize and retains its metallic state. In the marine environment, however, chloride ions (Cl^-) from salt diffuse from the surface to the reinforcing steel and attack the protective film. In this case, the surface of the exposed metal can act as a mixed electrode upon which coupled anodic and cathodic reactions take place.

The anodic (oxidation) reaction leads to corrosion of iron. The electrons produced by the anodic reaction flow through the iron to the cathodic site where oxygen is reduced to form hydroxide ions. During corrosion, the rate of oxidation of iron is equal to the rate of reduction of oxygen. Under these conditions, the electric potential of the reinforcing steel is defined as the corrosion potential, E_{corr}. The more positive E_{corr}, the greater the rate of corrosion. If the oxidation and reduction reactions occur at approximately the same site, the process is termed micro-corrosion. In macro-corrosion the electrons flow to a different location, while in macro-cell corrosion, a different rebar serves as the cathode. In these cases, the pore water in the concrete serves as an electrolyte to close the circuit and maintain electro-neutrality. For brevity, the term "concrete electrolyte" will be used.

1.2 CATHODIC PROTECTION

Cathodic protection is a major remedy for corrosion, especially for older reinforced concrete structures. In 1989, more than 275 bridges in the United States and Canada were being protected in this manner [4].

The principle of cathodic protection is to provide an alternative anodic reaction to that of iron oxidation. Consequently, some of the electrons needed to drive the oxygen reduction are supplied by an externally applied anode instead of the reinforcing steel, and the steel does not corrode as fast. In the limiting case, the applied anode supplies enough electrons to reduce all of the oxygen present at the reinforcing steel, and the iron corrodes at a negligible rate.

The behavior of a cathodic protection system depends on the electrochemical process occurring at the anode as well as the properties of the porous concrete electrolyte. Cathodic protection anodes include conductive graphite paint, catalyzed titanium, conductive polymeric wire, and sprayed zinc[4]. This report focuses on sprayed zinc anodes.

A schematic of the processes occurring in a sprayed zinc cathodic protection system is shown in Figure 1.2. A zinc anode is sprayed onto the outer surface of the corroding structure and electrically connected to the reinforcing steel through a voltage source. The zinc oxidation reaction "competes" with the oxidation of iron in supplying electrons to reduce oxygen. However, its effectiveness is limited by the highly resistive concrete electrolyte through which the negative charge must return to the zinc (in the form of ionic current). A schematic of the rate of the possible electrochemical reactions as a function of applied potential, E_{appl}, is shown in Figure 1.3.

2

Consider the cathodic protection system in the *absence* of an applied voltage but with the zinc connected to the steel in a short circuit. In this scenario, the total cathodic current increases relative to the free corrosion value. The additional anodic current comes from the oxidation of zinc. The cathodic current is proportional to the rate of all of the reduction reactions. An increase in the oxygen reduction rate corresponds to a lower electrical potential of iron compared to E_{corr}. Therefore the amount of current coupled to the iron half-cell decreases and corrosion is retarded. The lower the potential relative to E_{corr}, the lower the corrosion rate.
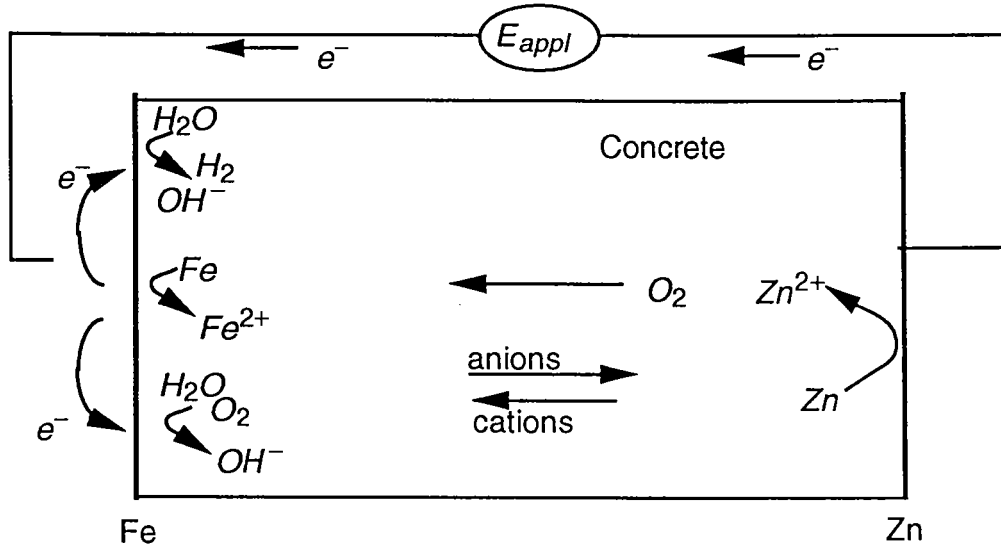
Figure 1.2 One-Dimensional Schematic of Processes Occurring in Cathodic Protection.
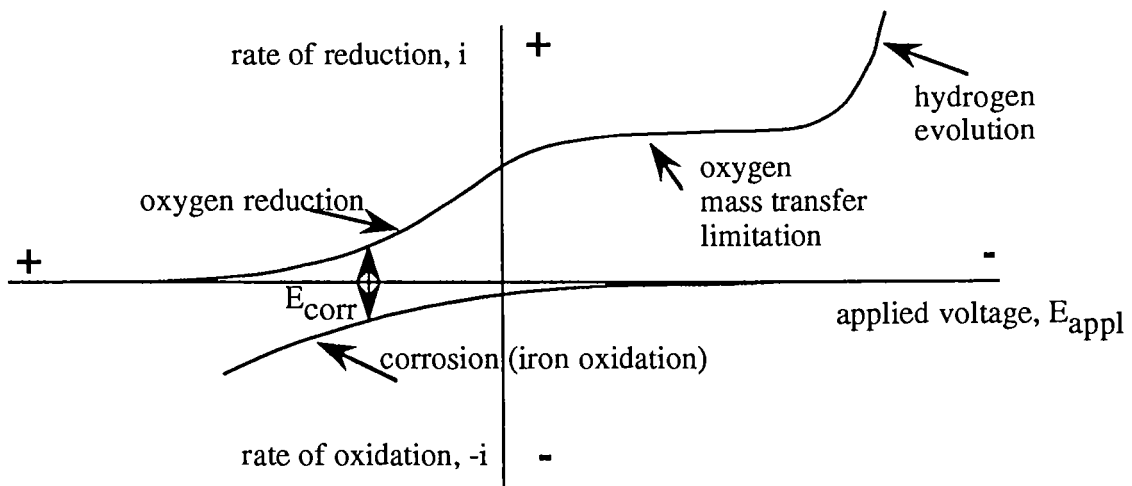
Figure 1.3 Schematic of the Rate of Oxidation and Reduction Processes as a Function of Applied Voltage for Cathodically Protected Reinforced Concrete.

The applied potential at which the cathodic current equals the corrosion current is labeled E_{corr}. In this case, the cathodic current equals the anodic current and no electrons flow in the external circuit. This is equivalent, in principle, to free corrosion where there is no CP system in place.

In order to decrease the rate of corrosion, a (negative) potential must be applied between the zinc and the iron. If the iron is made positive with respect to zinc, even more electrons will be supplied by the zinc to the reduction of oxygen. Again the total cathodic current will increase. Similarly the potential of iron will be more negative with respect to E_{corr}, and the oxidation of iron will be further retarded. This trend will continue until the concrete adjacent to the electrode is completely depleted of oxygen. This mass transfer controlled behavior is marked by the flat portion of the cathodic current curve.

As the applied potential is increased even further, other electrochemical processes occur. As Figure 1.3 illustrates, at sufficiently large potentials, hydrogen evolution commences. This can lead to hydrogen embrittlement of the iron and can also cause concrete cracking. Thus, there is an optimum applied potential. If the applied potential is too low, the iron is under-protected and corrosion still occurs at an appreciable rate. Too large an applied potential leads to overprotection, reducing the service life of the anode and possibly leading to the deleterious reduction of water to form hydrogen gas.

In order to optimize the performance of a CP system, it is important to apply the appropriate potential. This applied potential reduces the potential of iron with respect to E_{corr} and lowers the corrosion rate. However, if the potential of iron is too negative hydrogen evolution results. This suggests that a convenient monitor of the effectiveness of CP is achieved by measuring the potential of the protected reinforcing steel with respect to E_{corr} (see Figure 1.3). In order to implement this strategy, the proper value of ($E_{Fe} - E_{corr}$) must be determined. The measurement which is often made, the polarization decay, is related to this potential difference. The decay is determined by interrupting the protection current (open circuit) and monitoring the decay of potential relative to a stable reference electrode. Some investigators have reported 100 mV is an adequate potential decay for protection while others believe the value is closer to 150 mV[4-9]. In either case, a reliable and durable reference electrode is needed which can accurately track the iron potential.

1.3 POTENTIAL MEASUREMENT AND REFERENCE ELECTRODES

The potential of the reinforcing steel must be measured with respect to a reference electrode. Figure 1.4 shows a graphite reference electrode imbedded in the concrete near the steel. In this Figure, R_B and R_u are the bulk and uncompensated resistance, respectively. Since concrete is a highly resistive electrolyte, the reference electrode must be placed close to the reinforcing steel to minimize error in potential due to the uncompensated resistance.

The potential of the reference electrode needs to be as stable as possible. In selecting a reference electrode, a half reaction with a stable equilibrium potential and minimal polarization is desirable. The equilibrium potential can be affected by the chemical species around the reference electrode. An effective reference electrode's equilibrium potential is independent of the chemical species (especially pH) and temperature. Moreover, the passage of current leads to a departure from the equilibrium potential. These kinetic variations should also be minimized. Furthermore the reference electrode should be inexpensive and rugged enough to be embedded in concrete.
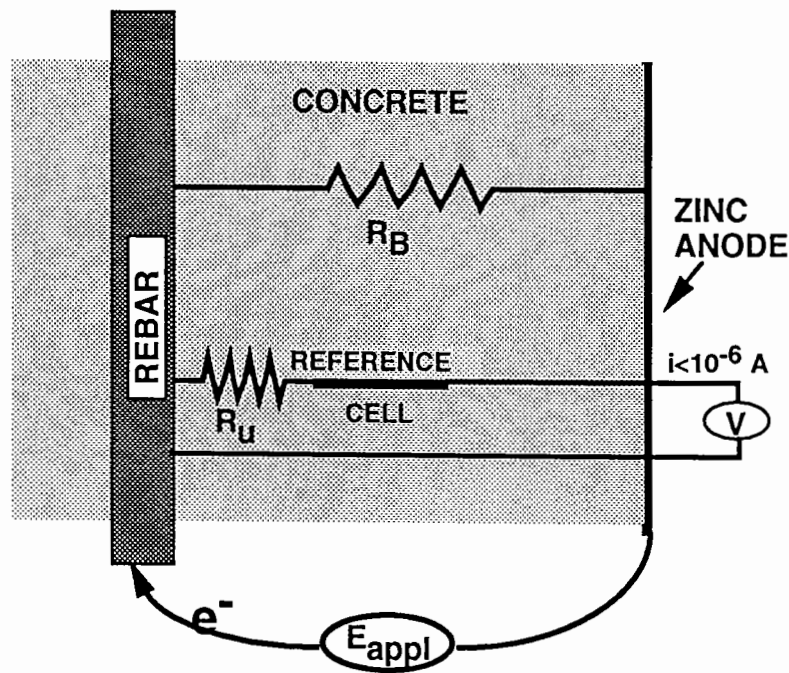
Figure 1.4 Schematic of the Placement of Graphite Reference Electrode.

Standard laboratory reference electrodes such as the silver-silver chloride electrode or the saturated calomel electrode have stable equilibrium potentials and are non-polarized. In these electrodes the half-reactions are also well defined. Unfortunately these electrodes are unsuitable for embedding in concrete due to leakage of electrolyte. Solid probes like graphite are more suitable in this regard. On the other hand, a graphite electrode does not have a well defined half reaction but is dependent on the species present in the concrete electrolyte. Hence their potential is not as stable as a standard laboratory electrode.

5

2.0 OBJECTIVES

The objective of this work was to evaluate the suitability of graphite electrodes for imbedded reference electrodes in reinforced concrete structures that are cathodically protected with a sprayed zinc anode and, if they are found suitable, to examine placement strategies. It was assumed that the 100-mV polarization decay criterion would be used.

The work plan was divided into two parts: computer simulation and laboratory scale experimentation.

1. Computer simulation.

The first objective was to develop a quantitative numerical model of the cathodic protection process and the 100-mV polarization decay criterion, with which sensitivity of the polarization decay measurement to the placement of electrodes could be examined. A finite difference code to solve for the potential and current distributions in a simplified rectangular geometry was to be used. Input parameters were to be based on available experimental data. With this code an analysis on the effects of variables such as moisture content of the concrete, depth of concrete cover, and applied potential were to be studied. These results were to be used to assess the performance of the system in terms of adequacy of protection and anode life. This steady-state model will also be the basis for future analyses of transient processes.

2. Laboratory study of graphite reference electrodes.

The second objective was to test the performance of commercially available and laboratory fabricated graphite electrodes for suitability as reference electrodes in the 100-mV polarization decay test, which is used to control cathodic protection systems. The performance of the graphite electrodes was to be compared to that of silver-silver chloride electrodes as a de facto standard. Silver-silver chloride electrodes are recognized as among the best available under controlled laboratory conditions, but are generally not rugged enough for field application.

The original work plan focused more on evaluating the reference electrode performance through experimental investigation. The rationale was that the erratic behavior of graphite electrodes observed in the field was caused by inherent instability in the electrodes. In fact, preliminary experiments suggested that the graphite reference electrodes behaved well when compared to standard laboratory reference electrodes in a controlled laboratory environment. Additionally it became clear that both the experimental and analytical work would require

much greater effort than was originally anticipated and that, in order to get meaningful results, the work would have to be concentrated in one area or the other. The experimental data suggested that the large variability of field graphite reference electrodes may be due to large variations in the potentials measured in the field rather than poor performance. To investigate this hypothesis, work on the numerical model was emphasized. Indeed the simulation results relate wide variations in measured potential directly to parameters such as pore saturation and concrete resistivity. Moreover this steady-state model provides a foundation for more complex transient analysis which is presently being undertaken by this group through investigation of chloride ion migration.

3.0 MODEL FOR CATHODIC PROTECTION

3.1 BACKGROUND

In this chapter, a mathematical model for corrosion and cathodic protection of reinforcing steel in concrete structures is developed. First the processes are described qualitatively, and then the mathematical expressions that are used to quantify these processes are presented. Many of the issues involved in cathodic protection are introduced through consideration of a system with a one dimensional geometry. The additional complexities of potential distributions and transport processes in two-dimensional systems are then considered, and finally a few comments on three-dimensional systems. As with any numerical modeling, many assumptions and simplifications are introduced. While the impact of critical assumptions are assessed, this model should be regarded as "a way of thinking about the problem" rather than "the direct basis for action."

To introduce the model, the simple one-dimensional system shown in Figure 1.2 is considered: a rectangular block of concrete with an iron plate on one face and a zinc plate on the opposite face. In the absence of cathodic protection, the two plates are not connected; for cathodic protection, the iron plate and the zinc plate are connected through a power supply.

Consider first the case of free corrosion, with the zinc plate disconnected from the rebar. The corrosion process is the oxidation of iron, which is represented by the reaction:

$$Fe \rightarrow Fe^{2+} + 2e^- \qquad (3\text{-}1)$$

which is coupled to the reduction of oxygen:

$$O_2 + 2H_2O + 4e^- \rightarrow 4OH \qquad (3\text{-}2)$$

Oxygen enters the system through the (hypothetically gas-permeable) zinc-plate boundary and moves through the pores and cracks of the concrete to the iron plate. The oxygen transport process is very complex, consisting of diffusion in the gas phase, diffusion in the liquids occupying the pore space, and capillary convection as pore fluids move in and out. The oxygen transport rate is thus highly dependent on the water content of concrete.

When the iron is cathodically protected, most of the electrons necessary to reduce the oxygen are supplied by oxidation of the zinc plate through the following reaction:

$$Zn \rightarrow Zn^{2+} + 2e^-$$
(3-3)

The electrons produced by the oxidation of zinc flow through the external circuit and reduce oxygen at the iron plate. Since the reduction of oxygen is supported by electrons from the zinc oxidation, the rate of iron oxidation (corrosion) is greatly reduced.

The cathodic protection circuit is completed by transport of ions through the pore structure in the concrete. The negative charge introduced through OH^- ions at the iron plate moves toward the zinc, and the positive charge introduced by the Zn^{2+} ions at the zinc plate moves toward the iron. The actual charge carriers are mobile ions in the concrete, for example, OH^-, Cl^-, SO_4^{2-}, Na^+, Ca^{2+}, etc. The rate of transport depends on the water content of the concrete: the greater the water content the higher the transport rates.

Thus, in the study of cathodic protection systems, there are five processes, the rates of which must be quantified:

    (i)   transport of oxygen from the surface of the concrete, through the concrete, to the surface of the steel;

    (ii)   electron transfer in the reduction of oxygen;

    (iii)   electron transfer in the oxidation of iron;

    (iv)   electron transfer in the oxidation of zinc;

    (v)   migration of ions through the concrete.

There are, of course, additional complications to this simple five-step process, such as the accumulation of reaction products at the Fe and Zn electrodes, which affect the rates of ion and electron transfer at these interfaces. These additional processes and time-dependent phenomena are not quantified in this study.

3.2 MODEL FORMULATION

A summary of the equations of the model is presented. This summary is followed by a detailed description of the major processes incorporated in the model, in which the

approximations and the selection of parameter values are discussed. The parameter values, some of which were obtained directly from the literature and some of which were derived in this study are summarized in Table 3.1 for the base case. The major processes in the model are:

(i)   transport of ions in the concrete,

(ii)   transport of oxygen in concrete, and

(iii)   electron transfer at the metal-concrete interfaces.

Table 3.1 Values of Parameters for the Base Case Model

Symbol	Units	Value	Source
PS	%	60	Typical value
ρ	Ω m	138	Gonzalez et al. (1993)[15]
k_O	m s^{-1}	1×10^{-7}	Derived from Kobayashi and Shuttoh (1991)[19] and Tutti (1982)[16]
H	$m_{liq}^3\ m_{gas}^{-3}$	33	
C_O^{air}	mol m^{-3}	8.6	Derived from ideal gas law at 298 K
i_O^0	A m^{-2}	7.7×10^{-7}	Derived from Locke and Siman (1980)[20]
E_O^{eq}	V vs SHE	0.509	Derived from Pourbaix (1974)[24]
	V vs CSE[a]	0.19	
b_O	V/decade	0.18	Derived from Locke and Siman (1980)[20]
i_{Fe}^0	A m^{-2}	7.1×10^{-5}	Derived from Locke and Siman (1980)[20]
E_{Fe}^{eq}	V vs SHE	-0.44	Derived from Pourbaix (1984)[24]
	V vs CSE[a]	-0.76	
b_{Fe}	V/decade	0.41	Derived from Locke and Siman (1980)[20]
pH		12	Typical value
i_H^0	A m^{-2}	1.1×10^{-2}	Frankenthal and Milner (1986)[23]
E_H^{eq}	V vs SHE	-0.710	Derived from Pourbaix (1984)[24]
	V vs CSE[a]	-1.030	
b_H	V/decade	0.15	Frankenthal and Milner (1986)[23]
E_{Zn}^{eq}	V vs SHE	-0.358	SHRP-S-670[4]
	V vs CSE[a]	-0.68	
L	m	0.0254	Typical value (ODOT)

[a]   Potentials are referred to standard hydrogen electrode (SHE) in the 1-D model and to the saturated $Cu/CuSO_4$ (CSE) in 2-D model; the potential of the CSE is - 0.32 V vs SHE[29] (i.e., E vs $Cu/CuSO_4$ = E vs SHE - 0.32 V)

3.2.1 SUMMARY

At steady-state, Laplace's equation governs the electric potential at any point in the bulk of the concrete:

$$\nabla^2 \phi = 0 \tag{3-4}$$

where ∇ is the gradient operator and ϕ is the electric potential(V) in the concrete which is discussed in more detail in Section 3.4.1.

At the zinc electrode, a constant potential boundary condition is chosen:

$$E_{Zn} = constant \tag{3-5}$$

where E_{Zn} is the potential of the Zn electrode (V vs. a reference electrode in the concrete immediately adjacent to the zinc electrode; see footnote Table 3.1).

At the iron boundary, the net current density is given by the mixed boundary condition:

$$i = \frac{i_L i_o^0 \exp\{\frac{-2.3(E_{Fe} - E_o^{eq})}{b_o}\}}{i_L + i_o^0 \exp\{\frac{-2.3(E_{Fe} - E_o^0)}{b_o}\}} - i_{Fe}^0 \exp\{\frac{2.3(E_{Fe} - E_{Fe}^{eq})}{b_{Fe}}\} = -\frac{\nabla\phi}{\rho} \tag{3-6}$$

where i is the *net* current density (A/m^2), E_{Fe} is the potential of the iron electrode (V vs. a reference electrode in the concrete immediately adjacent to the iron); for reactions 3-1 and 3-2, b_o and b_{Fe} are the Tafel slope parameters (V/decade), i_o^0 and i_{Fe}^0 are the exchange current densities (A/m^2), and E_o^{eq} and E_{Fe}^{eq} are the equilibrium potentials (V vs SHE); and ρ is the resistivity of the concrete electrolyte (Ω m). A derivation of equation 3-6 is presented in Appendix A.

The limiting current density, i_L, is given by:

$$i_L = nFk_o C_O^{air} \tag{3-7}$$

where k_O is the mass transfer coefficient of oxygen through the porous concrete (m/s) and C_O^{air} is the concentration of oxygen in air (mol/m³), n is the number of electrons transferred per molecule of O_2 (reaction 3-2), and F is the Faraday constant (C/mol). The values for these parameters that were used in the base case of this model are shown in Table 3.1 and are discussed in the following sections.

3.2.2 THE GOVERNING EQUATION FOR THE CONCRETE ELECTROLYTE

In this section the governing equation for the potential distribution in the concrete is developed. It is approached from first principles so that the basic assumptions are explicitly stated and evaluated.

The flux of an ion m in a single (homogeneous) phase can be expressed by the equation

$$J = - D_m \nabla C_m - \frac{F}{RT} z_m D_m C_m \nabla \Phi - C_m v \qquad (3\text{-}8)$$

where J_m is the flux of ion m (mol m^{-2} s^{-1}); D_m is the diffusion coefficient of ion m (m² s^{-1}); C_m is the concentration of ion m (mol m^{-3}); z_m is the charge on ion m (a signed integer, i.e., multiple of the elementary charge); R is the gas constant (8.314 J mol^{-1} K^{-1}); T is the temperature (K); and v is the bulk velocity of the fluid. The first term on the right hand side of equation 3-8 represents the flux of an ion due to diffusion (movement in a concentration or chemical potential gradient), the second flux term due to migration (movement in an electric potential gradient) and the third flux term due to convection.

Equation 3-8 is strictly valid for transport in a single phase. For a complex heterogeneous material such as concrete, transport is a multi-phase, multi-path process, which could be described by a series of equations of the form of equation 3-8. For the derivation that follows, the flux of ions in concrete is approximated as a process that occurs in a *single-phase*, which can be described by equation 3-8 with *effective* values of D_m and C_m. These values are not actually derived and used in this model, but it is important to define them more precisely in view of the heterogeneity of concrete.

The effective diffusion coefficient is represented as a scalar, independent of ion concentration and direction (i.e., the concrete is isotropic for ion transport). The effective diffusion coefficient incorporates diffusive transport of ions in the bulk liquid of the pore space, on the surfaces of solids surrounding the pore space, and through the solids of the concrete. Thus, it is highly dependent on water content of the

13

concrete. Similarly the concentration is an effective concentration, that is, moles per microscopic unit volume of concrete.

The current density at any point is found from the summation of the fluxes of ions (Faraday's Law):

$$i = \sum z_m F J_m \qquad (3\text{-}9)$$

where i is the current density (here a vector quantity, A/m^2).

The conservation of charge requires that the divergence of the current density equal zero, under the condition of no charge accumulation (electro-neutrality):

$$\nabla \cdot i = 0 \qquad (3\text{-}10)$$

Through combination of equations 3-8, 3-9, 3-10, and the application of the electro-neutrality condition, the governing equation for conservation of charge in the concrete becomes:

$$\Sigma [\nabla \cdot \frac{F^2}{RT} z_m^2 \, D_m C_m \nabla \Phi \,] + \Sigma [\nabla \cdot F z_{mD_m} \nabla C_m] = 0 \qquad (3\text{-}11)$$

where the convection term in equation 3-8 has dropped out due to electro-neutrality. This partial differential equation couples species transport to the potential distribution. Since data are not available for D_m and C_m, two approximations are made to solve equation 3-11.

First, it is approximated that diffusion is negligible compared to migration. This approximation is very accurate under either of the following conditions: (i) only one type of ion is mobile in concrete and responsible for virtually all the charge transport; or (ii) all the ions have equal diffusion coefficients. The first condition might be approached if the majority of the negative charge in the concrete were due to immobile -SiO⁻ or -AlO⁻ groups of the alumino-silicate lattice, while the majority of the positive charge were a single mobile cation such as Ca^{2+}. The second condition is unlikely to be approached under any circumstances, since different ionic species have different mobilities. However, as long as data for diffusion coefficients of ions in partially saturated porous concrete are unavailable, the assumption that diffusion is negligible compared to migration is necessary. Then the constant parameters in the

14

first term of equation 3-11 are grouped together to define the conductivity, κ, which is the inverse of resistivity, ρ:

$$\kappa = \frac{1}{\rho} = \frac{F^2}{RT} \Sigma z_m^2 D_m C_m \qquad (3\text{-}12)$$

and the second term of equation 3-11 is dropped.

In the second approximation, the conductivity is presumed constant in time and space. The use of this approximation is justified by the fact that bulk conductivity of the concrete is easy to measure while single ion diffusivities are unknown. It would be straightforward to modify this assumption to account for changes in environmental conditions. For example, conductivity could be related to water content of the concrete.

With these approximations, equations 3-8 and 3-9 can be combined to give

$$i = \kappa \nabla \phi \qquad (3\text{-}13)$$

which is just Ohm's Law. Moreover, with these two approximations, equation 3-11 reduces to Laplace's equation:

$$\nabla^2 \phi = 0 \qquad (3\text{-}14)$$

In summary, the governing equation for the concrete system is described by the coupled partial differential equation 3-11. However, due to the unavailability of data, this microscopic model must be abandoned for a much more macroscopic model expressed in terms of bulk conductivity. However, by considering the microscopic model from first principles, the assumptions of the macroscopic model can be evaluated.

Several points can be made about the effects of these assumptions on the application of the model. Many other published models just begin with equation 3-13 and implicitly incorporate the assumptions that have been made here explicitly. Thus, incorporation of these assumptions is common practice.

After these assumptions have been made, it is inconsistent to use the model for investigation of the transport of a particular type of ion; thus, questions about movement of specific ions (e.g., Cl^-) cannot be addressed directly with this model.

15

From a practical point of view, the use of different values of conductivity for different environmental conditions should be considered.

3.2.3 THE OXYGEN MASS TRANSFER COEFFICIENT

Both the Fe oxidation (equation 3-1) and the Zn oxidation (equation 3-3) are coupled to the reduction of oxygen at the rebar (equation 3-2). Since the availability of oxygen can limit the reaction rate, it is important to quantify the oxygen mass transfer through the porous concrete.

Concrete is a porous material with a tortuous mass transfer path. The pore structure is dependent on the hydration processes. In general there are many different size pores: gel pores about 0.2 nm, small capillary pores distributed around 6-8 nm, large capillary pores distributed around 100-1000 nm, and voids greater than 10 μm[10,11]. The pore structure complicates the transport process as the smaller pores can completely fill with water, while larger pores remain gas filled with only a film of water. Oxygen moves much more readily in the gas phase; the diffusion coefficient of oxygen in the gas phase is 4 orders of magnitude greater than in the liquid phase, and oxygen is 33 times more concentrated in the gas. Moreover, the gas filled pores can become bottlenecked with pockets of liquid, which slow the diffusion process. Oxygen could also move by capillary convection.

Data are lacking for a description of diffusion based on microscopic processes in this complex pore structure. Consequently, a macroscopic approach based on a bulk mass transfer coefficient, k_O (m s^{-1})[12], was used:

$$J_O = k_O(C_O^{air} - HC_O^{liq,y=L})$$
(3-15)

where H (m_{liq}^3/m_{air}^3) is the Henry's Law constant for the equilibrium distribution of oxygen between air and water, and $C_O^{liq,y=L}$ (mol m^3) is the concentration of oxygen in water at y = L (the surface of the iron electrode). Equation 3-15 is incorporated in the boundary condition equation 3-6 as described in Appendix A.

The source of oxygen in this system is the ambient air, in which oxygen is present in the gas phase at a constant concentration, C_O^{air}. However, the electrochemical reduction of oxygen probably occurs in association with a liquid phase or a liquid film at the electrode surface, in which ions that are generated in the reaction can be accommodated; furthermore the rates of the electrochemical reactions are generally written in terms of aqueous oxygen concentrations, C_O^{liq}. Thus, at some point, it is necessary to relate concentrations of oxygen in the gas phase to those in the liquid phase. The Henry's Law equilibrium provides this relation: $C_O^{gas} = H C_O^{liq}$.

The oxygen mass transfer coefficient depends on the percentage of water in the pores (pore saturation), as well as concrete cover depth. Values for the mass transfer coefficient can be obtained from the measured oxygen flux through concrete, as described in the next section.

3.2.4 VALUES FOR THE CONCRETE RESISTIVITY AND THE OXYGEN MASS TRANSFER COEFFICIENT VS. PORE SATURATION

Both the concrete resistivity and the oxygen mass transfer coefficient depend on the pore saturation. Rainfall, relative humidity and temperature are some of the environmental factors that influence pore saturation, but resistivity and oxygen mass transfer coefficient are most directly related to pore saturation. Values of these parameters that are relevant for conditions of the coastal bridges were estimated from data available in the literature.

Two studies of concrete resistivity as a function of pore saturation, PS, were found[14,15]. The data of Gjorv et al.[14] were used since their experiments were performed on concrete with water to cement ratio (w/c) = 0.4, while the other data were for mortar. An empirical representation of the data is shown in Figure 3.1. As a base case, a pore saturation of 60% was chosen. This value corresponds to a resistivity of 138 Ω m, typical for the coastal bridges.
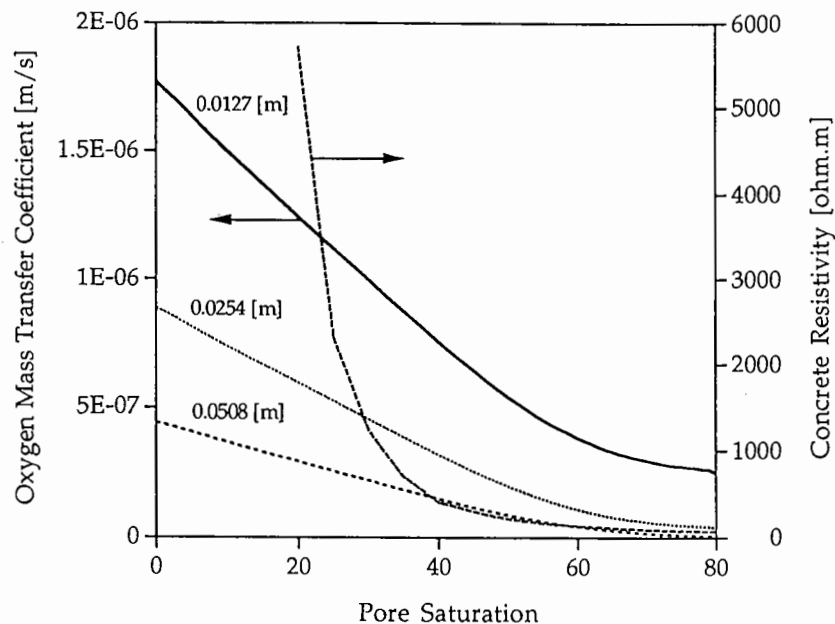
Figure 3.1 Oxygen Mass Transfer Coefficient and Concrete Resistivity Versus Percent Pore Saturation at Three Different Concrete Cover Thicknesses.

17

While several groups have studied the relationship between oxygen flux and relative humidity[11,16,17,18], only one group explicitly measured oxygen flux vs. pore saturation[19]. The following approach was taken to find the mass transfer coefficient of oxygen.

The value of the mass transfer coefficient of oxygen, k_O, depends on a number of factors, three of which were considered here:

     (i)   initial water to cement ratio of the concrete;

     (ii)   "pore saturation" of the concrete (volume fraction of the total pore space of the concrete that is occupied by water); and

     (iii)   thickness of the concrete cover through which oxygen transport occurs.

Additionally, the rate of mass transport of oxygen should be consistent with the oxygen-transport limited currents that are typically observed during cathodic polarization of the rebar. Thus, the goal is to integrate the results of several diverse studies of O_2 transport into conditional values that can be used in the cathodic protection model.

The first of these factors is the initial water to cement ratio (w/c), which influences the pore structure of the concrete. Kobayashi and Shuttoh[19] have shown data in which this ratio has relatively little influence on the mass transfer coefficient of oxygen; however, another study by Tutti[16] shows almost an order of magnitude variation in mass transfer coefficient over the range w/c = 0.2 - 0.8. In view of these conflicting results, an explicit dependence on w/c was not derived. However, experimental results for the other two factors, pore saturation and concrete thickness, were taken for concrete with initial w/c = 0.4 - 0.6, the range of the model system considered in this study.

The effective diffusion coefficient of oxygen in concrete, as a function of *pore saturation*, has been published by Kobayashi and Shuttoh[19]; the concrete thickness was 40 mm, and the initial water to cement ratio was 0.6.

The effective diffusion coefficient of oxygen in concrete, as a function of *thickness of concrete*, has been reported by Tutti[16]. From the strong dependence of apparent diffusion coefficient on thickness of concrete, it is quite apparent that the process is not Fickian diffusion. The relative humidity was reported as 50%, but the pore saturation was not given. The initial water to cement ratio was not reported. The pore saturation in Tutti's work[16] was estimated by finding the diffusion coefficient at 40 mm concrete thickness, and then finding the pore saturation in Kobayashi and Shuttoh's[19] study that gave a similar diffusion coefficient; the result was 80% pore saturation.

The dependence of mass transfer coefficient from these two studies were combined in the following way. First, it was assumed that the value of the effective diffusion coefficient of oxygen in concrete with 80% pore saturation was represented by the data of Tutti[16]. Second, it was assumed that the diffusion coefficient at 0% pore saturation (i.e., in dry concrete pores) was Fickian, independent of the concrete thickness, and equal to gaseous diffusion coefficient of O_2 modified by constant factors for the porosity and tortuosity of the concrete. Then, values of effective diffusion coefficients at values between 0% and 80% were obtained by linear interpolation between the two values. This procedure obviously involves a number of rough approximations, but makes the most use of the limited data available; furthermore, it points the way for future experimental work.

Finally, it was determined that the limiting currents predicted from these mass transfer coefficients were about an order of magnitude larger than those observed experimentally. The reason for this discrepancy is not clear. Thus, all values derived in this way were divided by a factor of 10; these are the values used in the model. The values of mass transfers coefficient derived in this manner as a function of pore saturation for three different thicknesses of concrete are presented in Figure 3.1. Values of oxygen mass transport coefficient for the sensitivity analysis were taken from this figure. For the base case, a concrete cover of 1 in (25mm) gave the oxygen mass transfer coefficient of 1×10^{-7} m/s (Table 3.1).

The studies from which these values were derived were all carefully designed for one-dimensional transport. In the cathodic protection model considered in Section 3.4, two-dimensional transport is considered. Obviously, the dependence of k_o on diffusion path length cannot be completely incorporated in the two-dimensional model through this approach. At this stage in model development, all transport of oxygen is represented as one-dimensional and is limited to the volume of concrete between the rebar and its projection on the opposing zinc face of the concrete. That is, oxygen effectively passes through only a small fraction of the opposing face of the concrete.

The experimental data for oxygen transport, from which the mass transfer coefficients were calculated, were obtained from experiments in which the concrete blocks were in contact with the gas phase at both boundaries. In the cathodic protection experiment, one of the boundaries of the concrete is in contact with an iron electrode, which is thought to be covered by a film or layer of water, as discussed above. Thus, it is of interest to estimate whether the mass transfer resistance of the water film at the iron electrode is significantly greater than the mass transfer resistance of the partially saturated bulk concrete (which may itself contain water films). An order of magnitude estimate can be made based on conditions that would yield equal fluxes of oxygen through the bulk concrete and the liquid film, that is, conditions at which $k_o = D_o^{liq} / \delta H$, where D_o^{liq} is the molecular diffusion coefficient of O_2 in water ($\approx 1 \times 10^{-9}$ m²/s) and δ is the water film thickness. For $\delta = 300$ μm, the mass transfer resistances are approximately equal. In view of the uncertainties about the

water film at the electrode and the nature of oxygen transport through porous concrete, one can say that this value of δ is large enough not to invalidate the treatment of mass transfer that has been used, but small enough to be of concern as the model is refined.

3.2.5 CHARGE TRANSFER KINETICS

Charge transfer kinetics at the electrodes are often described by an equation of the following form:

$$i = i^o \exp \left[\frac{-2.3(E - E^{eq})}{b} \right] \qquad (3\text{-}16)$$

where the parameters were defined in discussion of equation 3-6. This form is rigorously accurate for a single process, but it is often used to describe multi-step reaction sequences. In order to model the cathodic protection system, these parameters must be quantified for iron oxidation (3-1), oxygen reduction (3-2), zinc oxidation (3-3), and hydrogen evolution.

3.2.5.1 Iron Electrode

Three reactions occur at the iron electrode: iron oxidation, oxygen reduction and hydrogen evolution. The values of the parameters were determined directly from the experimental data of Locke and Siman[20], (Figure 3.2), through the following procedure.

First, the conditional equilibrium potentials for each half reaction (reactions 3-1 and 3-2) were calculated from the respective Nernst equations:

$$E_{Fe}^{eq} = E_{Fe}^0 + \frac{RT}{nF} \ln a_{Fe}^{2+} \qquad (3\text{-}17)$$

$$E_O^{eq} = E_O^0 + \frac{RT}{4F} \ln \left(\frac{p_{O_2}}{a_{OH^-}^4} \right) \qquad (3\text{-}18)$$
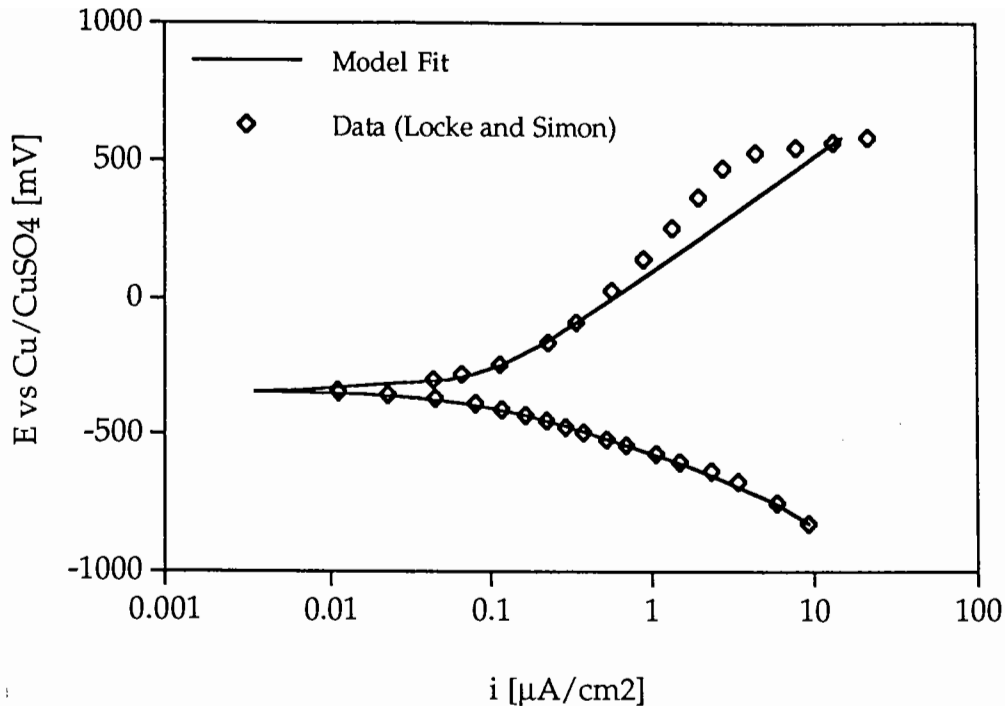
Figure 3.2 Data and Model for Polarization of Iron in Concrete With a 0.2% NaCl Concentration by Weight.

The standard potentials were taken from Pourbaix[24]. For the oxygen reduction reaction, the partial pressure of O_2, p_{O2}, was set to 0.21 atm, and the concentration (activity) of OH^- was set to 0.01 M, consistent with the estimated pH of concrete, pH = 12. For the iron oxidation reaction, the standard potential was used, i.e., the concentration (activity) of Fe^{2+} was set to 1 M. These values of the equilibrium potentials, which are relative to a standard hydrogen electrode, were then re-expressed relative to a saturated $Cu/CuSO_4$ electrode, (E vs $Cu/CuSO_4$ = E vs SHE - 0.32 V). These values are reported in Table 3.1. These values provide "reference potentials" at which comparisons of electrode kinetic data can be made. However, the values of the equilibrium potential and the exchange current densities (E^{eq} and i^0) in equation 3-16 co-vary completely, and in the final model, any appropriate pair could be used; it is just important that the values are internally consistent.

Polarization data taken from Locke and Siman[20] at a chloride concentration of 0.2% (their Figures 3 and 4) were used to determine the values of the electrode kinetic parameters. They reported that the data were not corrected for the IR drop associated with the high concrete resistivity. Thus, two methods were used to determine the values of these parameters. First, equation 3-6 was fit to the original data of Locke and Siman with no IR compensation. Second, their data were corrected with a term to account for the IR drop: $E_{Fe} = E_{appl} + \rho il + E_{ref}$, where E_{appl} is the value from Locke

21

and Siman, and l is the distance between the electrodes determined from the cited geometry to be 2.7 cm. Since the actual concrete resistivity was unknown, values of 20, 40, 60, 80 and 100 Ω m were tried. The kinetic equation, equation 3-6, was fit to the corrected values of E_{Fe} using nonlinear least squares optimization. In both methods, the term for mass transfer limitations represented by limiting current density, i_L, in equation 3-6 was used. This parameter was determined for each of the data sets and was found to be approximately 20 $\mu A/cm^2$. This value is reasonable and is consistent with the limiting current values calculated by the model parameters for a cover thickness of 1 in (25 mm). At a cover thickness of 1 in (25 mm) and pore saturation of 70% the limiting current has this value.

Of the five values with IR compensation, the best correlation occurred at a resistivity of 80 Ω m. The fit with no IR drop gave almost as good a correlation and neither the actual resistivity of the concrete nor the extent of the IR drop was known. Thus, the values from the two methods were averaged, and the averaged values of b_O, b_{Fe}, i_O^0, and i_{Fe}^0, which are listed in Table 3.1, were used in this study. The original data of Locke and Siman[20] and the values calculated from the electrode kinetic model are in Figure 3.2.

The model for electrode kinetics here is simply an accurate representation of experimental data[20], especially for oxygen reduction where the current densities of the data reflect values typical for cathodic protection systems. The parameter values used in this study are consistent with other values reported in the literature[6,21,22]; however, in none of these other reports were raw data presented.

The combination of mass transfer resistance due to oxygen transport (Section 3.2.3) and charge transfer resistances of the oxidation and reduction reactions leads to the boundary condition described by equation 3-6. This expression is derived in Appendix A.

The rate constants for hydrogen evolution:

$$2H_2O + 2e^- \rightarrow 2OH^- + H_2 \tag{3-19}$$
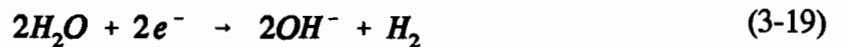
i_H^0 and E_H^0, were obtained by fitting the data of Frankenthal and Milner [23]. However, these experiments were performed at a pH of 8.3. The equilibrium potential, E_H^{eq}, was corrected for hydroxide concentration using the Nernst equation[24]. The parameter values are listed in Table 3.1.

3.2.5.2 Zinc electrode

The potential of the zinc electrode, E_{Zn}, was treated as a constant, the value of which was found experimentally to be -0.358 V vs. SHE[25]. Thus, charge transfer resistance at this electrode was neglected in the current model. This simplification does not affect the results of the model with regard to the 100-mV polarization decay criterion, since no current is flowing during the 4-hour polarization decay period, as will be discussed in Section 3.3. However, this simplification does affect values calculated for the applied potential during cathodic protection. To remove this simplification and evaluate the charge transfer resistance quantitatively, experimental data for the Zn-concrete interface, similar to those of Locke and Siman[20] for the Fe-concrete interface, are necessary.

An attempt was made to explain the potential E_{Zn} by a simple equilibrium model based on the solubility of Zn^{2+} in concrete pore solution and the Zn^{2+}/Zn couple (Appendix B). The potential calculated from the model was $E_{Zn} = -1.49$ V vs SHE, far from the experimental value of -0.358 V vs SHE[25]. It is currently unclear what controls the experimental value. A better understanding of the processes occurring at the zinc electrode is needed[26].

3.2.6 EQUIVALENT CIRCUIT REPRESENTATION AND SIGN CONVENTIONS

The net current density is the sum of the cathodic (positive) and anodic (negative) contributions:

$$i = i_{O_2} + i_{Fe} \qquad (3\text{-}20)$$

where i is the net current density, which, at the Fe electrode, is positive for a net cathodic process and negative for a net anodic process. To restate the sign convention, flow of electrons from zinc to iron in the external circuit, (or, equivalently, flow of positive charge from zinc to iron in the internal circuit) is positive current.

An equivalent circuit of the system, based on the approximations and assumptions stated above, is illustrated in Figure 3.3. The potential differences around the circuit include E_{appl}, the applied potential; E_{Fe} and E_{Zn}, the two metal-electrolyte interfacial potential differences; and E_{ohm}, the Ohm's law potential drop in the bulk of the concrete. Continuity requires that where the signs are consistent with Figure 3.3 and the definition of i. While E_{Zn} is represented by a constant potential with neglect of

charge transfer over-potential (equation 3-5), E_{Fe} also includes a mass transfer over-potential due to oxygen mass transfer resistance, R_{mt}, and a charge transfer over-potential due to the charge transfer resistance in both oxygen reduction and iron oxidation, R_{ct}.

$$E_{appl} = E_{Fe} - E_{ohm} - E_{Zn} \qquad (3\text{-}21)$$
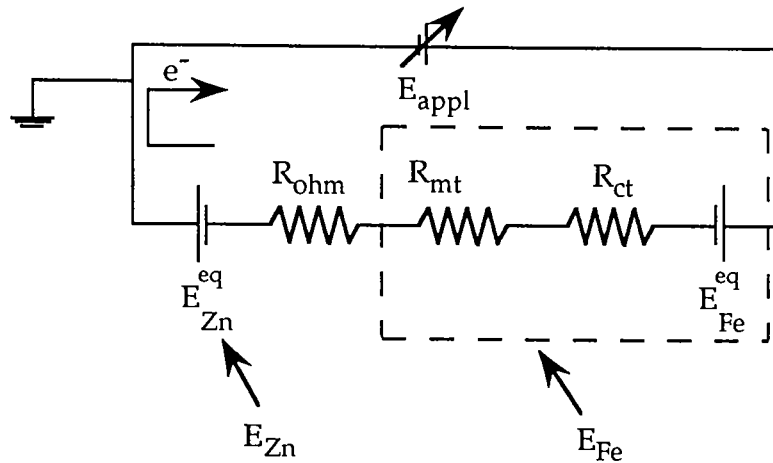
Figure 3.3 Equivalent Circuit of the Cathodic Protection System

3.2.7 METHODS OF APPLYING CATHODIC PROTECTION

The cathodic protection circuit can be controlled in three ways, as illustrated by Figure 3.3:

1.   control the voltage applied between zinc and iron, E_{appl} (constant voltage);

2.   control the current applied between zinc and iron, $I = I_{appl}$ (constant current);

3.   control, as nearly as possible the potential at the Fe-concrete interface (constant potential). This mode offers the best control for cathodic protection, since the

variable and generally unknown voltage drop represented by E_{ohm} in Figure 3.3 no longer interferes. This mode of control is implemented with a "three-electrode cell." In addition to the Fe and Zn electrodes, the circuit includes a reference electrode, which is located as close to the Fe electrode as possible. The potential between the Fe electrode and this reference electrode is measured and used in a feedback circuit to control the voltage between Zn and Fe, in order to bring the Fe-reference electrode potential to the desired set point. A high-impedance voltmeter is used to avoid polarization of the reference electrode. These circuits are commercially available and used widely in electrochemistry laboratories.

The control E_{appl} paradigm (constant voltage) is used for the presentation here, although the results would be the same if any of the other methods were used.

3.3 RESULTS IN ONE DIMENSION

The one-dimensional model can be formulated as follows. Laplace's equation can be integrated over the bulk (from y=0 to y=L) to give:

$$E_{ohm} = i\rho L \qquad (3\text{-}22)$$

The zinc boundary (y=0) is at constant potential:

$$E_{Zn} = -0.358 \ V \ vs \ SHE \qquad (3\text{-}23)$$

Oxygen transport is represented by equation 3-15. At steady state, the current due to oxygen reduction must be balanced by the flux of oxygen through the concrete:

$$i_O = nFk_O(C_O^{air} - HC_O^{liq,y=l}) \qquad (3\text{-}24)$$

Under the condition that $C_O^{air} >> H\ C_O^{liq,y=L}$, the current reaches the "limiting value"

$$i_L = n F k_O C_O^{air} \qquad (3\text{-}25)$$

The currents due to oxygen reduction and iron oxidation are given by the equations:

$$i_O = i_O^0 \frac{HC_O^{y=l}}{C_O^{air}} \exp\left[\frac{-2.3(E_{Fe} - E_O^{eq})}{b_O}\right] \qquad (3\text{-}26)$$

and

$$i_{Fe} = i_{Fe}^0 \exp\left[\frac{2.3(E_{Fe} - E_{Fe}^{eq})}{b_{Fe}}\right] \qquad (3\text{-}27)$$

where the net current density is given by equation 3-20:

$$i = i_{O_2} + i_{Fe} \qquad (3\text{-}20)$$

and the potentials are related by equation 3-21:

$$E_{appl} = E_{Fe} - E_{ohm} - E_{Zn} \qquad (3\text{-}21)$$

with $E_{ohm} = i \rho L$. Equations 3-20 - 3-27 completely define the one-dimensional model. These were solved by a BASIC computer program, which is listed in Appendix C.

With this one-dimensional model some very basic questions concerning cathodic protection, the 100-mV polarization decay criterion, and the placement of reference electrodes can be examined:

(i)   What process ultimately controls the rate of corrosion and will ultimately be the key in protecting against corrosion?

(ii)   What is an "acceptable" rate of corrosion (not a subject of this study but still a fundamental question)? What potential must be imposed at the Fe electrode to reduce corrosion to this acceptable level?

(iii)   How can the 100-mV polarization decay criterion be explained in terms of this model?

26

(iv)   To what extent is the 100-mV polarization decay criterion a satisfactory indication that the iron is satisfactorily protected?

(v)   To what extent is the placement of the reference electrode critical in the 100-mV polarization decay criterion.

(vi)   Under what conditions does evolution of Hydrogen become likely?

To address these questions, the one-dimensional model was run for three cases:

(i)   *free corrosion* in the absence of any protection;

(ii)   *cathodic protection* at an applied potential that results a polarization decay in potential change of exactly 100 mV; and

(iii)   "*instant-off*," to simulate the system immediately after the cathodic protection system has been switched off, but before polarization decay has occurred.

The results from these cases are presented in Table 3.2 and are discussed in the following sections.

3.3.1 CONTROL OF CORROSION RATE

The first step is to determine which process controls the rate of corrosion. The results of the model for the case of free corrosion are presented in Table 3.2, Case A. (Actually this case represents values calculated when the circuit is closed but the applied potential is such that no electrons flow in the external circuit. This case is identical to free corrosion.) As seen in the table for this case, the oxygen reduction current is less than 1% of its limiting value and the concentration of oxygen at the electrode surface is within 99% of its saturation value.

Thus, with the parameters used in this model, the rate of free corrosion is not controlled by oxygen transport, but by charge transfer kinetics. Then the next question is, how do charge transfer kinetics depend on E_{Fe} and E_{appl}?

According to equation 3-27, the log of the corrosion rate (actually i_{Fe}) is directly proportional to the potential difference at the iron-concrete interface, E_{Fe}.

The relation between E_{Fe} and E_{appl} can be understood by considering the net current (Figure 3.4), the IR drop (Figure 3.5), and the plot of E_{Fe} vs. E_{appl} (Figure 3.6). At values of E_{appl} close to the free corrosion value (0.331 V, Table 3.2, Case A), the current is low, the IR drop is negligible, and the value of E_{Fe} varies linearly with E_{appl},

as seen in Figure 3.7. At more negative values of E_{appl}, the current increases, the IR drop becomes significant, and the change in E_{Fe} with E_{appl} becomes less than 1:1.

Ultimately, the current reaches the oxygen transport controlled limit, the IR drop levels off, and E_{Fe} once again varies 1:1 with E_{appl}. The magnitude of the ohmic potential drop under limiting conditions depends on the ratio of the oxygen mass transfer coefficient in concrete to the ionic conductivity of concrete, but is independent of the dimensions of the concrete block.

Table 3.2. Solutions[a] to 1-D Model. The Model is Defined by Equations 3-20 to 3-27. The Parameter Values Appear in Table 3.1.

Symbol	Units	A Free Corrosion	B Protection	C Instant Off
Current				
i_o	A m^{-2}	0.00072	0.28	0.00041
i_{Fe}	A m^{-2}	0.00072	0.000024	0.00041
i	A m^{-2}	0	0.28	0
Potential				
E_{appl}[b]	V	0.331	-1.258	0.231
E_{Fe}[c]	V vs SHE	-0.027	-0.637	-0.127
E_{ohm}	V	0	0.979	0
E_{Zn}[c]	V vs SHE	-0.358	-0.358	-0.358
Oxygen concentration (effective concentration in concrete pore water)				
$C_o^{liq, y=L}$	mol m^{-3}	0.260	0.041	0.041
$C_o^{liq, y=0}$	mol m^{-3}	0.261	0.261	0.261
Current relative to limiting current[d]				
i_o/i_L	A m^{-2}	0.002	0.841	0.001
Corrosion velocity[e]				
V_{corr}	mm/yr	0.0008	0.00002	0.0005
	mm/yr	0.0330	0.00108	0.0188

[a]   Data are presented with several digits to allow balances to be calculated and comparisons between cases to be made; the number of digits is not to be interpreted as an indication of the precision.

[b]   In the absence of an applied potential (Cases A and C), this value is the free galvanic potential, E_{cell}.

[c]   V vs SHE at the electrode surface.

[d] $i_L = 0.33$ A m^{-2}.

[e]   Corrosion velocity is calculated from i_{Fe}, the density of Fe (7860 kg m^{-3}), the molar mass of Fe (0.055487 kg mol^{-1}), the number of electrons in the oxidation of Fe (2), and the number of seconds in a year (3.1536 x 10^7). A mil is 0.001 in.
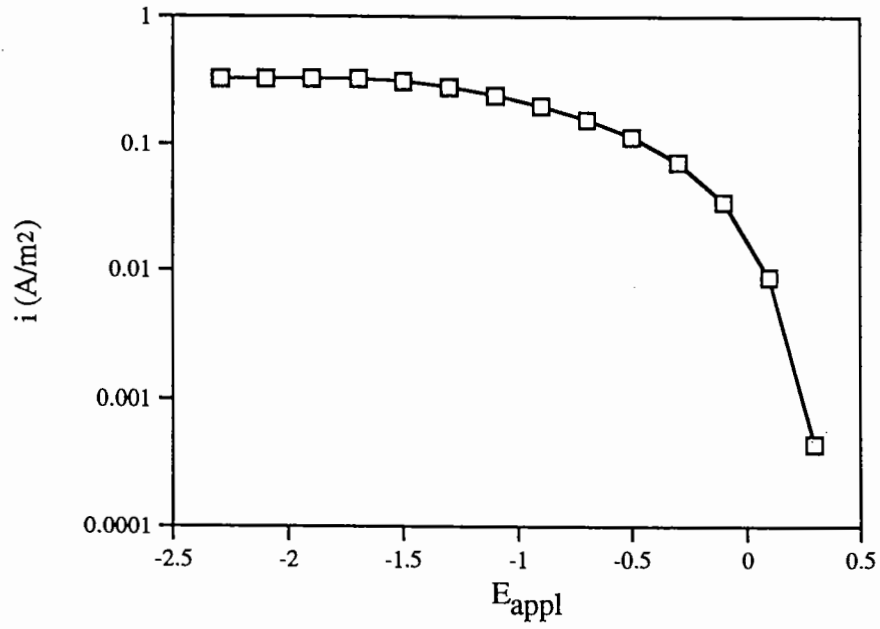
Figure 3.4 log i vs. E$_{appl}$

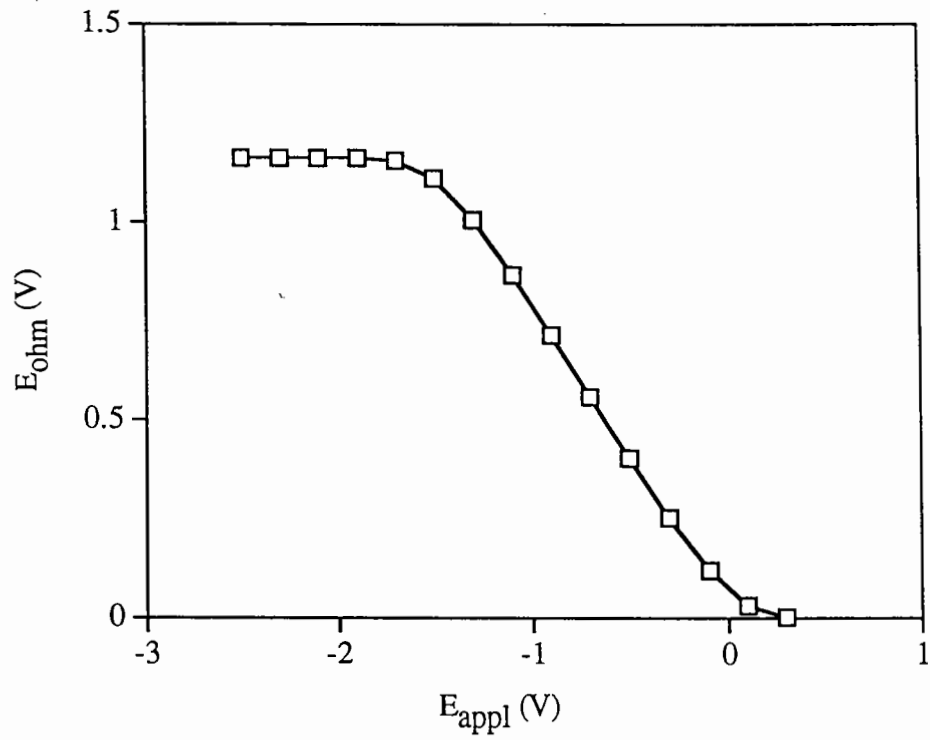**Figure 3.5 E$_{ohm}$ vs. E$_{appl}$**
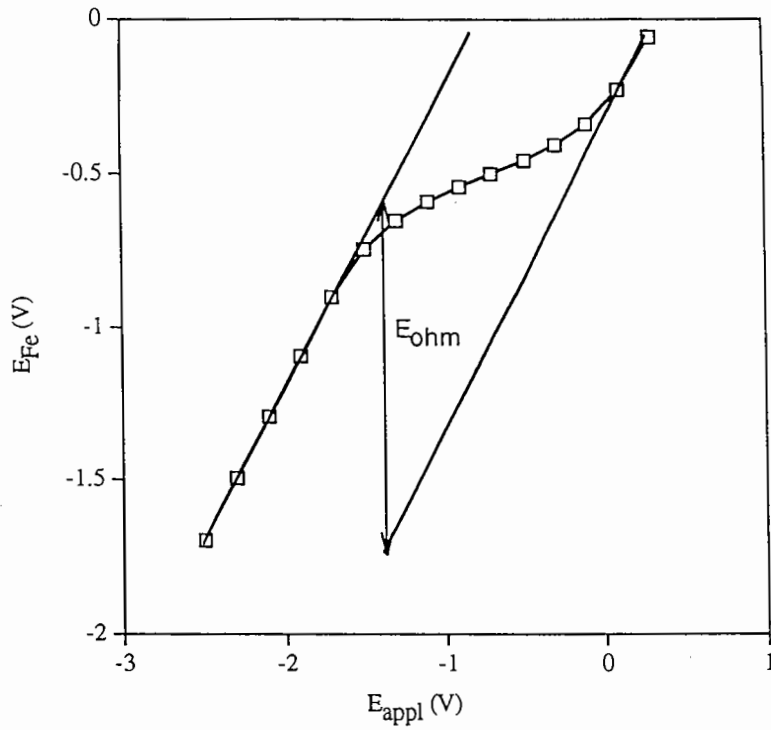
Figure 3.6 E_{Fe} vs. E_{appl} The Vertical Distance Between the Two Lines is the Value of E_{ohm} Under Conditions of Oxygen Transport Limited Current.
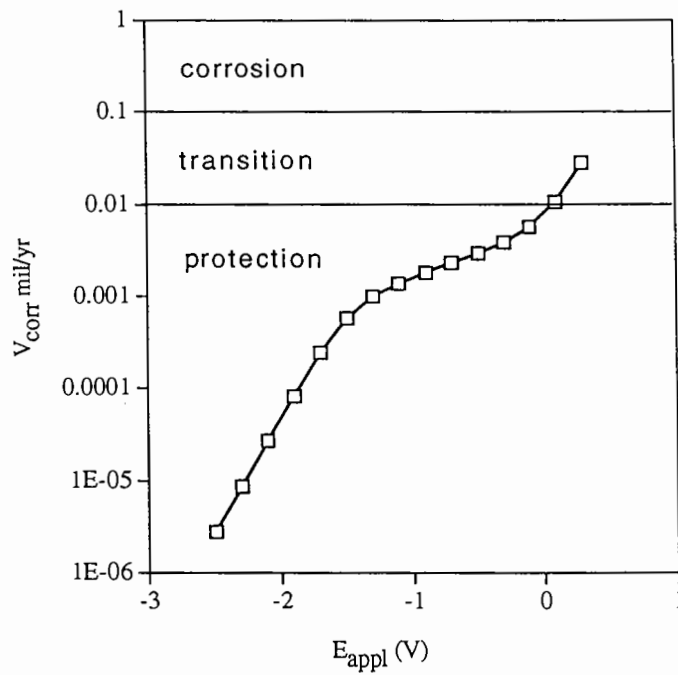
Figure 3.7 v_{corr} vs. E_{appl}

Thus, with the incorporation of a small offset due to the ohmic potential drop, the log corrosion current and corrosion velocity tracks E_{Fe}, and varies with E_{appl} as shown in Figure 3.7. The magnitude of the offset depends on the ratio of the oxygen mass transfer coefficient in concrete to the ionic conductivity.

3.3.2 ACCEPTABLE RATES OF CORROSION

The corrosion velocity of iron in concrete, in the absence of chloride, has been cited to be in the range 0.01 - 0.1 mil/yr[4,20]. If this range represents the transition between "acceptable" and "unacceptable" corrosion rates as shown in Figure 3.7, it is seen that any values of E_{appl} more negative than about +0.1 V yield "acceptable" rates of corrosion, which are less than 0.01 mil/yr. This estimate is very rough, but this procedure does provide a framework for quantitative analysis of the problem and does support the general notion that a few hundred millivolts change in E_{Fe} is necessary for protection, but more than several hundred millivolts are not necessary.

One might note that, even in the case of free corrosion (Case A, Table 3.2), the corrosion velocity is predicted to be only 0.03 mil/yr, which is not far from the "acceptable" range of 0.01 - 0.1 mil/yr[4,20]. One might expect free corrosion rate in concrete with 0.2% $NaCl$[20] to be well beyond the acceptable range. However, in making these comparisons, one should bear in mind that estimates of corrosion rates from log i vs. E data depend critically on the method used to deconvolute the data-traditional high over-potential Tafel linearization, low over-potential linearization, nonlinear fit of both anodic and cathodic branches with or without correction for IR drop or mass transfer limitation, etc. as discussed in Section 3.2.5.1. Different methods can yield different rates from the same set of data. Presumably the corrosion rates in the absence of Cl⁻ (0.01 - 0.1 mil/yr) cited above were determined with methods different from the one used here, and the thresholds of acceptability suggested above may not be strictly applicable. It is generally very difficult to find enough of the raw data from studies reported in the literature to ensure a consistent interpretation among different studies. Nonetheless, the approach taken here does provide a framework for quantitative analysis and points out important subjects for future work.

3.3.3 THE 100-mV POLARIZATION DECAY CRITERION

The current procedure for control of cathodic protection systems is the 100-mV polarization decay procedure. In this procedure, the cathodic protection current is shut off and the potential between the iron rebar and a reference electrode that is imbedded in the concrete near the rebar is monitored for four hours. If the difference between the "instant off" potential and the 4-hour potential is at least 100 mV, protection is deemed sufficient.

31

In the framework of this 1-D model there is one process that could contribute to this 100-mV relaxation in the concrete:

(i) diffusion of oxygen and change in the free corrosion potential as a function of oxygen concentration at the iron surface. Three other processes, which are not part of the simple model, could also contribute:

(ii) the relaxation from local corrosion immediately after the current is turned off, to macro-corrosion, in which a larger area of rebar is available for oxygen reduction;

(iii) the relaxation of ions with different electric mobilities that were displaced from an equilibrium position during the transport of current through the concrete; and

(iv) transformations within reactive oxide layers at the iron surface.

These last three processes might contribute significantly, but at this point there are no data with which to assess the magnitude of theses effects. Thus, the 100-mV relaxation is discussed in terms of the oxygen concentration at the electrode surface.

When the protection potential/current is shut off, several changes begin to occur simultaneously at the Fe-concrete interface. A quantitative description of these changes is beyond the scope of the simple steady-state model, but insight into the relaxation process can be gained from a qualitative examination of events accompanying the cessation of potential control:

(i) The Fe oxidation current must increase in magnitude and the O_2 reduction current must decrease in magnitude until the two are equal and the net current through the external circuit is zero;

(ii) Accompanying these changes in current, the potential at the iron-concrete interface, E_{Fe}, becomes more positive; as seen in equation 3-6 this change in potential is correct for the stated changes in currents;

(iii) Since the rate of oxygen reduction at the iron surface decreases when potential control is shut off, the concentration of oxygen at the iron surface slowly begins to increase back to its value at the free corrosion potential.

Thus, in summary, both the potential, E_{Fe}, and the concentration of oxygen at the surface of the Fe electrode, $C_O^{y=L}$ slowly begin to increase back to their E_{corr}, i_{corr} values in such a way that i_O is always equal to i_{Fe} (equations 3-26 and 3-27).

32

Although the exact path of these concomitant increases in E_{Fe} and cannot be predicted without a time dependent model, a two-step scenario can be taken as a limiting case:

    (i)   the concentration of oxygen at the electrode surface doesn't change (remaining at its original value, which was established at the "protection" potential), while E_{Fe} changes immediately to ensure that $i_{O2} = i_{Fe}$;

    (ii)   after this initial step-change in E_{Fe}, the oxygen concentration slowly rebuilds at the iron surface, ultimately allowing E_{Fe} to return to E_{corr}.

Now the 100-mV protection criterion can be interpreted in terms of this two-step limiting case: Step 1 yields the "instant off" potential, and Step 2 yields the 4-hour drift period, over which the 100-mV difference should be observed. In the absence of a time-dependent model, an estimate of the diffusional relaxation time τ can be obtained from $\tau = L / k_{O2}$, which, for this model (L and k_{O2} in Table 3.1) is approximately 70 hours, somewhat longer than the specified 4-hour test period.

These steps are seen quantitatively in Table 3.2: the system under protection is described in Case B, the system at instant off is described in Case C, and the system back at free corrosion is described in Case A. The protection potential was selected such that the difference between E_{Fe} in Cases C and A was exactly 100 mV.

3.3.4 ADEQUACY OF PROTECTION

At the protection potential used in this exercise, the corrosion velocity of iron is predicted to be 1×10^{-3} mil/yr, compared to 3×10^{-2} mil/yr in free corrosion. According to some of the studies cited by Locke and Siman[20], corrosion in the absence of chloride is of the order of the 2×10^{-2} mil/yr; hence, one might conclude that protection is adequate. However, one should bear in mind the caveats about the comparison of corrosion rates that were discussed in Section 3.3.2.

However, still of interest is an examination of the mechanistic relevance of the 100-mV polarization decay criterion. Under the protection conditions calculated for this case (Table 3.2, Case B), the concentration of oxygen at the iron surface is still relatively high, and the current is only 84% of the oxygen transport limited case. Thus, the conditions are by no means extreme.

An alternative approach to clarifying the physical significance of the 100-mV criterion involves stepping backwards through the cases described above:

33

(i)   first calculate the value of $C_O{}^{y=L}$ that is necessary in the protection phase to yield a 100-mV difference between E_{Fe} at instant off and E_{Fe} at free corrosion;

(ii)   determine the value of E_{Fe} that is necessary to create this value of $C_O{}^{y=L}$ while in the protection mode; and

(iii)   determine the effect of this value of E_{Fe} on the corrosion current, i_{Fe}.

This procedure is tedious, but it can be done; still, it still delivers no particular mechanistic insight as to why the 100-mV polarization decay should correspond to adequate protection.

3.3.5 PLACEMENT OF THE REFERENCE ELECTRODE

As shown in Table 3.2, Case B, when the system is in the protection mode, an IR drop of 979 mV occurs over a distance of 2.54 cm, for a gradient of 385 mV / cm. Thus, *in the protection mode*, not only placement of the reference electrode, but also the size of the reference electrode could make a difference, since a difference of 1 cm translates to difference of 385 mV. However, *in considering the 100-mV polarization decay criterion alone*, the current is negligible, the IR drop is negligible, and electrode placement should not be a matter of concern.

3.3.6 HYDROGEN EVOLUTION

If the value of E_{appl} is too large in the negative direction, hydrogen gas will begin to be evolved at the Fe electrode. The value of E_{appl}, at which E_{Fe} is equal to the equilibrium potential of the $H^+/H_2(g)$ couple (at pH 12, $p_{H2} = 1$ atm), is operationally defined as the "potential of the onset of hydrogen evolution," $E_{appl,H2}$. This quantity can be re-expressed as the "maximum E_{appl} before hydrogen evolution," with "maximum E_{appl}" $= -E_{appl,H2}$. This value of maximum E_{appl}, as a function of pore saturation for three different cover thicknesses, is shown in Figure 3.8. The derivation of Figure 3.8 is explained graphically in Appendix D. Evolution of hydrogen is favored in thick, dry concrete.
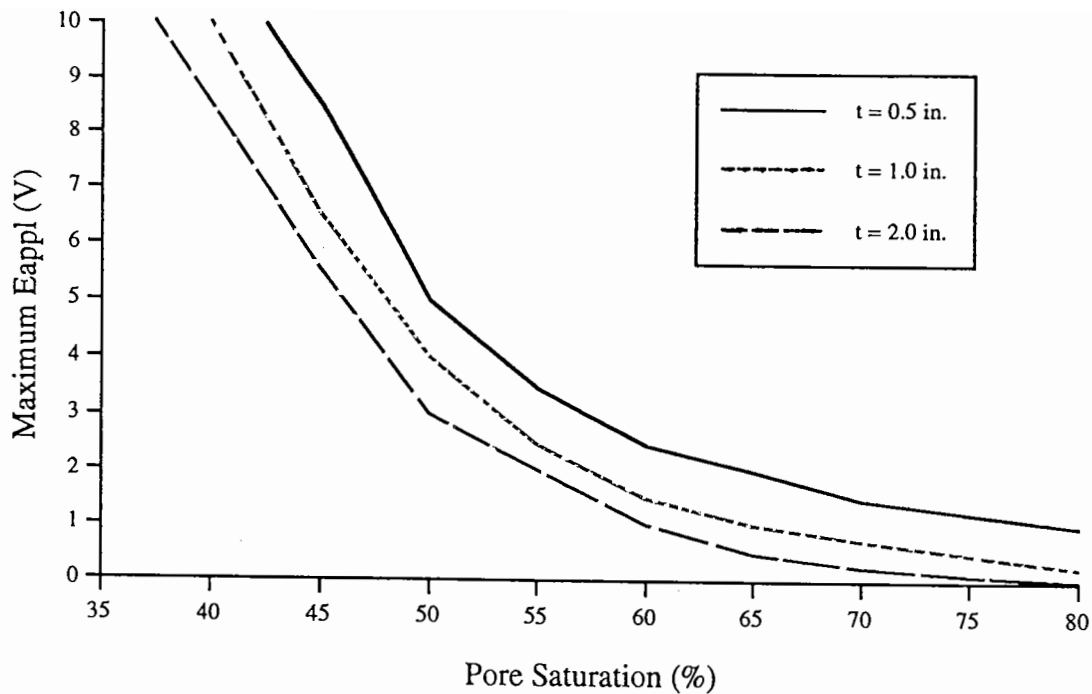
Figure 3.8 The Value of "Maximum E$_{appl}$" Before H$_2$ Evolution vs. Pore Saturation and Cover Thickness; "Maximum E$_{appl}$" is Defined in the Text.

3.4 SIMULATION IN TWO DIMENSIONS

Consideration of one-dimensional processes did not indicate that the 100-mV polarization decay test depended on placement of the reference electrode. However, when the model was extended to two dimensions, a significant dependence on reference electrode placement due to non-uniform current distribution was seen.

3.4.1 METHODOLOGY

Figure 3.9a shows a simplified representation of a bridge deck, reduced to a repeating rectangular unit. A plane of symmetry at the centerline of the rebar allowed the simulation area to be divided by two. Figure 3.9b shows the geometry used for the simulations. For a base case, the distance between the zinc and rebar is 2.54 cm (1 in). The rebar width is 1.27 cm (0.5 in), the distance between the centerline of the rebar and the edge of the rebar is 0.635 cm (0.25 in) and the distance from the centerline of one reinforcing bar to the next is 30.48 cm (12 in). Different concrete cover depths are also studied. Dimensions were chosen to represent typical values for the Yaquina Bay Bridge, Newport, Oregon.

35
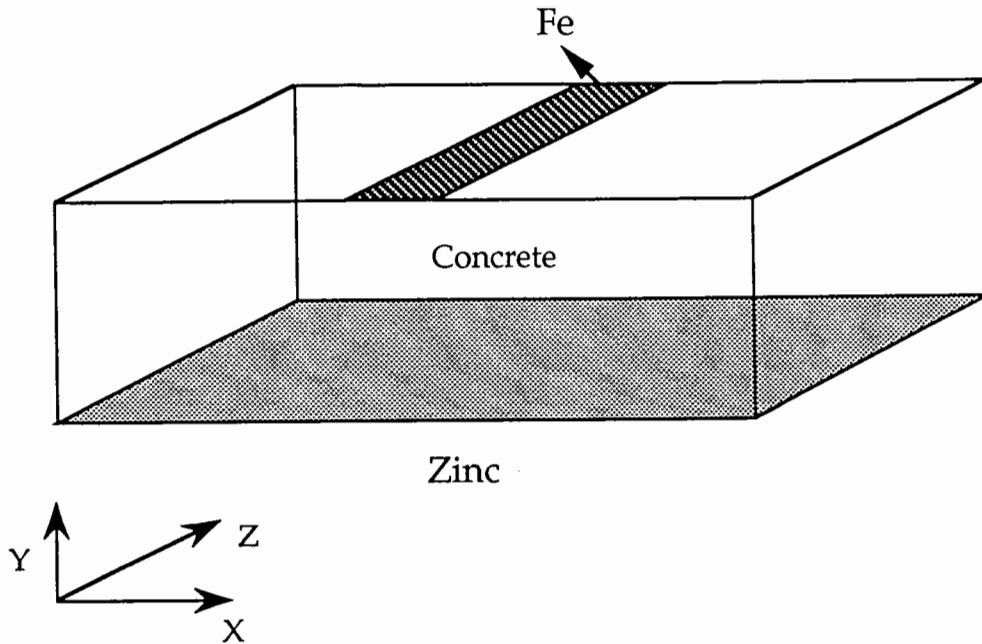
Figure 3.9a Two-Dimensional Geometry of Fe-Concrete-Zn System.

A finite difference code (Appendix E) was developed to solve Laplace's equation, equation 3-4, with boundary conditions described by equation 3-5 at the zinc and equation 3-6 at the rebar. All other boundaries were considered to be insulating:

$$\nabla \Phi \cdot n = 0 \qquad (3\text{-}30)$$

where **n** is a unit vector normal to the insulating surface.

The equations were solved by means of a Gauss-Siedel iterative method with the help of an over-relaxation factor. An interval halving method was used to solve for the nonlinear boundary condition at the rebar. Iteration concluded when potentials of all points in the domain changed less than a given convergence criterion for two successive iterations. The self-consistency of the solutions was tested as follows: the current density at the rebar surface was calculated independently according to Ohm's Law and by the mass transfer - reaction kinetics equation 3-6. These two calculations yielded identical values.

Five different quantities are reported as output of the model:

   (i)   The potential as a function of position in the concrete, $\phi(x,y)$, is
           reported. Actually it is the differences in potential, rather than the
           potentials themselves, that are the significant quantities. However, as a
           point of information, the origins of the absolute potentials are described.

36

In accordance with the boundary condition in equation 3-5, the value of ϕ in the concrete adjacent to the zinc electrode is set to a constant value; this constant is chosen to be $\phi_{Zn} = + 0.678 \text{ V} = - E_{Zn}$ vs. CSE; CSE refers to saturated $Cu/CuSO_4$ electrode. With this value of $\phi_{Zn} = \phi(x,0)$, the value of $\phi(x,y)$ that is reported then corresponds to the potential that would be measured between an ideal CSE at point x,y in the concrete vs. the Zn electrode.

(ii) The total or net current for the cell (i.e., current that would flow in the external circuit) is reported. This value can be converted to an "average current density" using either the surface area of the rebar in the model (0.635 cm^2) or the surface area of the zinc electrode in the model (15.24 cm^2), whichever is appropriate.

(iii) The "average rebar potential" is reported. Actually, this value is the arithmetic average of each of the rebar-concrete interfacial potential differences at each of the nodes in the model. The average is plotted (instead of individual space-dependent values) since the size of the reference electrodes in actual experiments (approximately 1.5 cm) is about the size of the rebar, and the "average potential" is an approximation of the value that would actually be determined experimentally.

(iv) The difference between the rebar-concrete interfacial potential differences at the "centerline" and "edge" of the rebar, as defined in Figure 3.9b, is reported.
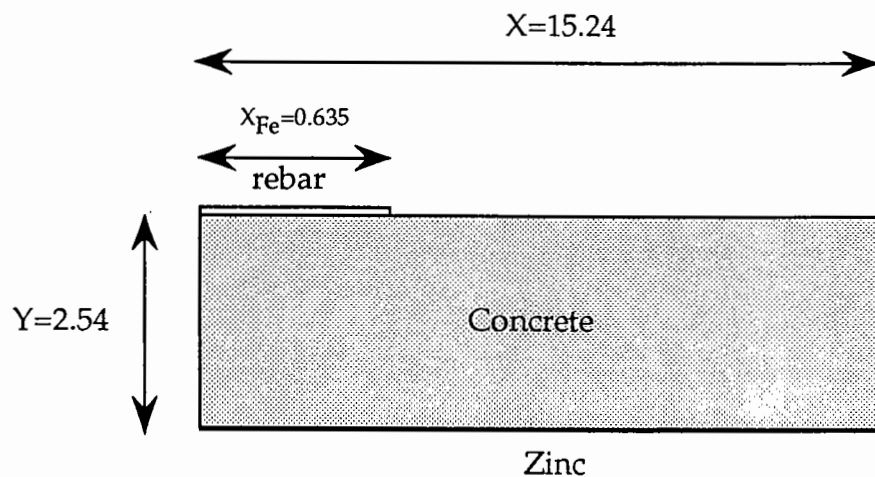
Figure 3.9b Schematic of Two-Dimensional Fe-Concrete-Zn System, Dimensions in cm.

37

(v)   The difference between the percentage saturation of oxygen at the centerline and at the edge of the rebar surface is reported. The saturation value was calculated for water in equilibrium with atmospheric oxygen. These values are used to calculate the polarization decay potentials of the rebar-concrete interface.

3.4.2 EQUIPOTENTIAL MAPS

Maps were drawn to show lines of equipotential in an X-Y cross-section of the concrete that was shown in Figure 3.9b. Calculations were made for three values of concrete thickness, L, 0.5, 1, 2 in (12.5, 25, 50 mm) and three values of E_{appl} (0, -1, -2 V), (for a total of nine cases) with all other parameters at the base-case values in Table 3.1. Results are summarized in Table 3.3 and discussed in more detail below. For each of the nine cases, the maps are shown in Figures 3.10 - 3.13.

Equipotential lines at an applied potential of -1.0 V for the three cover thicknesses are shown in Figure 3.10. For all three cover thicknesses, the greatest gradients in electric potential, and hence the greatest current densities, lie directly between the Fe and the Zn electrodes. This result suggests that the effective area of zinc as an anode is considerably less than the entire area of sprayed zinc, and that the anode will be preferentially consumed directly opposite the iron. **Consequently, calculations of anode life should be based on actual local current densities at the zinc anode rather than the average current density.** It should be borne in mind that relaxation of the simplistic model for oxygen transport (oxygen transport occurs only in the volume of concrete between Fe and its projection on the Zn, Section 3.2.4) could influence the appearance of the potential maps; this subject should be given attention in future studies.

Equipotential lines at a cover thickness of 25 mm. and the three values of E_{appl} are shown in Figure 3.11. As seen in the figure, the potential maps at E_{appl} = -1 V and -2 V (Figures 3.11b and 3.11c) are quite similar, and the values in these two maps are more negative than those in the map at E_{appl} = 0 V (Figure 3.11a), as would be expected. The similarity of the maps at E_{appl} = -1 V and -2 V is explained by the fact that the overall currents are limited by O_2 transport in both of these cases; the mass transport limitation results in similar currents (Table 3.3) and similar IR potential drop through the concrete. Furthermore, as shown in Table 3.3, at E_{appl} = 0 V the iron-concrete interfacial potential difference varies by 7 mV from the centerline to the edge, while at the limiting current (E_{appl} = - 1 and - 2 V) it varies by 100 mV.

38

Table 3.3 Calculated Values for Two-Dimensional Simulation

Concrete Thickness mm	E_{appl} V	I^a mA	"Average" E_{Fe}^b V vs $Cu/CuSO_4$	ΔE_{Fe}^c mV
12.7	0	0.20	-0.65	8
	-1	4.54	-0.95	98
	-2	7.94	-1.39	324
25.4	0	0.18	-0.64	7
	-1	2.24	-1.17	99
	-2	2.27	-2.16	102
50.8	0	0.15	-0.63	7
	-1	0.87	-1.42	41
	-2	0.87	-2.42	41

[a]   Current in the external circuit.
[b]   Average of E_{Fe} calculated at each of the nodes.
[c] E_{Fe}(centerline of rebar) - E_{Fe}(edge of rebar).
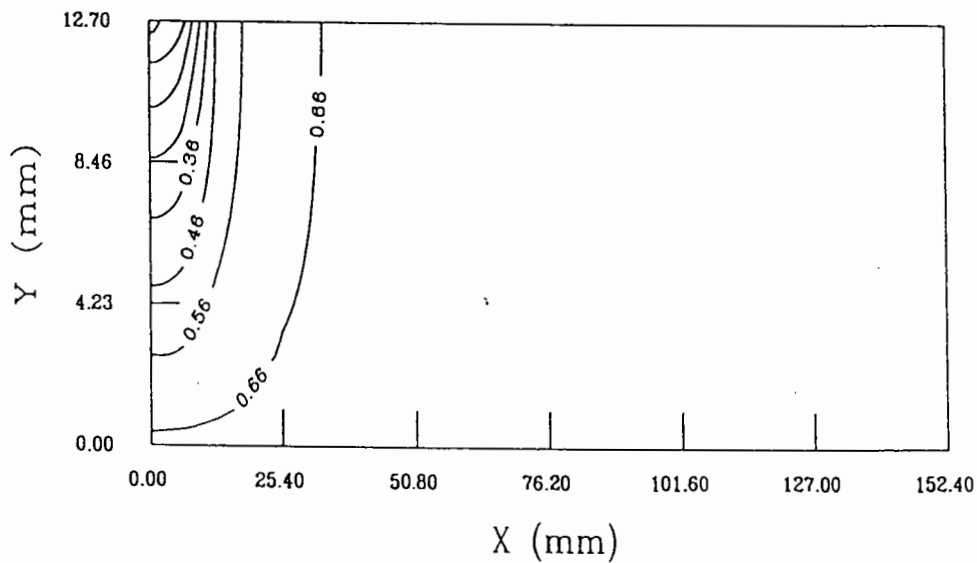
Figure 3.10a Equipotential Lines at an Applied Potential of -1 V and a Cover Thickness of 12 mm.
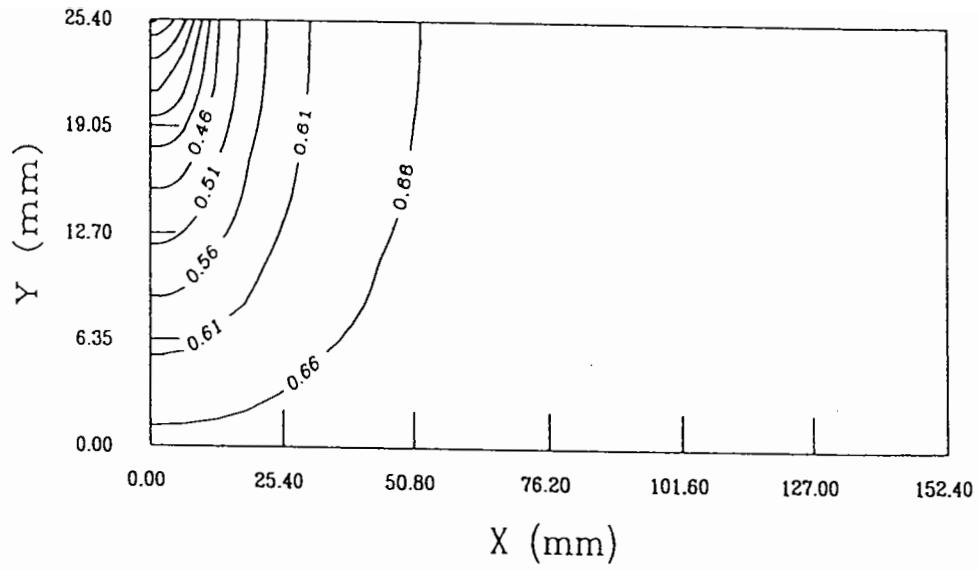
Figure 3.10b Equipotential Lines at an Applied Potential of -1 V and a Cover Thickness of 25 mm.
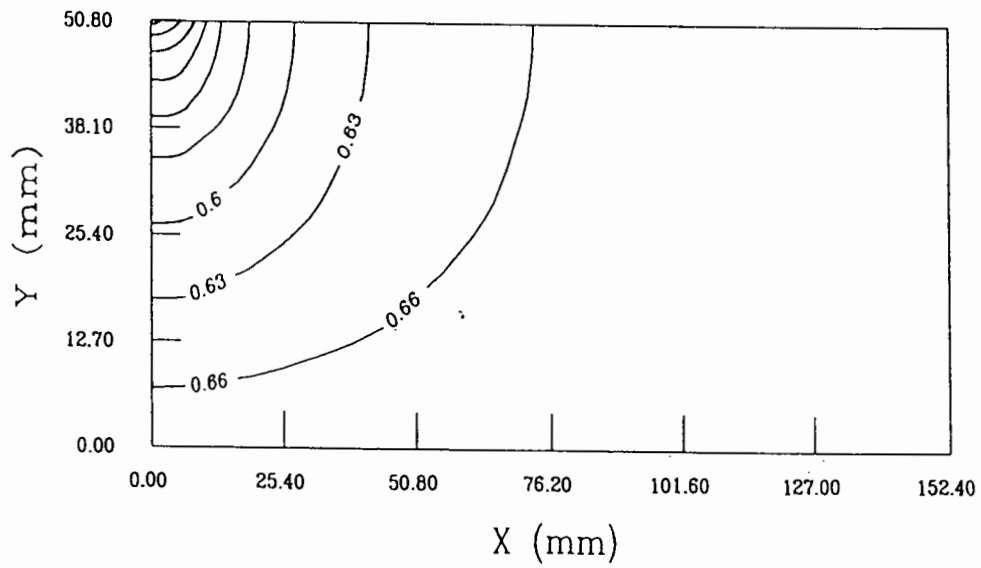
Figure 3.10c Equipotential Lines at an Applied Potential of -1 V and a Cover Thickness of 50 mm.
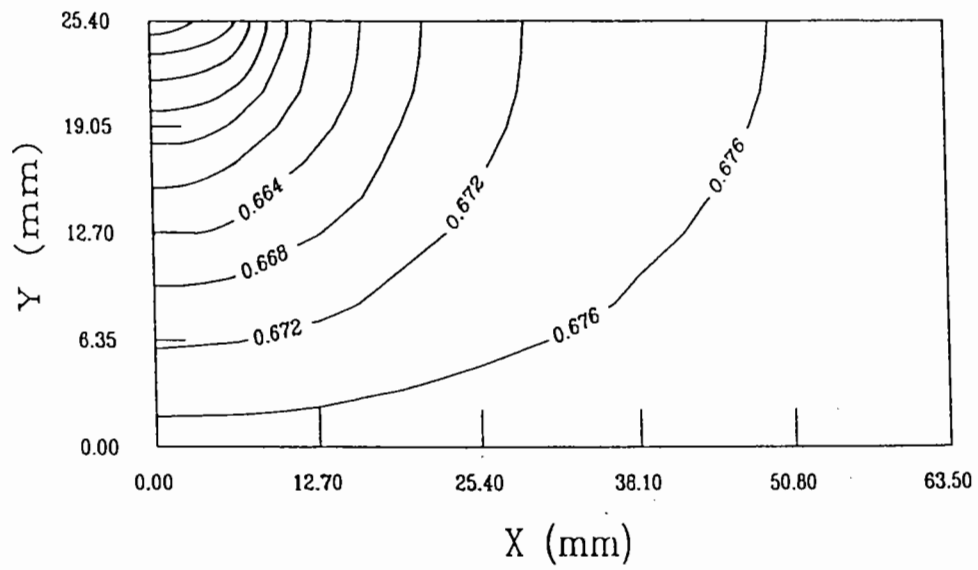
Figure 3.11a Equipotential Lines at an Applied Potential of 0 V and a Cover Thickness of 25 mm.
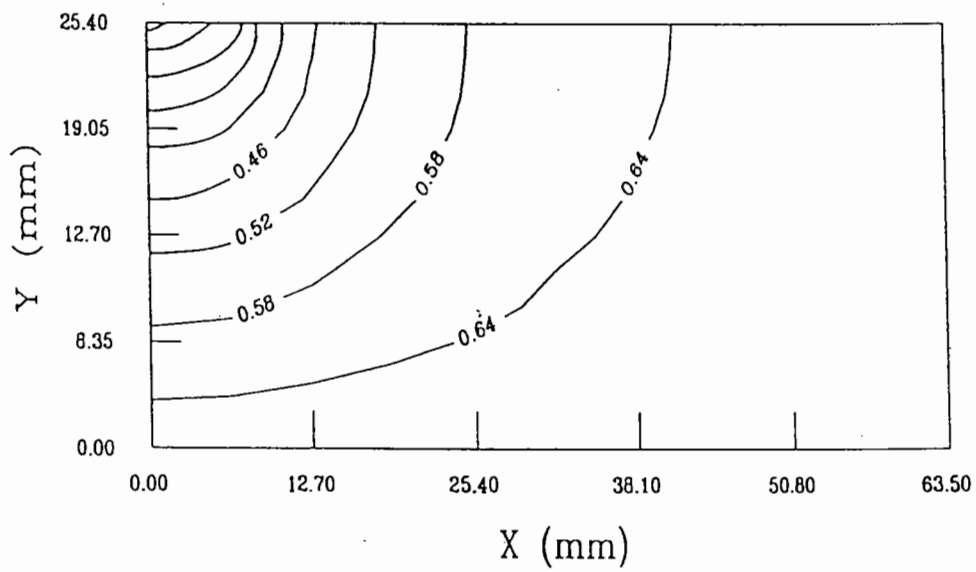
Figure 3.11b Equipotential Lines at an Applied Potential of -1 V and a Cover Thickness of 25 mm.

41
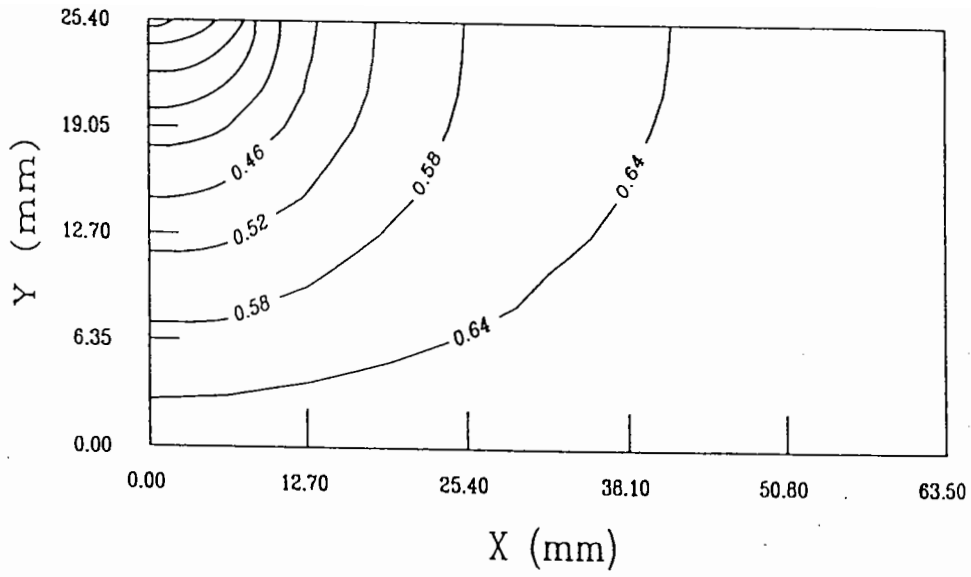
Figure 3.11c Equipotential Lines at an Applied Potential of -2 V and a Cover Thickness of 25 mm.
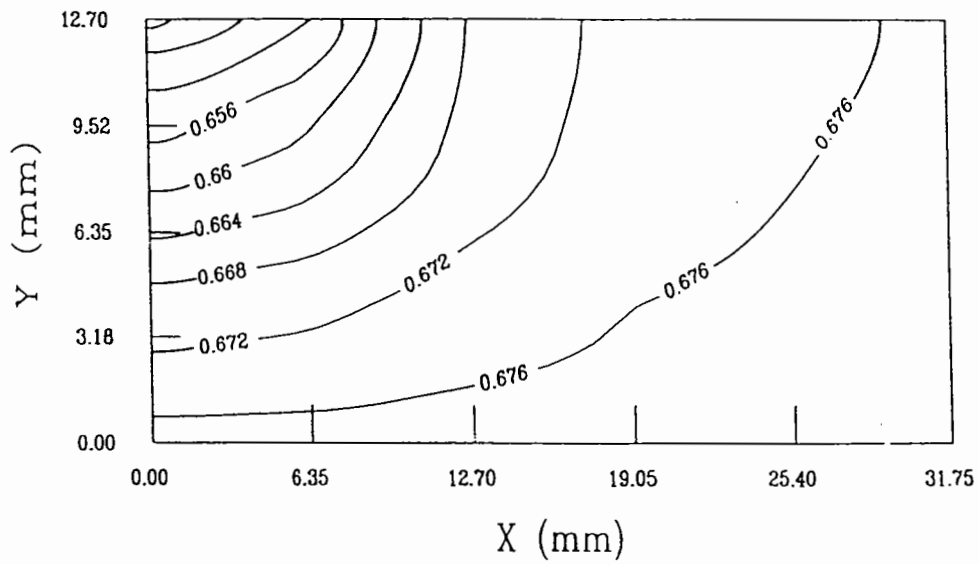
Figure 3.12a Equipotential Lines at an Applied Potential of 0 V and a Cover Thickness of 12 mm.
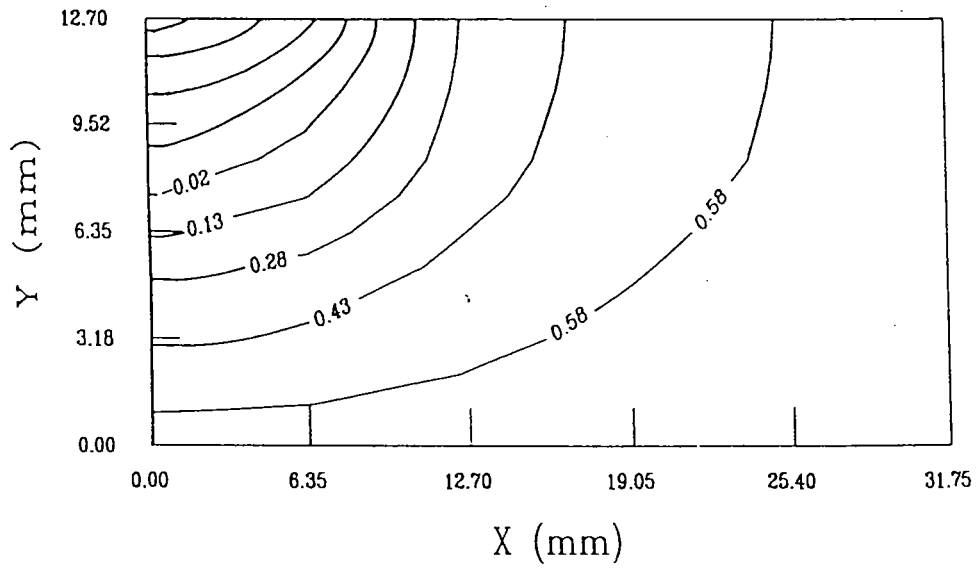
Figure 3.12b Equipotential Lines at an Applied Potential of -2 V and a Cover Thickness of 12 mm.
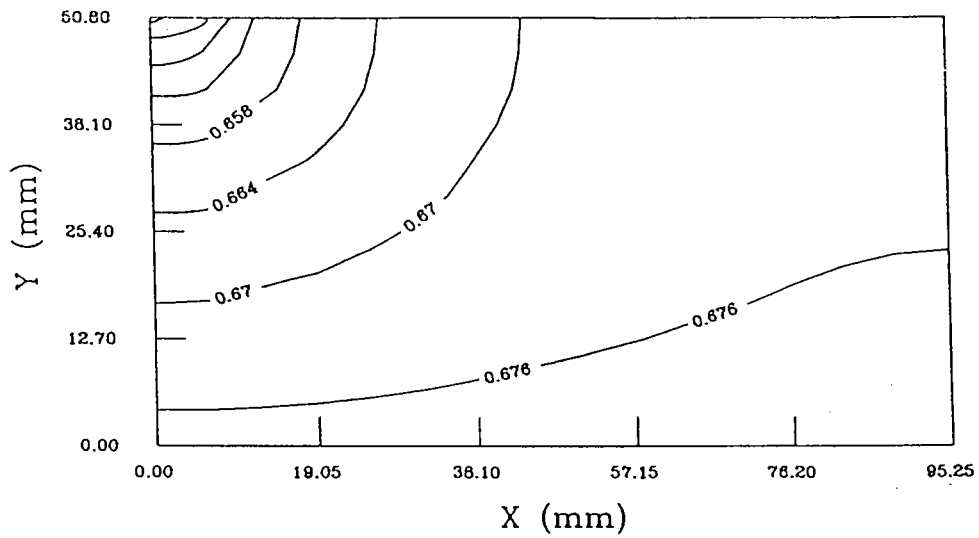
Figure 3.13a Equipotential Lines at an Applied Potential of 0 V and a Cover Thickness of 50 mm.

43
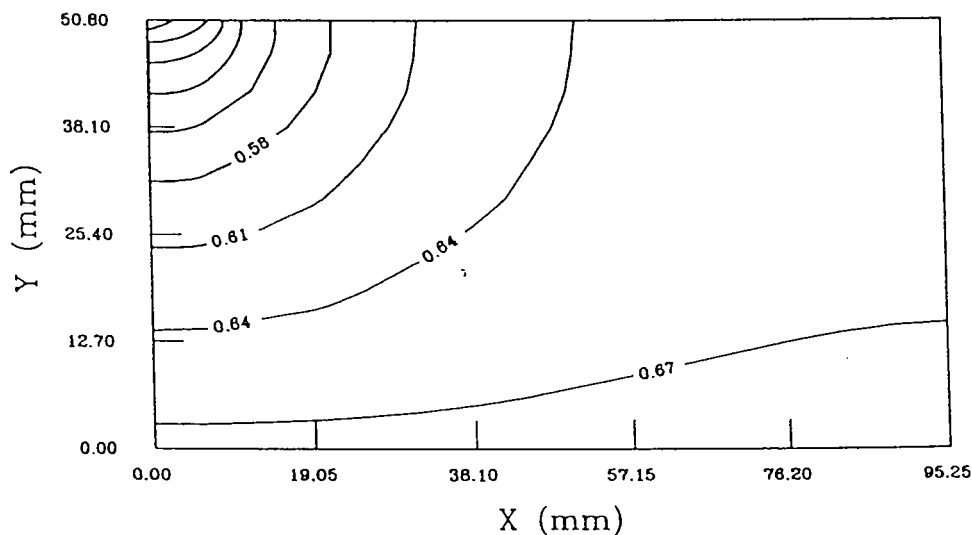
Figure 3.13b Equipotential Lines at an Applied Potential of -2 V and a Cover Thickness of 50 mm.

Equipotential lines for the remaining cases (cover thicknesses of 12 mm. and 25 mm., at E_{appl} = 0 and -2 V) are shown in Figures 3.12 and 3.13. Note that the scales are different. The total current, the rebar potential and the difference in E_{Fe} between the centerline and the edge are shown in Table 3.3. As the cover thickness decreases to 0.5 in, there is more oxygen available and the current increases. In this case, there is a difference between -2 V and -1 V applied potential. Accordingly, the difference in the potential between the centerline and the edge exceeds 300 mV. Thicker concrete cover shows the opposite trend.

In all cases, the potential at the edge of the rebar is more negative than that of the centerline suggesting the centerline is less protected. When the CP circuit is opened the rebar relaxes to a more uniform value, E_{corr}. **Therefore, the reference electrode should be located as close to the centerline of the rebar as possible.** In extreme cases, protection at the centerline may coincide with hydrogen evolution at the edge.

3.4.3 EFFECT OF PORE SATURATION

The degree of pore saturation effects the cathodic protection system both through the electrical resistivity of the concrete and through the resistance to mass transport of oxygen to the iron electrode. Since the degree of pore saturation can exhibit large

44

variations, a study on the effect of pore saturation on the system response was performed. The results are shown in Figures 3.14 - 3.17.

The total current as a function of pore saturation at E_{appl} of 0, -1, and -2 V is shown in Figure 3.14. At E_{appl} = 0 V, the current is small and increases with pore saturation. In this case, the applied potential is too small to deplete oxygen at the rebar and the bulk resistivity of the concrete controls the current. Since the resistivity decreases with pore saturation, the current increases. The other two cases of applied potential exhibit much larger currents (maximum 4 mA) and go through a maximum with respect to pore saturation. At low pore saturation resistivity controls current. At high pore saturation, the availability of oxygen limits the current. In fact, above 60% PS, the -1 and -2 V curves coincide as mass transfer resistance completely dominate electrode kinetics. The current peaks when there is a tradeoff between low resistivity and high oxygen availability for a given reaction rate. This maximum occurs at a lower PS for an applied potential of -2 V, since more oxygen is needed for the faster reaction kinetics.
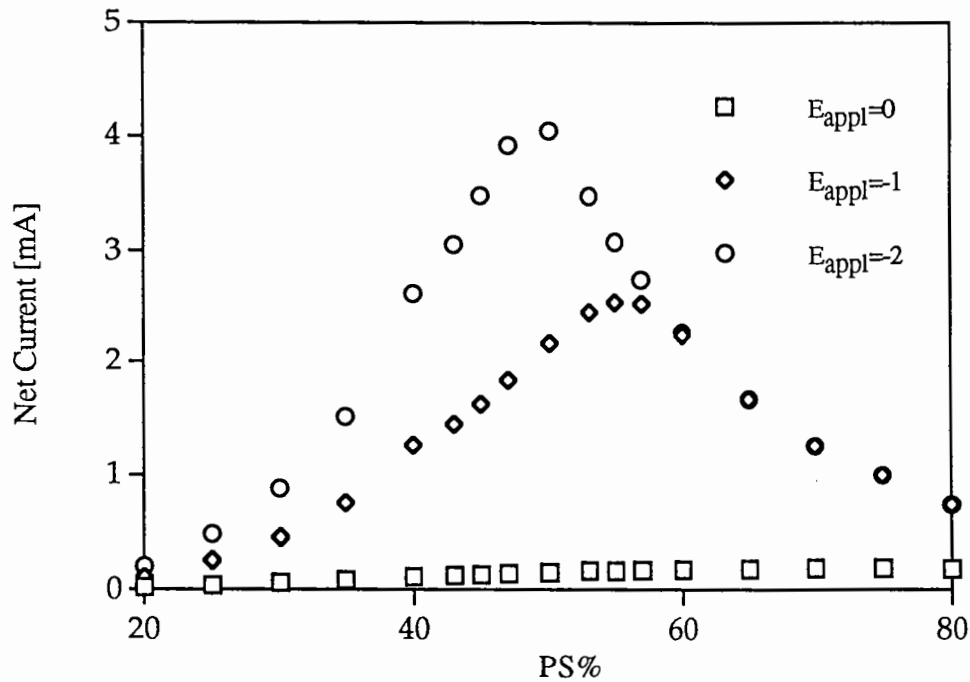
Figure 3.14 Net Current vs. Pore Saturation for a Concrete Cover of 25 mm.

The rebar potential (E_{Fe} vs. saturated Cu/CuSO$_4$) as a function of pore saturation at E_{appl} of 0, -1, and -2 V is shown in Figure 3.15. The sign convention for potential is consistent with the equivalent circuit of Figure 3.3. At high PS, the bulk resistance of the concrete is small compared to the charge transfer resistance at the Fe electrode; then E_{Fe} approaches E_{appl} + E_{Zn} (see equation 3-21). At low PS, the bulk resistance of the concrete is large compared to the charge transfer resistance at the Fe electrode;

then the circuit is effectively opened across the concrete, the rebar potential goes to E_{corr}, and the external current goes to zero.
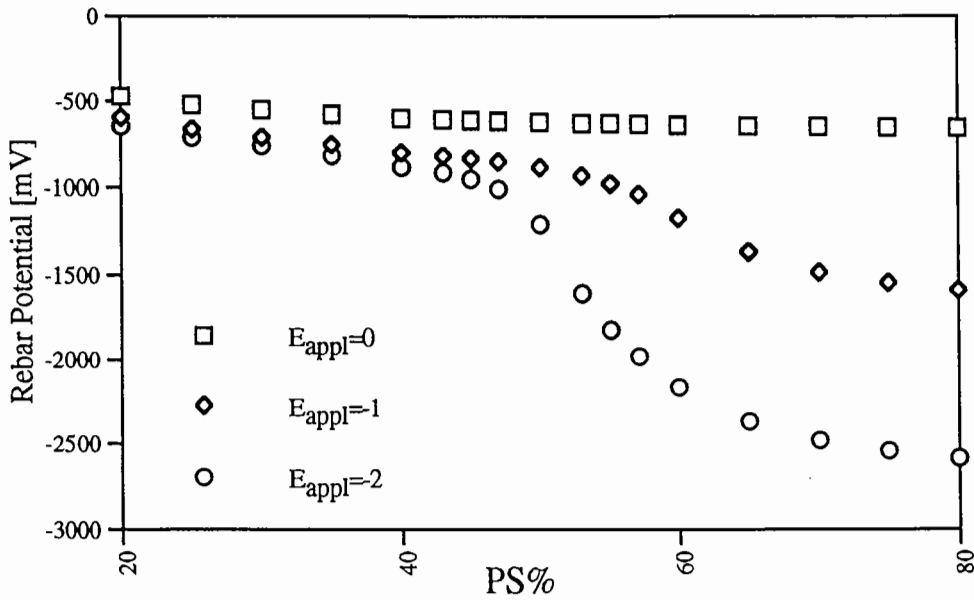
Figure 3.15 Rebar Potential vs. Pore Saturation.

The difference in E_{Fe} between the centerline and the edge of the rebar vs. pore saturation, at E_{appl} of 0, -1, and -2 V, is shown in Figure 3.16. In the case of the maximum current discussed above (an applied potential of -2 V and a PS of 50%), the value of E_{Fe} at the centerline of the rebar is 270 mV more positive than it is at the edge. For most cases with significant protection, the difference in E_{Fe} between the centerline and the edge of the rebar is greater than 50 mV.
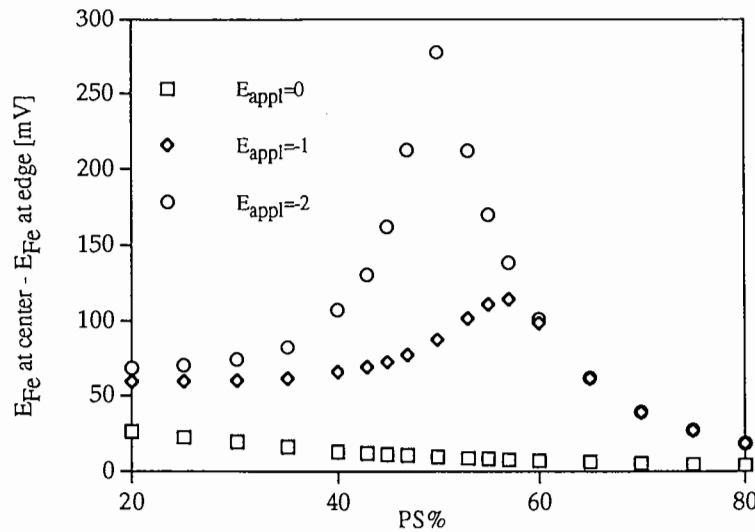
Figure 3.16 Difference in E_{Fe} Between the Centerline and the Edge of the Rebar vs. Pore Saturation.

46

The oxygen concentration at the centerline and at the edge of the rebar vs. pore saturation, at E_{appl} of 0 and -2 V, is shown in Figure 3.17. The criterion for adequacy of protection is the 100- (or 150-) mV polarization decay test. A major component of the polarization decay can be related to the change in oxygen concentration at the rebar surface, according to the model presented in Section 3.3.2. From examination of the oxygen concentrations at the edge vs. the centerline of the rebar, polarization decay values for the two locations can be assessed. **At pore saturation above 50%, where all the oxygen is consumed, reference electrode placement is not critical; however from 30-50% PS, placement of the reference electrode can have a large effect on the polarization decay measurement.** For example at a PS of 45%, (using the same analysis as described in the 1-D model) a reference electrode placed on the edge would depolarize by 125 mV, which would be interpreted as adequate protection, while one placed at the centerline would depolarize by only 38 mV.
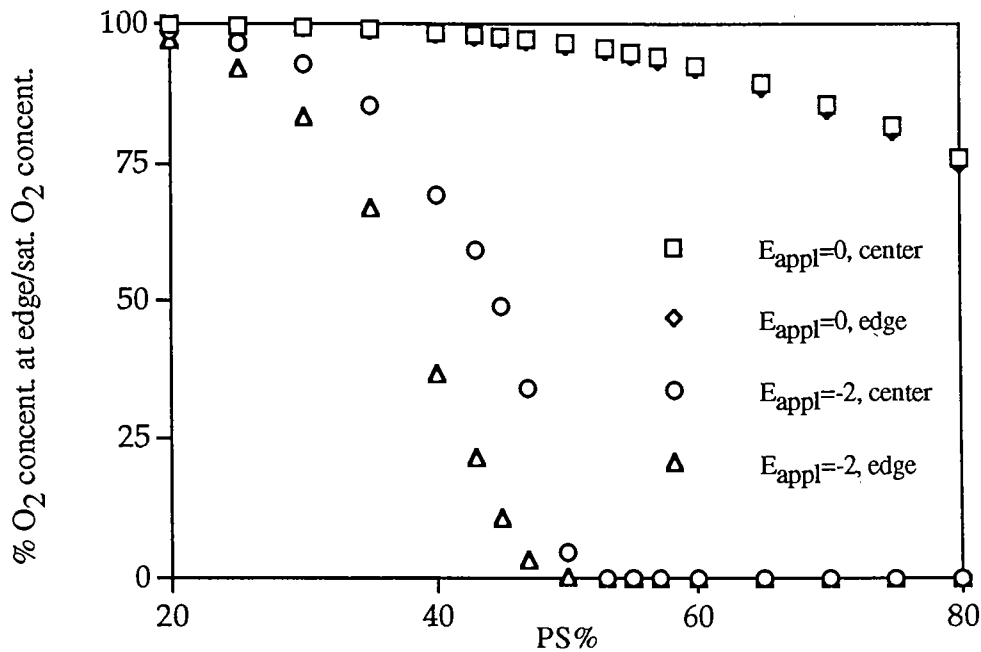
Figure 3.17 Oxygen Concentration at the Centerline of the Rebar and at the Edge vs. Pore Saturation.

This analysis should not be interpreted a complete description of the polarization decay mechanism. Other processes probably contribute to the polarization decay, as discussed in Section 3.3.2. However, care should be taken to place reference electrodes as close as possible to the centerline of the rebar for drier concrete decks.

47

3.4.4 SENSITIVITY ANALYSIS

In this section, the sensitivity of the output of the model to several of the input parameters is evaluated. The parameters evaluated are: (i) the resistivity of the concrete (Figure 3.18); (ii) the oxygen mass transfer coefficient (Figure 3.19); (iii) the oxygen exchange current density (Figure 3.20); and (iv) the Tafel slope for oxygen reduction (Figure 3.21).

Other parameters were considered for the sensitivity analysis, but not incorporated. The equilibrium potential and the exchange current density co-vary, as shown by equation 3-16; thus, for the sensitivity analysis, the former was fixed at its base case value and only the latter was varied. Similarly, the value for oxygen concentration at $y = 0$ is not expected to vary from its base-case value. Finally, the iron kinetics were not incorporated, since they do not contribute to the results discussed in the last two sections, although they are important in determining corrosion rates.

The sensitivity analysis consists of varying the four input parameters from their base case values and plotting: (i) current; (ii) rebar potential; (iii) difference in E_{Fe} between the centerline of the rebar and the edge of the rebar; and (iv) difference in $C_O^{y=L}/C_O^{y=0}$ at the centerline of the rebar and the edge of the rebar. A brief summary of theses sixteen figures (four parameters x four model outputs; Figures 3.18a-d, 3.21a-d) follows, additional information can be gained from inspection of the figures.
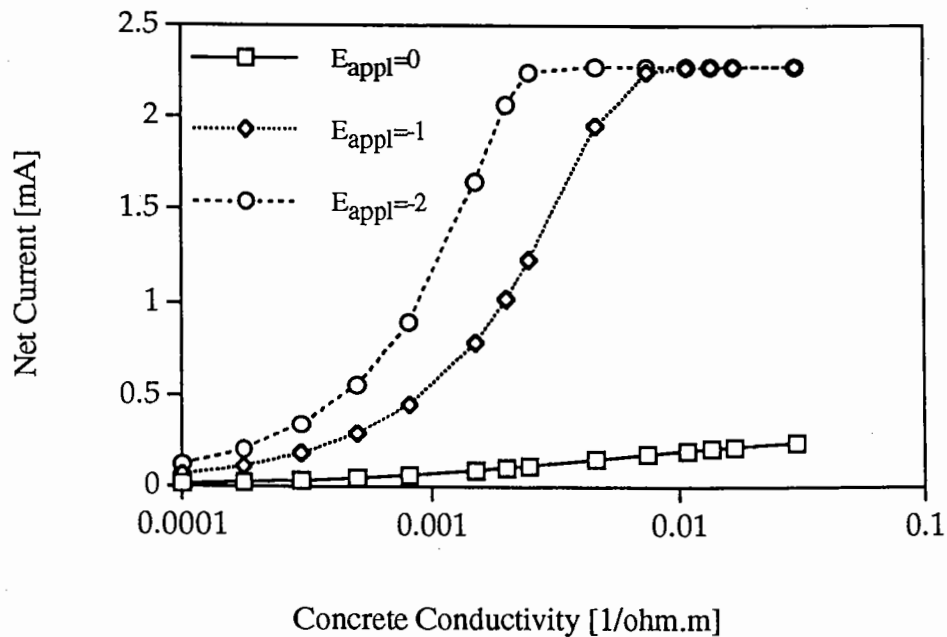
Figure 3.18a Net Current vs. Concrete Conductivity.
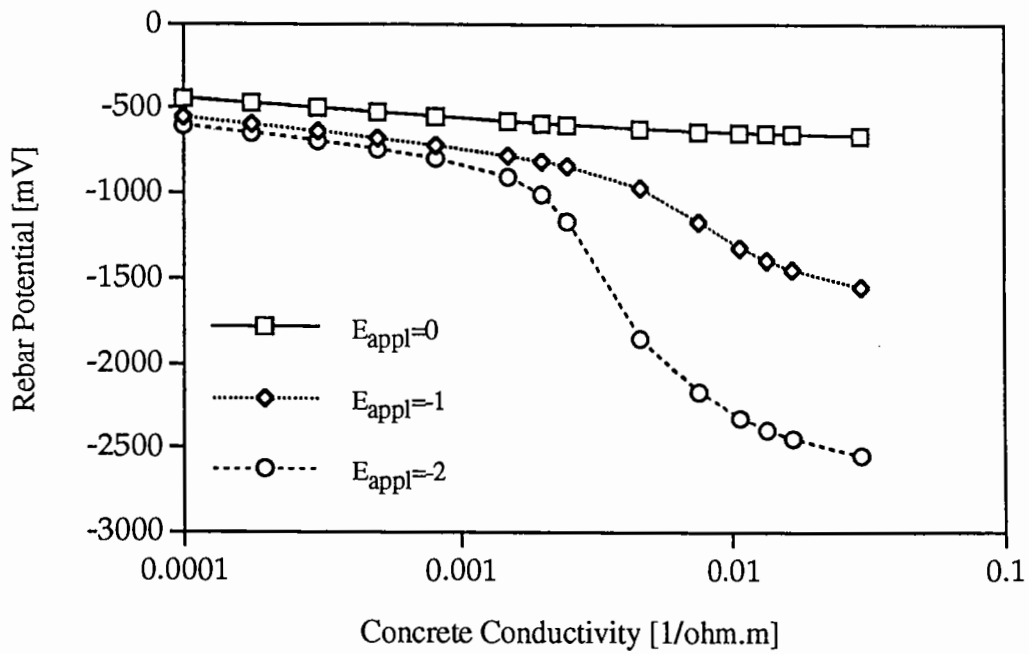
Figure 3.18b Rebar Potential vs. Concrete Conductivity.
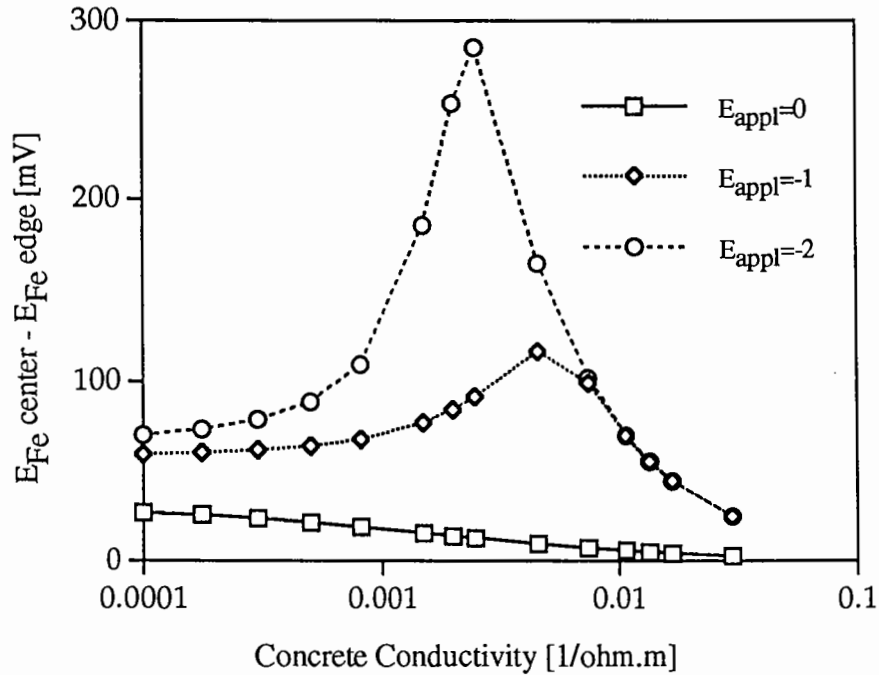
Figure 3.18c Difference in E_{Fe} Between the Centerline of the Rebar and the Edge vs. Concrete Conductivity.

49
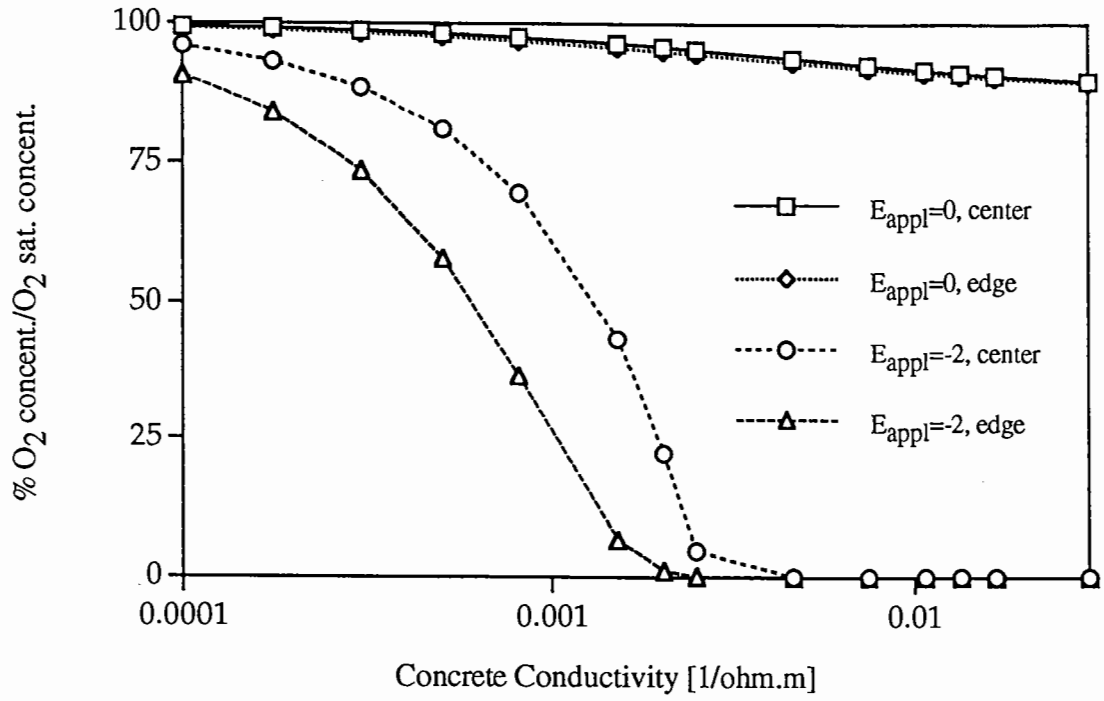
Figure 3.18d Oxygen Concentration at the Centerline of the Rebar and at the Edge vs. Concrete Conductivity.
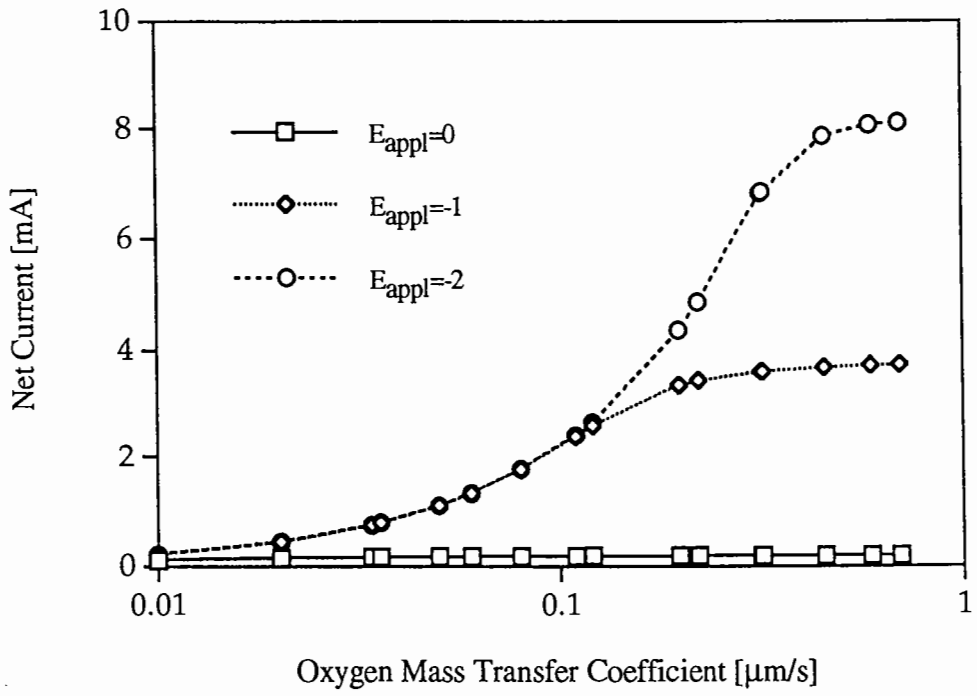
Figure 3.19a Net Current vs. Oxygen Mass Transfer Coefficient.
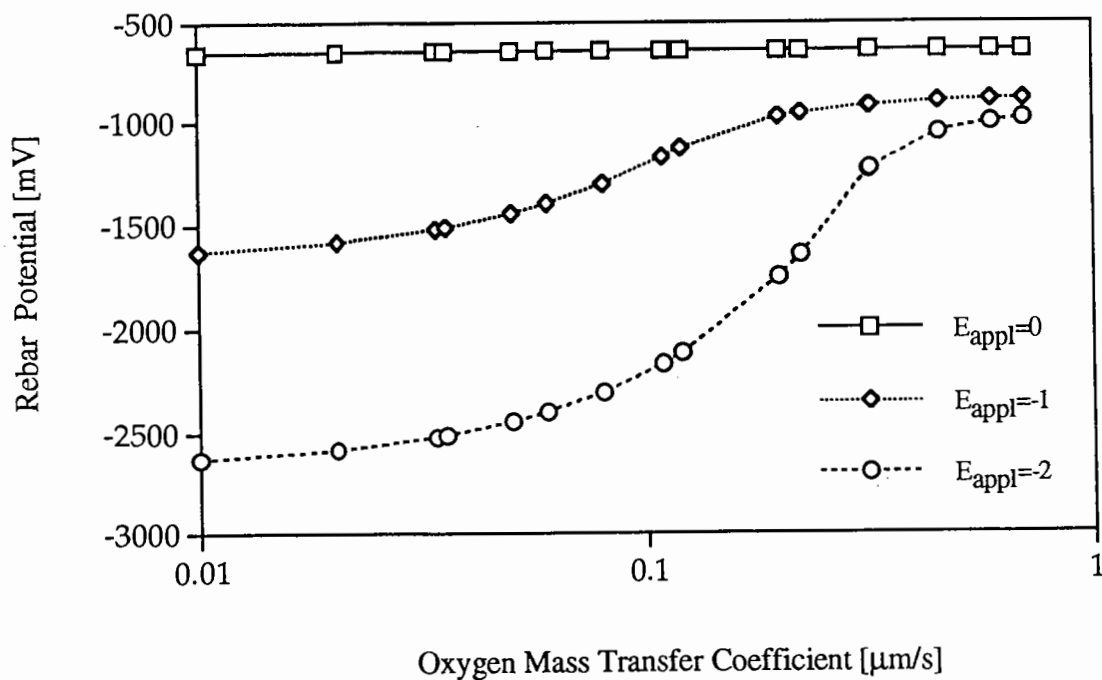
Figure 3.19b Rebar Potential vs. Oxygen Mass Transfer Coefficient.
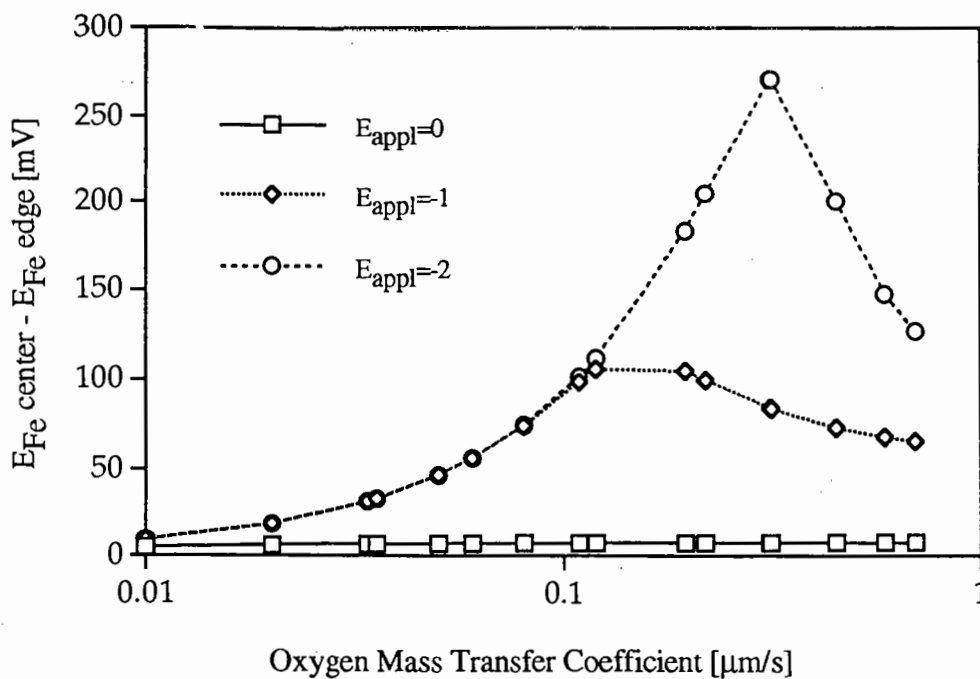
Figure 3.19c Difference in E_{Fe} Between the Centerline of the Rebar and the Edge vs. Oxygen Mass Transfer Coefficient.

51
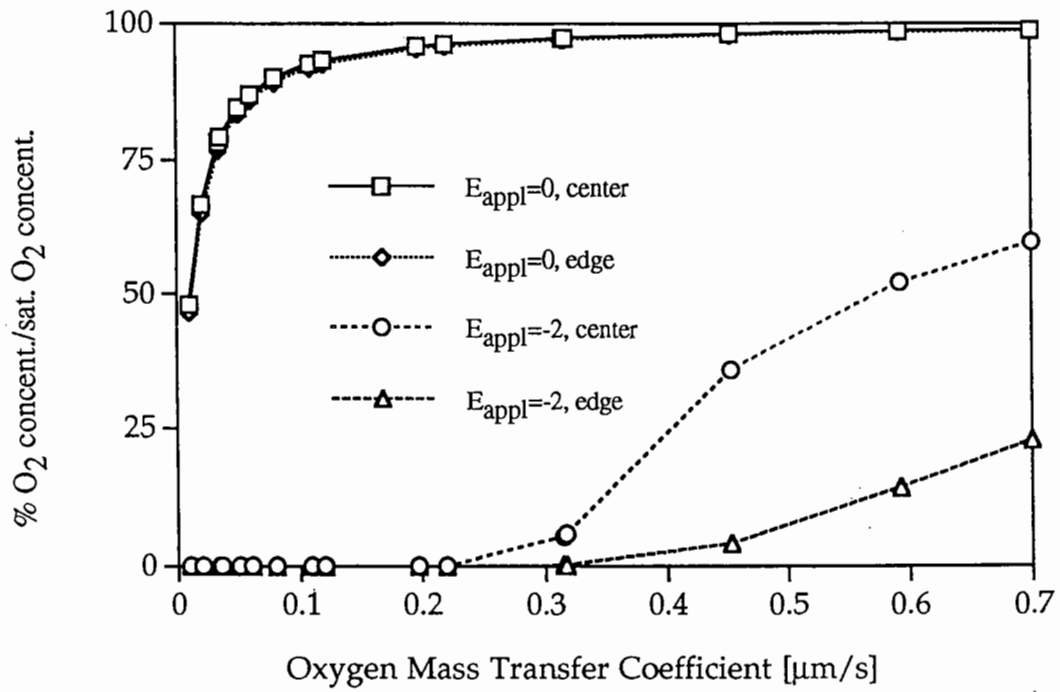
Figure 3.19d Oxygen Concentration at the Centerline of the Rebar and at the Edge vs. Oxygen Mass Transfer Coefficient.
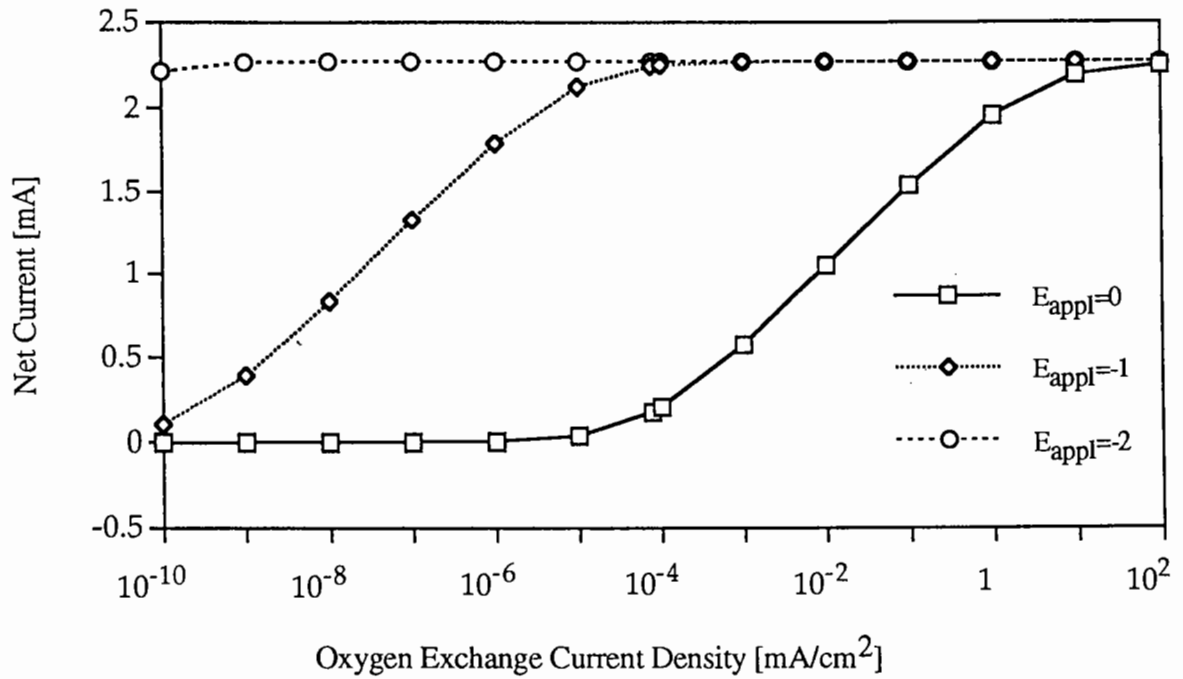
Figure 3.20a Net Current vs. Oxygen Exchange Current Density.

52
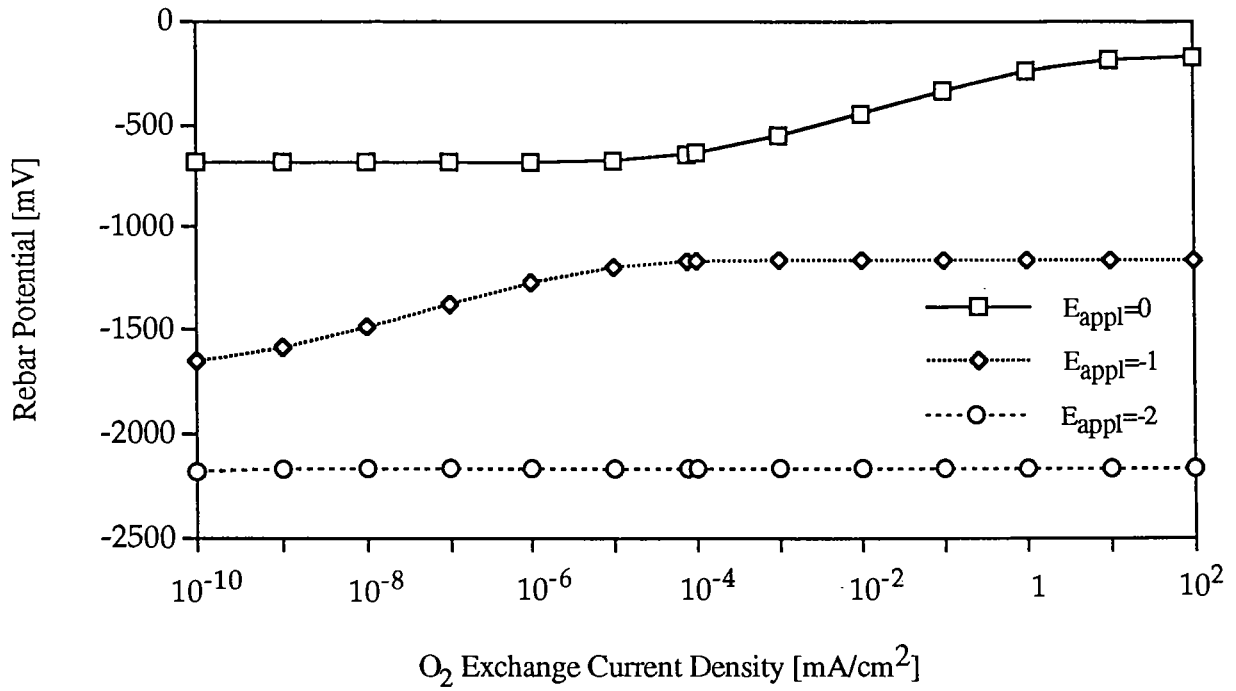
Figure 3.20b Rebar Potential vs. Oxygen Exchange Current Density.
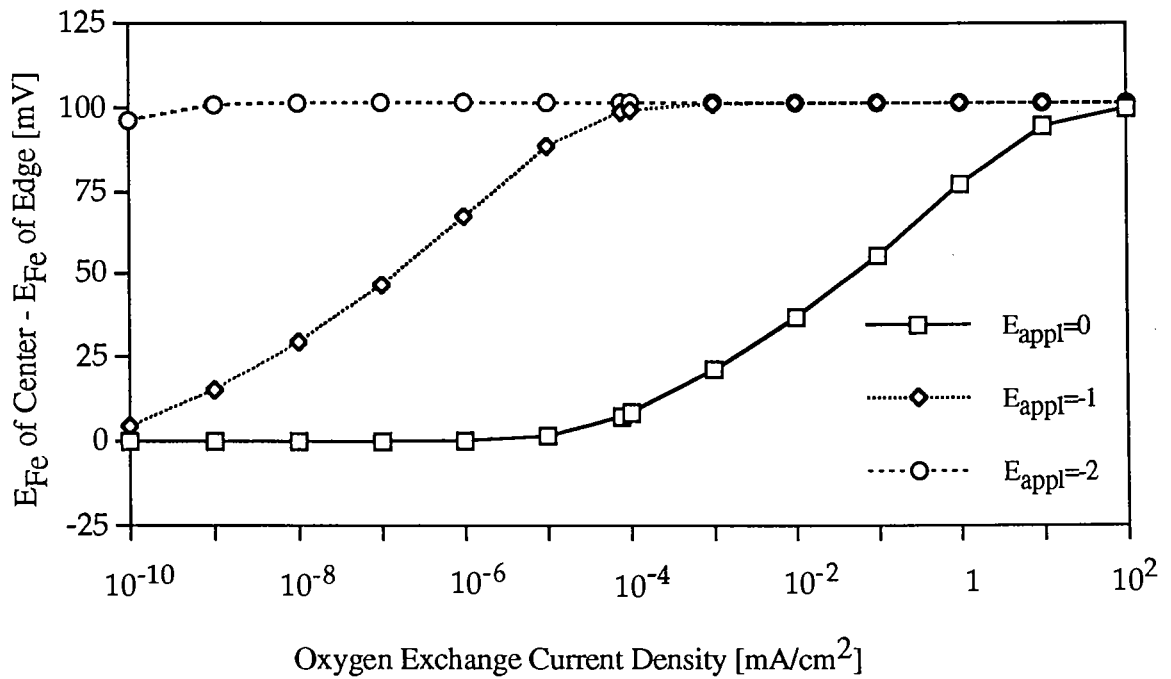
Figure 3.20c Difference in E_{Fe} Between the Centerline of the Rebar and the Edge vs. Oxygen Exchange Current Density.
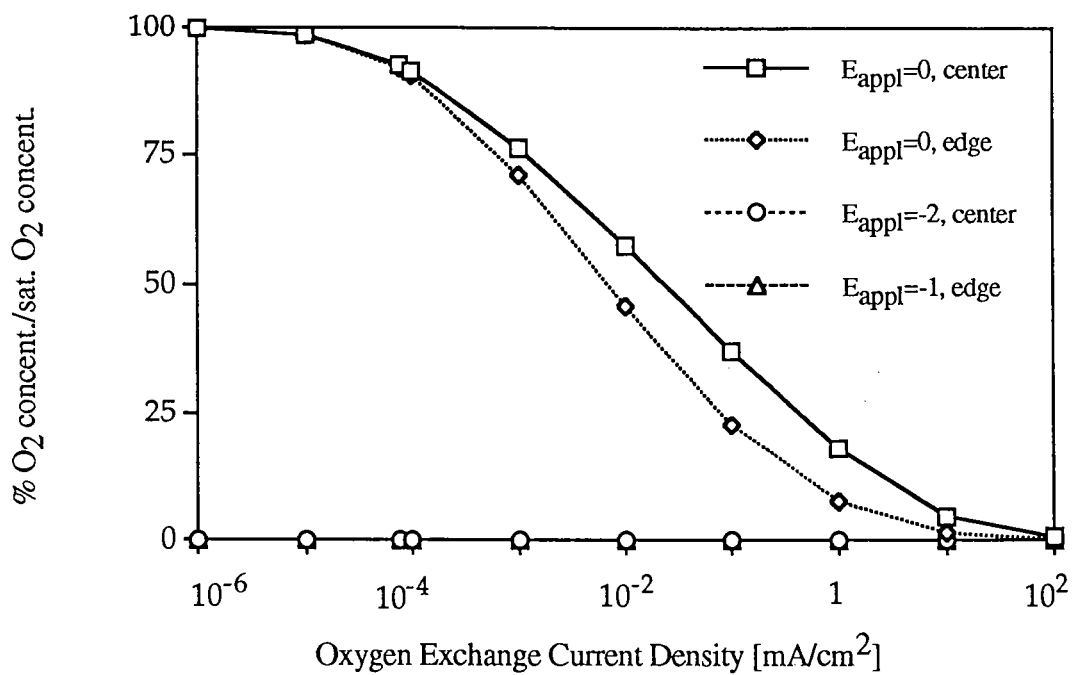
Figure 3.20d Oxygen Concentration at the Centerline of the Rebar and at the Edge vs. Oxygen Exchange Current Density.
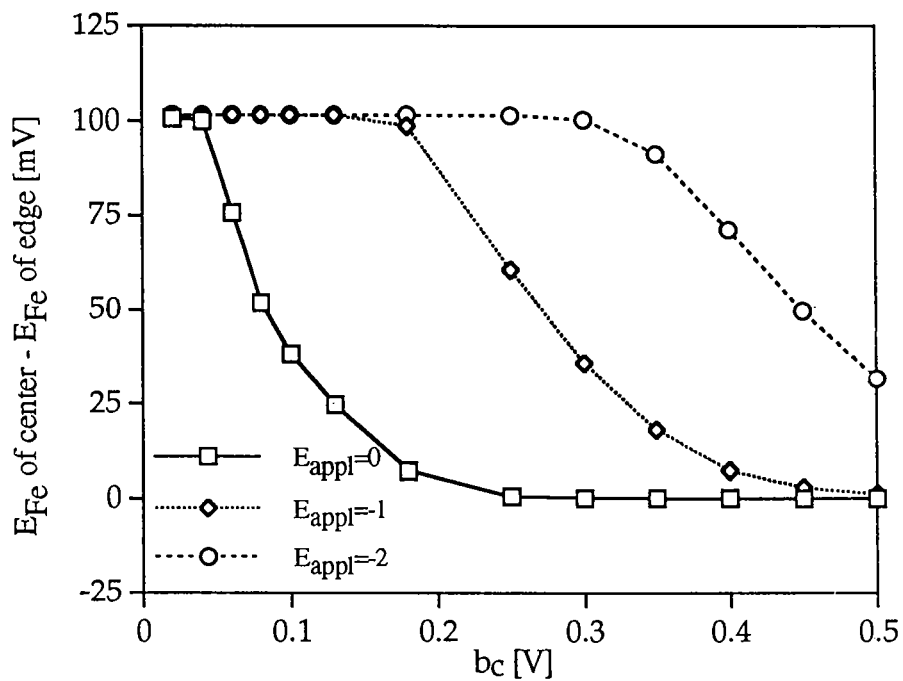
Figure 3.21a Net Current vs. Anodic Tafel Slope.
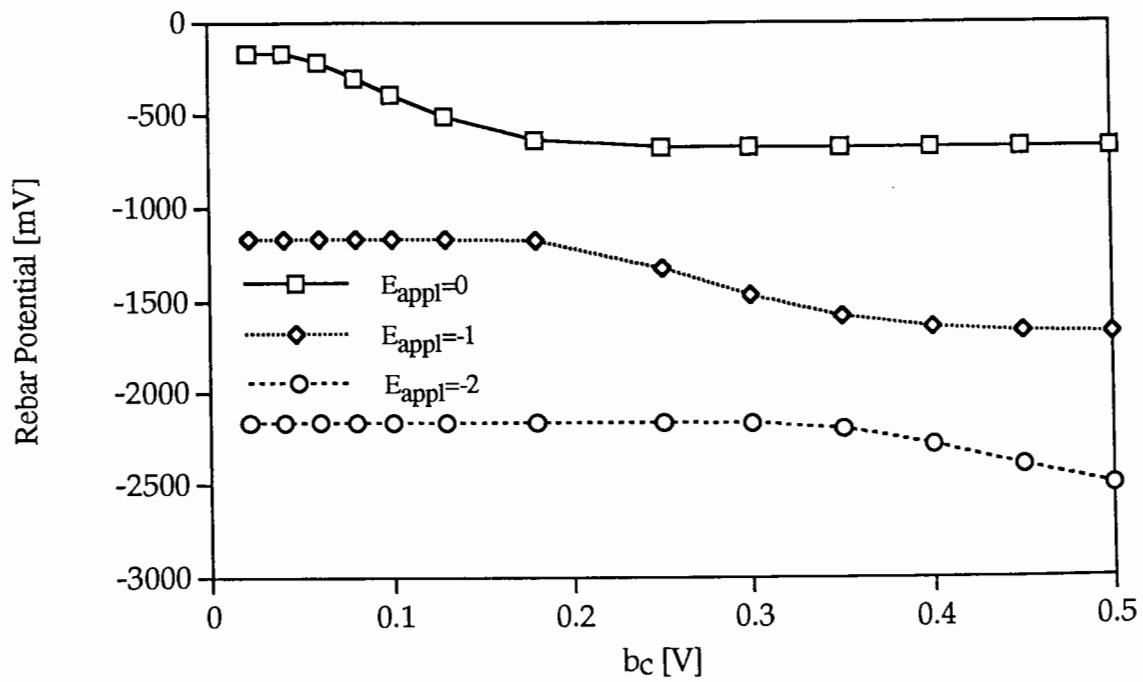
Figure 3.21b Rebar Potential vs. Anodic Tafel Slope.
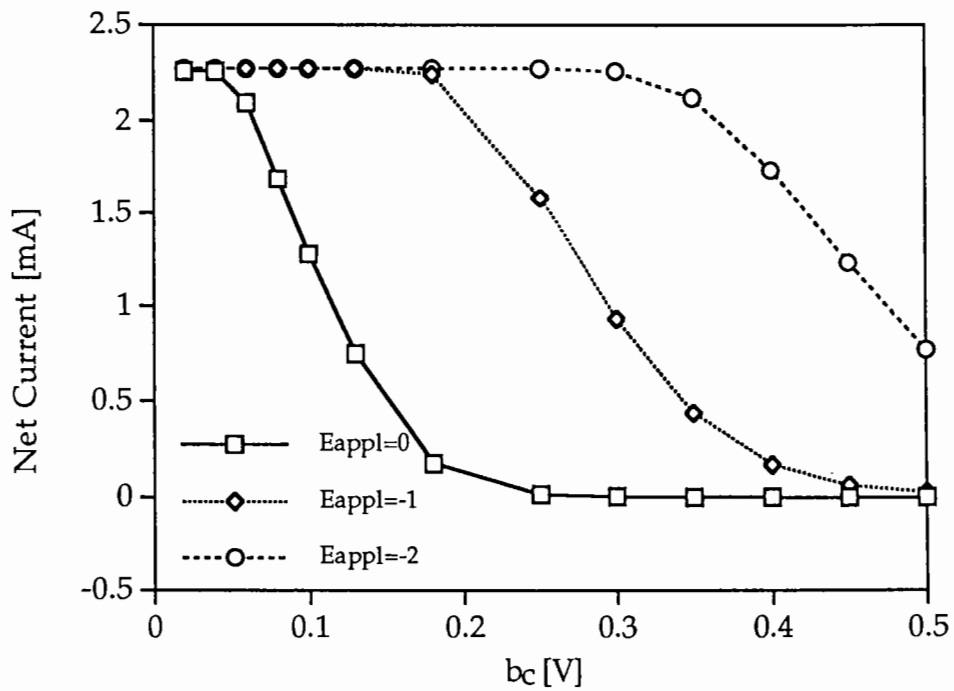
Figure 3.21c Difference in E_{Fe} Between the Centerline of the Rebar and the Edge vs. Aodic Tafel Slope.

55

Figure 3.21d Oxygen Concentration at the Centerline of the Rebar and at the Edge vs. Anodic Tafel Slope.

As Figure 3.18a illustrates, when the resistivity is high (conductivity is low), the system acts as an open circuit and protection is ineffective. At low resistivity all the available oxygen is consumed and the current goes to the limiting current value. The effect of concrete resistivity on rebar potential (Figure 3.18b), the difference in E_{Fe} between the centerline and the edge (Figure 3.18c) is similar to the effect of pore saturation, as discussed in the last section. The behavior of the percentage of oxygen concentration with respect to concrete conductivity for E_{appl} of 0 and -2 V is shown in Figure 3.18d. Again for -2 V and low values of resistivity, the mass transfer resistance of oxygen dominates.

As shown in Figure 3.19, as the oxygen mass transfer coefficient goes to zero, the net current goes to zero. At large mass transfer coefficients, the concentration of oxygen approaches the saturation value. In this case, the intrinsic kinetics (as related to E_{appl}) of oxygen reduction and the IR drop determine the system response. Significant differences in oxygen concentration between the edge and centerline, and corresponding differences in polarization decay potential, occur for mass transfer coefficients greater than 3×10^{-7} m/s.

Figure 3.20a illustrates that the are three regions of behavior for the oxygen exchange current density. At very low values, oxygen reduction is negligible and no net current flows. Of course, corrosion would also occur at slow rates. At high values, the current is limited by oxygen availability. At intermediate values charge transfer

56

resistance controls the current. The higher the applied potential the lower the transition to this intermediate region. In fact, for Eappl of -2 V, an exchange current density as low as 10^{-10} μA cm^{-2} still yields limiting current conditions. The behavior for the difference in E_{Fe} between the centerline and the edge (Figure 3.20c) mirrors the behavior of current. The functionality with Tafel slope (Figure 3.21) is opposite the exchange current density.

3.5 SIMULATION IN THREE DIMENSIONS

Two types of rebar exist in reinforced concrete bridges: king rebar to which the cathodic protection circuit is directly connected, and cross rebar, to which the cathodic protection system is not directly connected. However, the cross rebar is indirectly connected through contact with the king rebar. A concrete block with the surfaces of these rebars on one side and sprayed zinc on the other side is shown in Figure 3.22.

The Oregon Department of Transportation ensures low bar-to-bar resistance by measuring the resistance between the king bar and the cross rebar with a four-probe AC resistance meter. The four-probe technique eliminates probe contact resistance from the measurement by separating the current leads from the voltage sensing leads. Bars with a resistance to the king bar of greater than one ohm are welded to the nearest bar with less than one ohm resistance to the king bar to ensure low resistance rebar junctions.
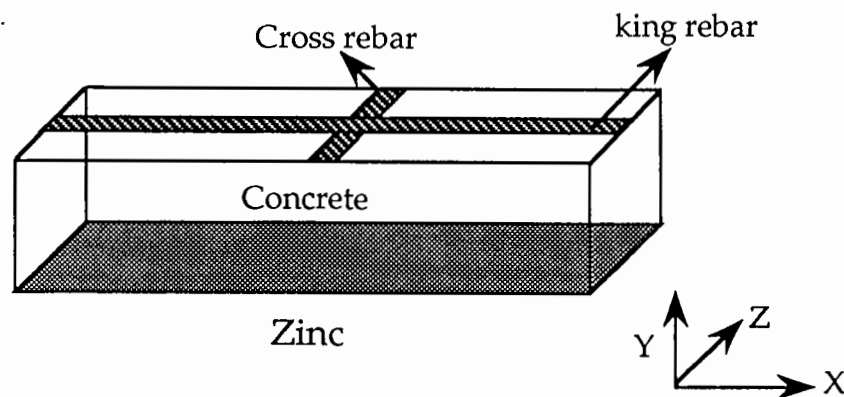
Figure 3.22. Schematic of a Three-Dimensional Geometry

57

A three-dimensional model was developed to determine the adequacy of protection of the cross rebar. The potential applied to the cross bar was obtained by subtracting the ohmic potential drop between the bars from the potential applied to the king rebar. For bar to bar resistance of 1 Ω or less, the potential drop between the bars was only a few millivolts. This potential drop was negligible compared to potential drop across the rebar (from centerline to the edge) for the cases studied in two-dimensional geometry. This result suggested that bar to bar resistance of 1 Ω is insignificant in cathodic protection.

However, another three-dimensional effect, which might have a very significant impact on the efficacy of cathodic protection, was beyond the scope of this study and was not investigated. In the two dimensional model, the cathodic protection cell was represented as a three layer sandwich of zinc-concrete-iron; in actuality, the cell consists of four layers: zinc-concrete-iron-*concrete*; that is, the "back" side of the rebar and the last layer of concrete has been neglected in the two dimensional model. Control of the potential and protection of the rebar at this "back" iron-concrete interface is certain to be a difficult task, and it cannot be simulated with a simple two dimensional model. Modification of the geometry for a better representation of this problem is recommended.

4.0 LABORATORY TESTS OF REFERENCE ELECTRODES

4.1 INTRODUCTION

The long-range goal of this part of the study was to test reference electrodes for their suitability in circuits with which cathodic protection systems are controlled. The current standard for control of cathodic protection systems is the 100-mV 4-hour Polarization decay criterion; thus, the primary objective of this study was to determine the *suitability of reference electrodes in the 100-mV 4-hour Polarization decay test*. A secondary objective of the laboratory study was to evaluate the *suitability of the reference electrodes for continuous monitoring* of the cathodic protection process. As described in Section 3.2.7, cathodic protection can be applied in one of three modes: (i) constant applied current; (ii) constant applied voltage between Fe and Zn; and (iii) constant potential at the Fe-concrete interface with a 3-electrode potentiostat. The third electrode allows the potential at the *Fe-concrete interface* to be controlled, not just *overall voltage between Fe and Zn* (i.e., the 3-electrode potentiostat corrects for the ohmic potential drop across the concrete). The 3-electrode potentiostat mode provides the best control for cathodic protection *if* the reference electrode continuously operates properly. Thus, the secondary objective was to determine the suitability of reference electrodes for continuous monitoring.

Two characteristics that are important for the reference electrode are ruggedness and reproducibility. These two characteristics are difficult to attain in the same electrode. For example, the silver - silver chloride (Ag/AgCl) reference electrode is extremely reproducible when it is used under controlled laboratory conditions and the liquid junction is carefully maintained. Furthermore, its potential can be understood from first principles; thus, the effects of various environmental factors (such as pH, O_2, etc.) on electrode response can be predicted. However, careful maintenance of the liquid junction is virtually impossible under field conditions. In contrast, the graphite reference electrode requires virtually no maintenance, but it is not recognized as a particularly reproducible electrode, its response is not easily understood from first principles, and thus one cannot be sure how it will be affected by various environmental factors (e.g., pH, O_2, temperature, water activity, etc.).

This study was done in two steps:

1.   Characterization of a system in which reference electrodes could be tested.

         The first step was to use the Ag/AgCl electrode as a "best case scenario" to verify the performance of the testing procedure.

59

2. Comparison of the graphite electrodes and Ag/AgCl electrodes.

The second step was to evaluate how graphite electrodes responded in comparison to Ag/AgCl electrodes. Furthermore, the reproducibilities of the types of graphite electrodes were compared, with and without pre-conditioning. These tests were carried out under ambient laboratory conditions (21 - 23 °C, 50 - 80% RH).

Two additional steps would be useful to complete the characterization of reference electrodes used in cathodic protection:

3. Effect of environmental variables (temperature, water content of the concrete) on electrode response.

Another step of this procedure would be to evaluate the performance of the electrode under controlled variations in environmental conditions (e.g., temperature 0 - 30 °C, relative humidity 40 - 100%). For the graphite electrode, of which the response mechanism in concrete is unknown, this step is important. Other environmental variables such as O_2 content and pH value could play a role as well. The results of this experimental portion of the study should be considered to apply only to a fixed set of environmental conditions until this step is completed.

4. Mechanism of response of the graphite electrode.

The chemical species that poise (fix) the potential of the graphite electrode in concrete are unknown. It would be useful to determine the reactions that are responsible for poising the electrode in order to predict the sensitivity of the electrode to environmental variables. These last two steps were not completed as part of this study.

4.2 MATERIALS AND METHODS

The goal was to create a well characterized environment within which electrodes could be tested. A rectangular concrete block was cast and incorporated in a sandwich composed of an Fe plate, a sponged soaked 0.1 M NaCl, the concrete block, another sponge soaked in 0.1 M NaCl, and a Zn plate, as shown in Figure 4.1. The purpose of the sponges was to reduce the charge transfer resistance at the metal plates to the point that it was negligible compared to the ohmic resistance of the concrete. Then, if the concrete block was homogeneous in electrical conductivity, the performance of reference electrodes could be tested by two methods: (i) if a constant potential is maintained between Fe and Zn, the potential between the reference electrode and the Fe plate should vary linearly with distance from the Fe plate; (ii) if the reference electrode is maintained at a fixed location in or on the concrete, the potential difference between the reference electrode and the Fe plate should vary linearly with potential difference between Fe and Zn plates.

60
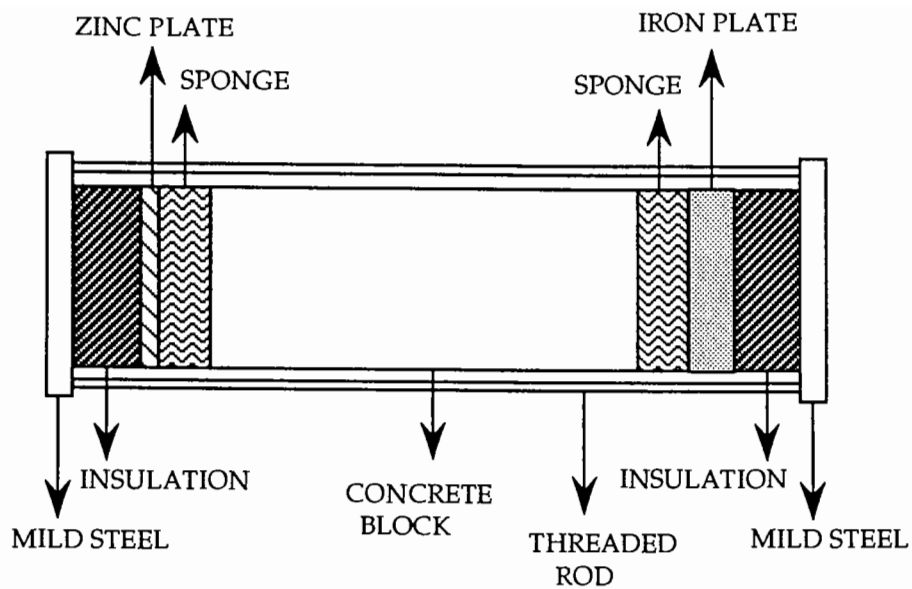
Figure 4.1 Schematic of the Electrochemical Cell.

4.2.1 CONCRETE BLOCKS

A block of concrete (35 cm x 15 cm x 15 cm) was cast and cured according to a formulation used in a 1953 bridge project. The composition of the concrete was (dry weights per cubic yard): 256 kg. of cement, 953 kg. of 19 mm. to 38 mm. aggregate, 506 kg. sand, and 122 kg. water. To this mix was added 0.9 kg. sodium chloride per cubic yard. Sufficient air entraining agent was added to provide 3-6% air content. The block was cast in the OSU Cement Laboratory.

4.2.2 ELECTRODES

The iron electrode was a 15 cm x 15 cm x 1 cm cast steel plate purchased from Gerlinger company in Salem, OR. The zinc electrode was a 15 cm x 15 cm x 0.08 cm Zn metal plate purchased from VWR Scientific.

Three types of reference electrodes were used. The Ag/AgCl reference electrodes were Orion Research Model 90-02 double junction reference electrodes. The inner compartment was filled with Orion Model 90-00-02 filling solution, which poises the electrode at + 0.242 V vs. the standard hydrogen electrode at 25 °C (i.e., equivalent

to a saturated calomel electrode). The outer filling solution was 1 M KCl. Commercial graphite electrodes were obtained from Electrochemical Devices, Inc. (EDI Model CG-GRA). "Laboratory" graphite electrodes were made from graphite rods (grade 8k-05, 1.6 cm X 30 cm) purchased from McMaster-Carr Supply Company. These rods were cut into pieces 6.5 to 7 cm in length, and a piece of wire was connected to each by a stainless steel screw. The graphite electrodes were used as received and preconditioned by soaking in saturated $Ca(OH)_2$ for 24 hours.

4.2.3 TEST CELL

The Fe and Zn electrodes were connected to the concrete block through sponges as shown in Figure 4.1. The sponges had been soaked with 0.1 M NaCl and squeezed to remove excess water. The potential difference between the Fe and Zn electrodes was maintained with an EG&G Princeton Applied Research Corporation (PAR) Model 173 potentiostat (in a 2-electrode mode) connected to a PAR Model 175 Universal Programmer. The total charge passed was monitored with a PAR Model 179 digital coulometer.

Two reference electrodes were attached to the cell as shown in Figure 4.2. A Ag/AgCl reference electrode was placed in a hole in the sponge at the Fe plate, and another reference electrode, which was to be tested, was attached to the concrete block, in one of two ways: (i) in a hole bored in a sponge cube (2.5 cm x 2.5 cm x 2.5 cm, treated with 0.1 M NaCl), which was then held on the surface of the block with a clamp; and (ii) embedded in the concrete block and sealed with a mixture of cement, concrete powder from the hole, and water. The reference electrode at the iron plate and the reference electrode to be tested were connected directly to a Keithley Model 197 digital voltmeter (DVM) with 1 Gohm input impedance. Independent tests showed that the ground of the Keithley 197 was isolated from the ground of the potentiostat.

4.3 RESULTS AND DISCUSSION

4.3.1 EVALUATION OF THE TEST PROCEDURE WITH Ag/AgCl ELECTRODES

The potential between two identical Ag/AgCl reference electrodes as a function of position and the potential applied between the Zn and Fe plates is shown in Figure 4.3. As indicated by the straightness of the lines, the concrete is reasonably homogeneous, the potential differences at the Fe and Zn interfaces are negligible compared to the potential difference across the concrete, and the Ag/AgCl electrodes do behave as would be predicted from first principles. The resistivity of the concrete was calculated from the current and voltage data from all of the experiments to be 330

Ω m. Thus, one concludes that the test cell is indeed a satisfactory system for testing other reference electrodes. However, it should be noted, that as additional experiments were performed, there was evidence that NaCl solution introduced from the sponges at both ends of the block and the sponge in which the reference electrode was placed reduced the resistivity of the block and led to inhomogeneities of the electric field.
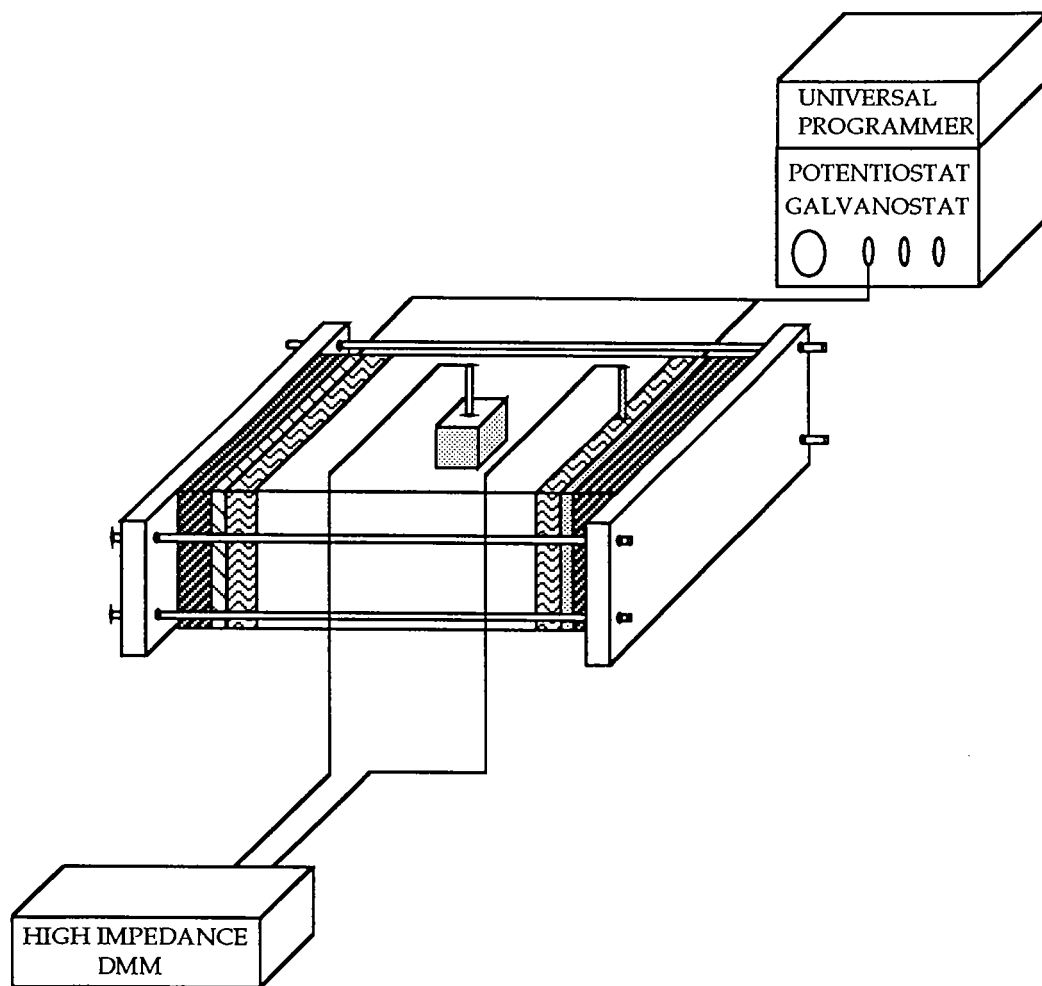
Figure 4.2 Experimental Apparatus for the Case Where the Reference Electrode is Placed on the Surface of Concrete Through a Sponge.
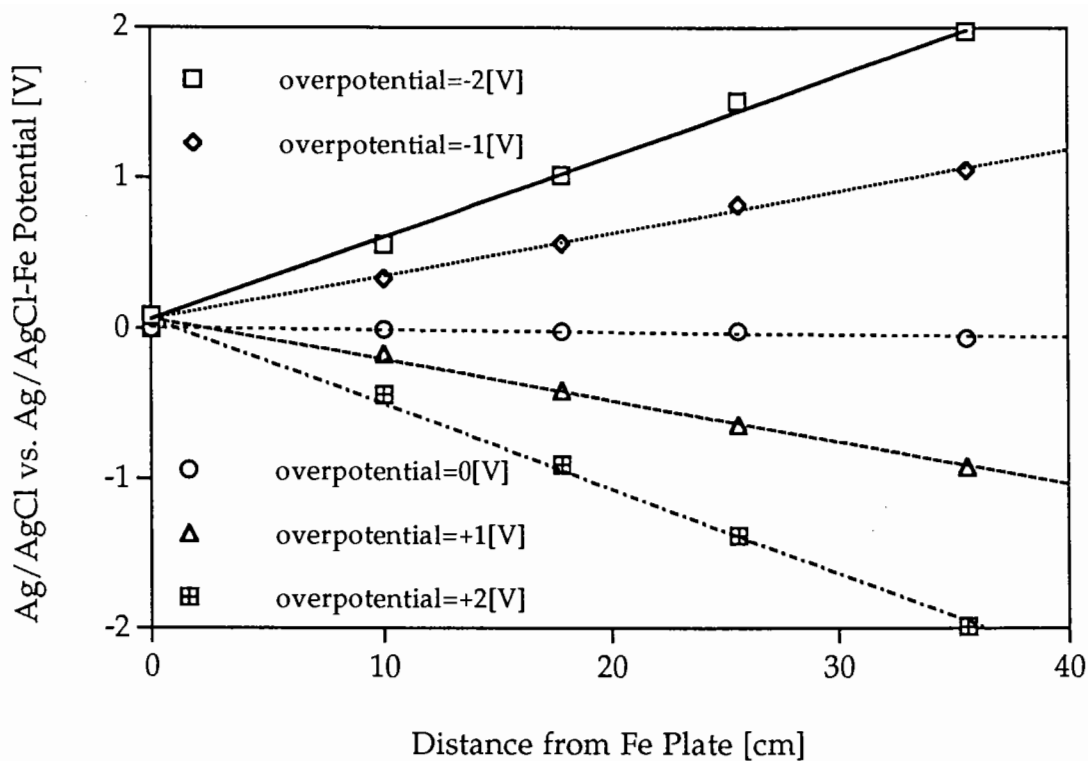
Figure 4.3 Electric Potential Difference Between the Two Reference Electrodes vs Distance at Different Fe-Zn Over-Potentials.
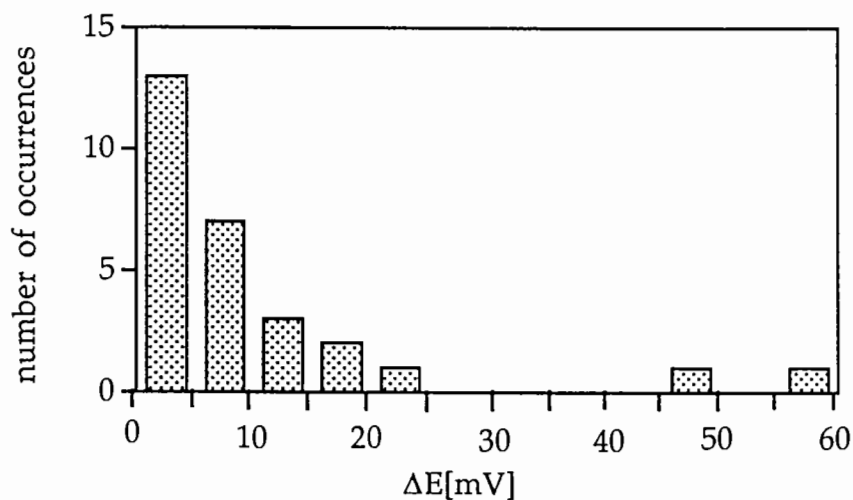
Figure 4.4 Reproducibility Between Runs with a Ag/AgCl Electrode. The Time Between Runs was a Few Hours.

64

In order to examine the reproducibility, the entire experiment was repeated within several hours. A histogram of the magnitude of the differences between the first run and the second run is presented in Figure 4.4. With the exception of a few outlier's, all readings were reproducible within 25 mV, and 70% were within 10 mV. It should be pointed out that, with a potential drop of 2000 mV across 35 cm, the gradient is 6 mV/mm; thus, the placement of the reference electrode could be major source of error.

4.3.2 COMPARISON OF THE Ag/AgCl AND GRAPHITE ELECTRODES

In a second phase, the entire test procedure (with reference electrodes attached to the block through sponges) was repeated several weeks later with both a Ag/AgCl reference electrode (Figure 4.5a) and an EDI graphite electrode (Figure 4.5b). By this time, the homogeneity of the concrete had been reduced by local intrusions of NaCl from the sponges. The reproducibility between runs conducted a few hours apart is shown in Figure 4.5a and 4.5b. The graphite electrode in a 0.1 M NaCl soaked sponge performed as well as the Ag/AgCl reference electrode in a sponge. Again the position of the reference electrode may be a major source error.

4.3.3 COMPARISON AMONG GRAPHITE ELECTRODES

In a third phase, the performance of laboratory-made graphite electrodes, commercial graphite electrodes, and Ag/AgCl reference electrodes were compared. The reference electrode to be tested was connected to the concrete block through the 0.1M NaCl soaked sponge. Over-potentials of 0, -1 and -2 V were used. Graphite electrodes were conditioned (soaked in saturated $Ca(OH)_2$ solution for 24 hours) and the test was repeated. All of the test conditions for this phase of the study are outlined in Table 4.1.
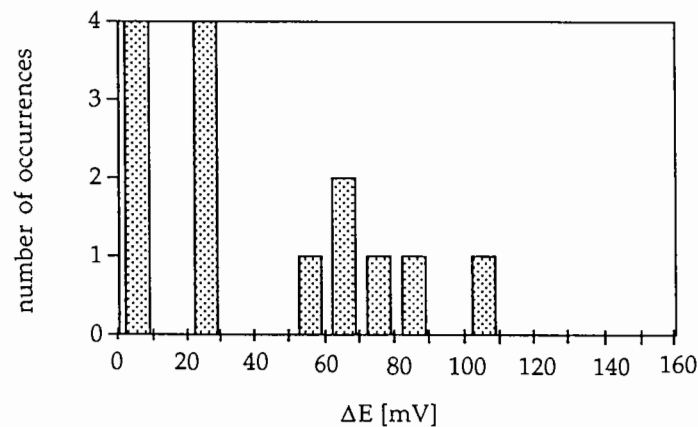
Figure 4.5a Reproducibility Between Runs with a Ag/AgCl Electrode. The Time Between Runs was a Few Hours.

65
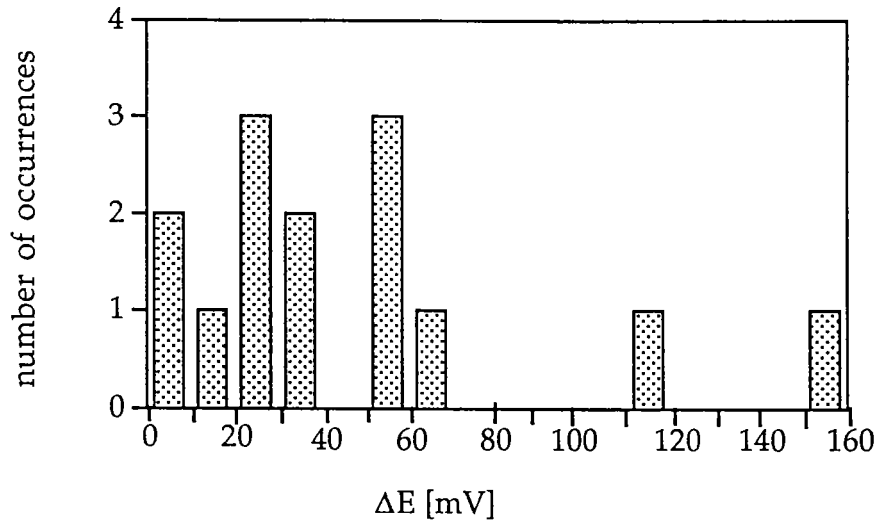
Figure 4.5b Reproducibility Between Runs with a Commercial Graphite Electrode. The Time Between Runs was a Few Hours.

Table 4.1 Tests performed on graphite and Ag/AgCl electrodes in the third phase.

Electrode	1st run $\eta = -2$ V	1st run $\eta = -1$ V	2nd run $\eta = -1$ V	2nd run $\eta = -2$ V
Orion Ag/AgCl	√	√	-	-
EDI # 1	√	√	-	-
EDI # 2	√	√	√	√
laboratory # 1	√	√	√	√
laboratory # 2	√	√	√	√
EDI #1, conditioned	√	√	√	√
EDI #2, conditioned	√	√	√	√
laboratory # 1, conditioned	√	√	√	√
laboratory # 2, conditioned	√	√	√	√

All of the electrodes appear to follow the potential along the concrete block reasonably well, as shown in Figures 4.6 and 4.7. The "kink" that appears in the potential at about 26 cm from the Fe plate is attributed to inhomogeneity in the concrete caused by

66

intrusion of salt solution from the sponge in which the electrode was mounted; no additional work was performed to confirm this supposition. Moreover, laboratory graphite probes behaved as well as the EDI electrodes and the Ag/AgCl reference electrode. This result allows more flexibility in experimentation since the laboratory probes are much less expensive than the commercial ones. Furthermore, the conditioned graphite probes showed potential values closer to each other than those of the unconditioned ones, as a comparison of Figures 4.6 and 4.7 illustrates. **Conditioning causes the probes to behave more uniformly.**

Histograms for unconditioned and conditioned probes are shown in Figures 4.8 and 4.9, respectively. **These data show that the reproducibility of the probes increase after conditioning.**

4.3.4 COMPARISON OF EMBEDDED GRAPHITE AND Ag/AgCl ELECTRODES

In a fourth phase, the performance of *embedded* reference electrodes was evaluated. The potential of one reference electrode embedded in the concrete block relative to the reference electrode in the sponge at the Fe plate was recorded as the potential applied between the Zn and Fe electrodes was changed. As seen in Figure 4.10, both the conditioned laboratory graphite electrode and the Ag/AgCl electrodes follow the applied potential well.
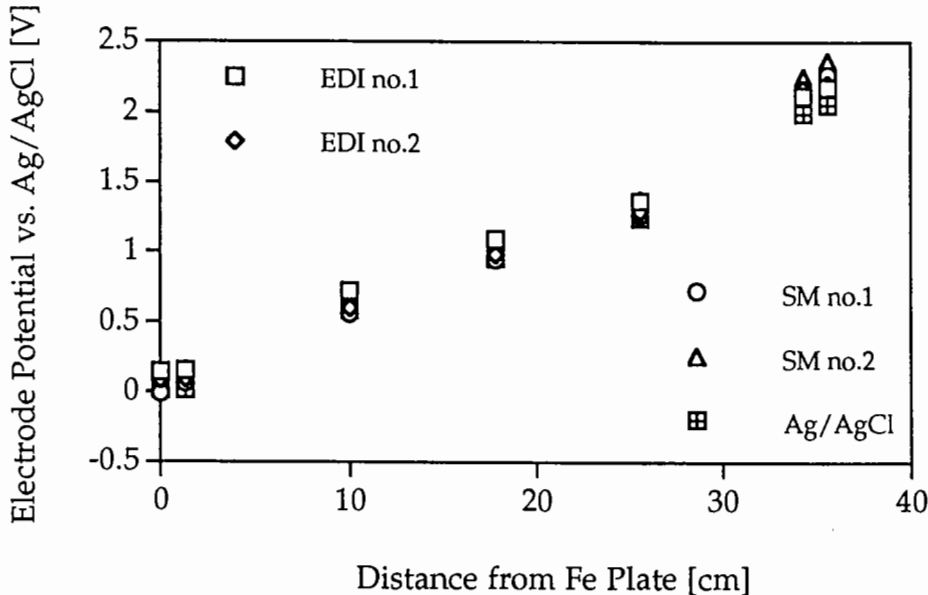
Figure 4.6 Electric Potential Difference Between Unconditioned Graphite Probes and Ag/AgCl, (Over-Potential = - 2 V).
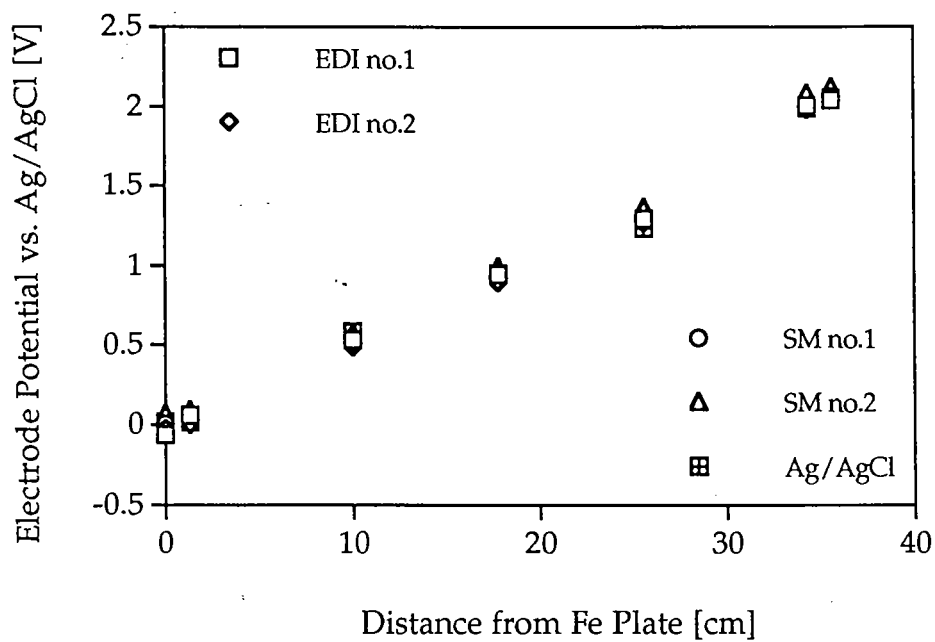
Figure 4.7 Electric Potential Difference Between Conditioned Graphite Probes and Ag/AgCl, (Over-Potential= - 2 V).
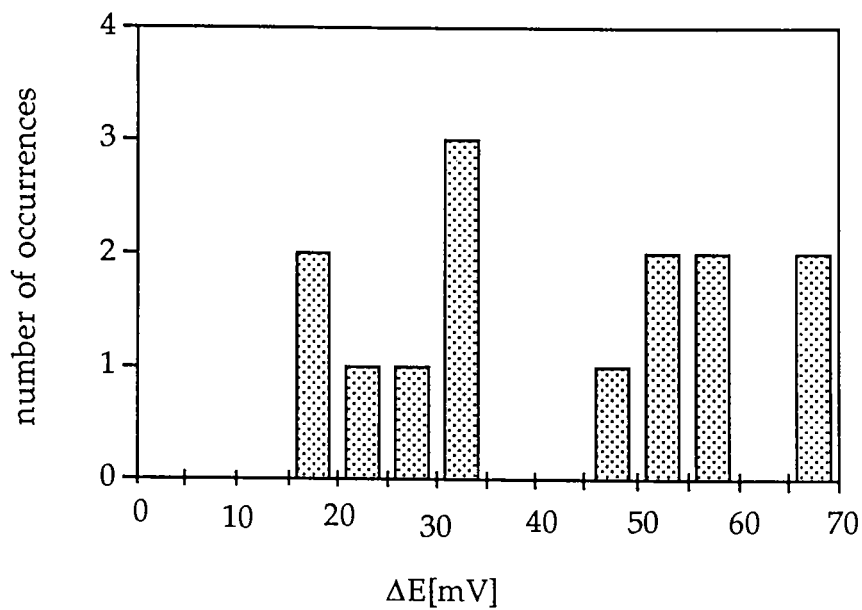
Figure 4.8 Reproducibility Between Runs with an Unconditioned Commercial Graphite Electrode. The Time Between Runs was a Few Hours.
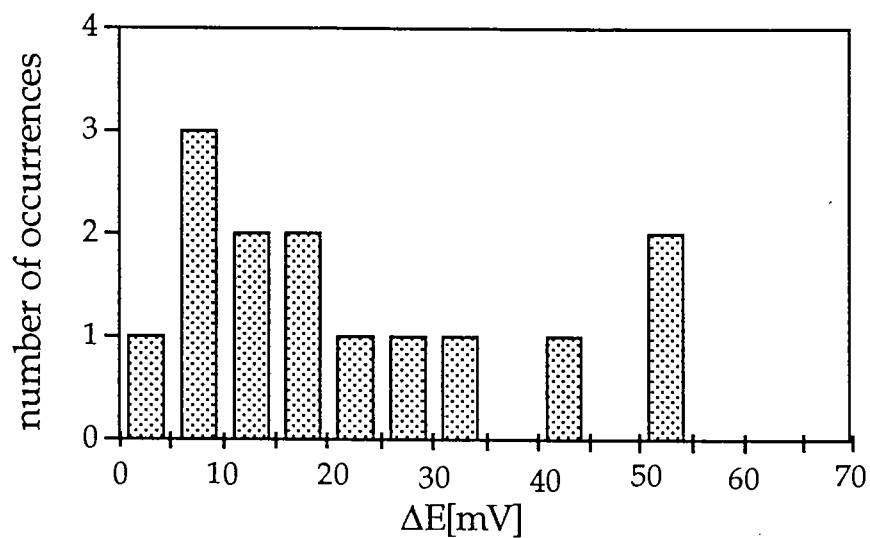
Figure 4.9 Reproducibility Between Runs with a Conditioned Commercial Graphite Electrode. The Time Between Runs was a Few Hours.
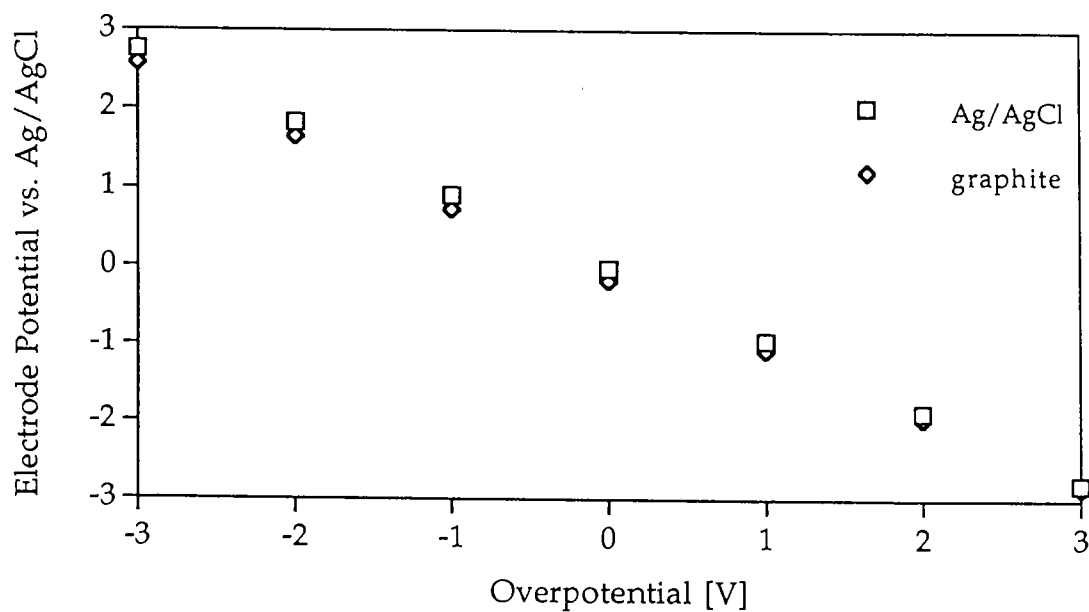
Figure 4.10 A Comparison Between Embedded Conditioned Graphite and Embedded Ag/AgCl Electrodes.

4.4 SUMMARY

At the level of testing performed here, their seemed to be no striking difference between the conditioned laboratory and EDI graphite electrodes and the Ag/AgCl electrode. The tests with the movement of the reference electrode showed higher variability than one would like to see (approximately 50 mV deviation), but part of that variability is attributed to the placement of the reference electrode. Thus, it is recommended that future tests monitor long-term stability of embedded electrodes under conditions similar to those of the 100-mV Polarization decay test or the 3-electrode controlled potential protection circuit.

5.0 CONCLUSIONS AND FUTURE WORK

In this section the major conclusions from this work are presented followed by suggestions for future work.

5.1 CONCLUSIONS

The following conclusions are based on the mathematical model and experimental data from the literature:

1. The rate of free corrosion is controlled primarily by charge transfer kinetics; O_2 concentration at the rebar surface is near its saturation value.

2. As the voltage applied to the rebar becomes more negative, the concentration of O_2 at the rebar surface decreases; current ultimately becomes limited by mass transport of oxygen. At a sufficiently negative applied potential, hydrogen evolution will commence.

3. Any calculations of anode life should be based on the actual current distribution over the surface of the zinc electrode rather than just the total zinc electrode area.

4. Under many conditions, the potential at the edge of the rebar is more negative than that at the center, suggesting that the centerline is more susceptible to corrosion. Therefore, the reference electrode should be located as close to the center of the rebar as possible.

5. In galvanic base case, the potential difference between the iron/concrete interface varies only by 7 mV from the center to the edge of the rebar; however, at the O_2-transport limited current it varies by 100 mV.

6. The higher the current the larger the potential difference between the center and the edge of the rebar.

7. As the cover thickness decreases, there is more oxygen available and the current increases at large applied potentials. Accordingly, the difference in the potential between the center and the edge also increases.

8. The degree of pore saturation has a significant effect on the characteristics of the cathodic protection system both in terms of the concrete resistivity and the flux of reacting oxygen to the iron electrode. Since the degree of pore saturation can exhibit large variations, a study on the effect of pore saturation on the system performance is warranted.

9. Current, as a function of pore saturation, goes through a maximum at intermediate values of pore saturation. At high values of pore saturation, current is limited by availability of oxygen. At low values of pore saturation, current is limited by the ohmic resistance of the concrete.

10. At pore saturation above 50% all the available oxygen is consumed and reference electrode placement is not critical; however from 30-50% pore saturation, placement of the reference electrode can have a large effect on the Polarization decay measurement.

The following conclusions are based on experimental results obtained with a concrete block, at approximately constant temperature and water content.

11. The concrete block was reasonably homogeneous, the potential differences at the Fe/sponge/concrete and Zn/sponge/concrete interfaces were negligible compared to the potential difference across the concrete, and the Ag/AgCl electrodes affixed to the block through a sponge did behave as would be predicted from first principles. Thus, the test cell was indeed a satisfactory system for testing other reference electrodes.

12. The position of the electrode on the concrete block could be a major source of error.

13. When the various reference electrodes were connected to the concrete block through a 0.1 M NaCl soaked sponge, the laboratory-constructed graphite electrodes behaved as well as the commercial graphite electrodes and the commercial Ag/AgCl reference electrode.

14. The conditioned graphite probes showed potential values closer to each other than those of the unconditioned ones. Also the reproducibility of the probes increased after conditioning.

15. Embedded graphite probe behaved similarly to the Ag/AgCl reference electrode. They both tracked the applied potential.

5.2 FUTURE WORK

1. The performance of the electrodes under controlled variations in environmental conditions (e.g., temperature 0-30 C, relative humidity 40-100%) is proposed for study.

2. The chemical species that poise the potential of the graphite electrode in concrete are unknown. It would be useful to determine the reactions that are responsible for poising the electrode in order to predict the sensitivity of the electrode to environmental variables.

3. In order to represent field systems more accurately, it is recommended that future tests be performed on concrete blocks with embedded iron and zinc plates. These tests should monitor long-term stability of embedded graphite electrodes under conditions similar to those of the 100-mV Polarization decay test and the 3-electrode controlled potential protection circuit.

4. Concentrations and mobilities of the charge carriers in concrete need to be evaluated so that conduction in concrete can be elucidated.

5. In the current model, the potential difference at the zinc/concrete interface was treated as a constant. However, a better understanding of the processes occurring at the zinc electrode is needed.

6. The geometry used for the two dimensional simulation was simple. However, this configuration is unable to predict the potential distribution on the "back" of the rebar, which is buried in concrete in actual field systems. Modifying the geometry for a better representation of the actual systems is recommended.

7. Only quasi steady state processes have been examined in this model; a time-dependent model needs to be developed.

6.0 IMPLEMENTATION

As a result of this research, the following guidelines should be used in regard to installation of embedded reference electrodes in reinforced concrete bridges which are cathodically protected with a sprayed zinc anode:

- Potential mapping of concrete surfaces remains an effective method to locate actively corroding rebar. The simulation performed in this study suggests that, even accounting for non-uniform current densities, reference electrodes should still be placed at locations with the most negative potential. However, care should be taken to place the electrode in the concrete as close to the centerline of the rebar as possible.

- Care should be taken to account for the environmental conditions at the bridge when assessing the cathodic protection system. In dry environments (low pore saturation), placement of the reference electrode has a large affect on the Polarization decay measurement. Conversely, in wet environments electrode placement is much less critical.

- In wet environments, the magnitude of the applied potential should be limited to prevent hydrogen evolution.

- Graphite electrodes appear to be a suitable choice for a reference electrode to monitor the 100-mV Polarization decay.

- Graphite electrodes should be conditioned prior to use.

- Design calculations of anode life should be based on the effective anode area rather than the total sprayed area.

REFERENCES

1) K.F. Dunker and B.G. Rabbat. Why America's Bridges are Crumbling. <u>Scientific American</u>, March 1993, pp. 66.

2) R.F. Stratfull. Cathodic Protection of a Bridge Deck. <u>Material Performance.</u> Vol 13, 1974, pp. 24.

3) Florida, Oregon Project Bridge Substructures.<u>Civil Engineering.</u> Oct 1991,pp 18.

4) J. Bartholomew, J. Bennett, T. Turk, W.H. Hartt, D.R. Lankard, A.A. Sagues and R. Savinell. <u>SHRP-S-670: Control Criteria and Materials Performance Studies for Cathodic Protection of Reinforced Concrete</u>. Prepared for the Strategic Highway Research Program. 1993.

5) M. Funihashi and J.B. Bushman. Technical Review of 100mV Polarization Shift Criterion for Reinforcing Steel in Concrete. <u>Corrosion</u>, Vol 47, No. 5, 1989.

6) M. Funihashi and W.T. Young. Investigation of 100mV Polarization Shift Criterion for Reinforcing Steel in Concrete. Paper 193 <u>NACE Corrosion/92</u>, 1992.

7) J.E. Bennett and T.A. Mitchell. Polarization decay Testing of Cathodically Protected Reinforcing Steel in Concrete. <u>Materials Performance</u>. Dec, 1990, pp. 20.

8) J.E. Bennett and T.A. Mitchell. Polarization decay of Cathodically Protected Reinforcing Steel in Concrete. Paper 373 <u>NACE Corrosion/89</u>, 1989.

9) R.C.G. Laird. Performance Evaluation Testing of Conductive Cathodic Protection Systems on Thin Parking Garage Slabs. Paper 553 <u>NACE Corrosion/91</u>, 1991.

10) D.M. Roy, P.W. Brown, D.Shi, B.E. Scheetz, W. May. <u>SHRP-S-628: Concrete Microstructure Porosity and Permeability</u>. Prepared for the Strategic Highway Research Program. 1993.

11) V.G. Papadakis, C.G. Vayenes and M.N. Fardis. Physical and Chemical Characteristics Affecting the Durability of Concrete. <u>ACl Materials Journal</u>. Vol 8, 1991, pp. 186

12) R.B. Bird, W.E. Stewart and E.N. Lightfoot. <u>Transport Phenomena</u>. Wiley, New york, 1960.

13) S.I. Sandler. <u>Chemical and Engineering Thermodynamics</u>. John Wiley & Sons, 1989, pp 437.

14) O. Gjorv and O. Vennesland. Evaluation and Control of Steel Corrosion in Offshore Concrete Structures. SP 100-79 in <u>Concrete Durability</u>, John M Scanlon Ed., American Concrete Institute, 1987, pp. 1575.

15) J.A. Gonzalez, W. Lopez and P. Rodriguez. Effects of Moisture Availability on Corrosion Kinetics of Steel Embedded in Concrete. <u>Corrosion</u>. Vol 49, 1993, pp 1004.

16) K. Tutti. Corrosion of Steel in Concrete. <u>Swedish Cement and Concrete Research Institute</u>, Stockholm, 1982.

17) C.D. Lawrence. Transport of Oxygen through Concrete. <u>British Ceramics Proceedings</u>, Vol 35, pp 277, 1984.

18) H. Hurling. Durability of Concrete Structures under Normal Outdoor Exposure. <u>RILEM Seminar</u> 1984.

19) K. Kobayashi and K. Shuttoh. Oxygen Diffusivity of Various Cementatous Materials. <u>Cement and Concrete Research</u>, Vol 21, 273 (1991).

20) C.E. Locke and A. Siman. Electrochemistry of Reinforcing Steel in Salt-Contaminated Concrete. Corrosion of Reinforcing Steel in Concrete <u>ASTM STP 713</u>, pp. 3.

21) A.A. Sagues and S.C. Kranc. On the Determination of Polarization Diagrams of Reinforcing Steel in Concrete. <u>Corrosion</u>, Vol 48, pp 624, 1992.

22) C.C. Naish A. Harker and R.F.A. Carney. Concrete Inspection: Interpretation of Potential and Resistivity Measurements. <u>Corrosion of Reinforcement in Concrete</u>. Elsevier Applied Science, London-New York, 1990, pp. 314.

23) R.P.Frankenthal and P.C. Milner. Hydrogen Evolution Kinetics on a High-Carbon Steel and on Tin in Seawater. <u>Corrosion</u>, Vol 42, pp 51 1986.

24) M. Pourbaix. <u>Atlas of Electrochemical Equilibria</u>, National Association of Corrosion Engineers, Houston Tex, 1974.

25) A.A. Sagues and R.G. Powers.<u>SHRP-88-ID024: Low-Cost Sprayed Zinc Galvanic Anode for Control of Corrosion of Reinforcing Steel in Marine Bridge Substructures</u>. Prepared for the Strategic Highway Research Program, 1994.

26) ODOT HP&R Study #5264: The Effect of Film Growth on the Adhesion of Metallized Zinc Coatings to Concrete. Oregon Department of Transportation, 1994.

27) S. Mindess and J.F. Young, Concrete, Prentice-Hall, 1981.

28) D.S. Brown and J.D. Allison. MINTEQA1, An Equilibrium Metal Speciation Model. Environmental Research Laboratory, U.S. Environmental Protection Agency, 1987.

Appendix A

DERIVATION OF THE BOUNDARY CONDITION AT THE FE-CONCRETE INTERFACE

A.1 OXYGEN REDUCTION CURRENT DENSITY

The current density for reduction of oxygen is described by the equation:

$$i_O = i_O^0 \, H \, C_O^{liq,y=L} / C_O^{air} \exp\{- 2.3 \, (E_{Fe} - E_O^{eq}) / b_O\} \qquad (A\text{-}1)$$

where the parameters are defined with equation 3-6.

The steady-state oxygen reduction current density is related to the molar flux of oxygen at the electrode surface by Faraday's law:

$$i_O = n \, F \, J_O \qquad (A\text{-}2)$$

which, in combination with the definition of J_O (equation 3-15) leads to

$$i_O = n \, F \, k_O \, (C_O^{air} - H \, C_O^{liq,y=L}) \qquad (A\text{-}3)$$

If the concentration of oxygen in the pore space at the iron surface is negligible compared to the concentration of oxygen in the pore space at the air interface (i.e., $C_O^{air} >> H \, C_O^{liq,y=L}$), the current is said to be "diffusion limited" and equation A-3 reduces to the "diffusion limited current," i_L:

$$i_L = n \, F \, k_O \, C_O^{air} \qquad (A\text{-}4)$$

Division of equation A-3 by A-4 and incorporation of the result into equation A-1 results in a relation between current density and electrode potential with no explicit dependence on the concentration of oxygen at the electrode surface

$$i_O = \frac{i_L \, i_o^0 \exp\{-2.3 \, (E_{Fe} - E_o^{eq}) / b_o\}}{i_L + i_o^0 \exp\{-2.3 \, (E_{Fe} - E_o^{eq}) / b_o\}} \qquad (A\text{-}5)$$

A.2 IRON OXIDATION CURRENT DENSITY

The current density for oxidation of iron is described by the equation:

$$i_{Fe} = -i_{Fe}^0 \exp\{ 2.3 (E_{Fe} - E_{Fe}^{eq}) / b_{Fe}\} \qquad \text{(A-6)}$$

where the parameters were discussed in connection with equation 3-6.

A.3 THE NET CURRENT DENSITY VS. IRON POTENTIAL

The total current density is the sum of the cathodic (positive) and anodic (negative) contributions, given by equations A-5 and A-6 respectively:

$$i = i_O + i_{Fe} \qquad \text{(A-7)}$$

where i is the net current density in the external circuit. Continuity requires that the current density calculated from electrode kinetics through equation A-7 be equal to the current density calculated by Ohm's law at the electrode surface:

$$i = -\nabla\phi / \rho \qquad \text{(A-8)}$$

where the gradient of ϕ, $\nabla\phi$, is evaluated at the electrode surface. A combination of A-7 and A-8 yields the boundary condition 3-6.

$$i = \frac{i_L i_O^0 \exp\{\dfrac{-2.3(E_{Fe} - E_O^{eq})}{b_O}\}}{i_L + i_O^0 \exp\{\dfrac{-2.3(E_{Fe} - E_O^0)}{b_O}\}} - i_{Fe}^0 \exp\{\frac{2.3(E_{Fe} - E_{Fe}^{eq})}{b_{Fe}}\} = -\frac{\nabla\phi}{\rho} \qquad \text{(3-6)}$$

Appendix B

ZINC-CONCRETE EQUILIBRIUM MODEL

In this appendix, the concentration of zinc ions at the zinc-concrete interface are approximated from a simple local equilibrium model of the concrete. While this model cannot account for experimental values of the potential at the zinc-concrete interface, it does provide insight into the zinc-concrete chemistry.

During the course of cathodic protection, Zn^{2+} is produced at the concrete-zinc interface according to reaction

$$Zn \rightarrow Zn^{2+} + 2\ e^- \tag{B-1}$$

The Zn^{2+} that is produced at the interface will simultaneously react with constituents of the concrete and diffuse away into the bulk of the concrete.

In order to assess the interaction of Zn^{2+} with the concrete, an equilibrium model of Zn(II) in concrete was developed. The chemical equilibrium model is based on the representation of concrete as an assembly of pure mineral phases (from the MINTEQA1[28] database) and the corresponding pore water concentrations of the dissolved species. To create this equilibrium model, the number of moles of each of the chemical components of the concrete and the amount of "free" water in the pore space must be calculated. The elemental composition of portland cement is shown in Table B.1, and the composition of concrete per unit volume is shown in Table B.2. This composition is in accordance with ODOT mix formulation from a 1953 bridge project.

A porosity of concrete (volume of pore space / total volume) of 0.27 and a pore saturation of 48% was used. From these values, the number of moles of each element per liter of water in the pore space was calculated, as shown in Table B.3. The assemblage of mineral phases that would form from these elements and water as well as the resulting free activities (concentrations) of ions in the water phase at equilibrium were then calculated, using the geochemical equilibrium computer program MINTEQA1[28] for the thermodynamic data.

The result is a hypothetical, well defined matrix with which Zn^{2+} ions react when they are produced. This equilibrium representation of concrete is shown in Table B.4. The major features of this model are: pore water solution pH = 10.35 (this low pH represents an equilibrium state which, in practice, concrete does not reach); there are 9 chemical components, 7 solid phases, and 1 liquid phase, leaving only one degree of freedom in the solution phase composition. The major soluble ions are Na^+ and SO_4^{2-}, with concentrations in the 0.1 - 0.2 M range.

The major approximations in this approach are:

(i) temperature = 25 °C;
(ii) the water activity is unity;
(iii) the activity coefficients of the solution species are unity;
(iv) concrete can be represented by discrete mineral phases; and
(v) other components such as CO_2 and $NaCl$ were neglected.

Variations in the first three of these approximations might change the assemblage of mineral phases and the solution-phase concentrations by a small amount, but the basic result would be the same: a high-pH, moderate ionic strength solution, with SO_4^{2-} as the dominant anion. Further work would be required to investigate the impact of the last two approximations.

To represent this Zn-concrete interface during cathodic protection, it is approximated that the charge introduced by Zn^{2+} is exactly balanced by the charge introduced by the diffusion of SO_4^{2-} from the bulk of the concrete. (The loss of SO_4^{2-} is ultimately compensated by OH^- generated from Reaction (3-2), preserving charge balance.) When equal quantities of Zn^{2+} and SO_4^{2-} are added to the matrix described above, the following sequence of reactions takes place:

$$Zn^{2+} + CaSiO_3(s) \rightarrow Ca^{2+} + ZnSiO_3(s) \qquad \text{(B-2)}$$

$$Ca^{2+} + SO_4^{2-} \rightarrow CaSO_4(s). \qquad \text{(B-3)}$$

Thus, the net reaction is:

$$Zn^{2+} + SO_4^{2-} + CaSiO_3(s) \rightarrow ZnSiO_3(s) + CaSO_4(s) \qquad \text{(B-4)}$$
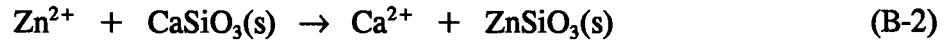
The solubility of $ZnSiO_3(s)$ is very low; thus, based on the local equilibrium model, the formation of $ZnSiO_3(s)$ is expected almost immediately when cathodic protection is begun. (A solution of the diffusion equation for semi-infinite, constant-current boundary conditions, with $D_{Zn} = 2 \times 10^{-12}$ m^2 s^{-1}, i = 1 mA m^{-2}, and corrected electrode area, shows that total Zn(II) concentration at the electrode surface reaches 5×10^{-10} M within 1 s of the current being turned on. As seen in Table B.4, only 4×10^{-10} M Zn(II) is soluble in the concrete matrix).

As cathodic protection proceeds, it is expected that the pore solution at the zinc electrode will be depleted in SO_4^{2-}, while deposition of $ZnSiO_3(s)$ and $CaSO_4(s)$ occurs near the electrode surface.

Under the initial conditions, after precipitation of $ZnSiO_3(s)$ but before significant depletion of SO_4^{2-}, the concentration of free Zn^{2+} can be calculated from the local equilibrium model of concrete (Table B.4C) and the potential E_{Zn} can be calculated from equation B-5:

$$E_{Zn} = E_{Zn}^0 + RT/nF \ln a_{Zn} \qquad \text{(B-5)}$$

These values are $[Zn^{2+}] = 0.0173$ picomole, and $E_{Zn} = -1.49$ V versus $Cu/CuSO_4$ (in the absence of charge transfer and mass transfer overpotential); the measured value of E_{Zn} is -0.678 V versus $Cu/CuSO_4$. Obviously, the zinc electrode does not appear to be poised by this sequence of reactions.

In the mathematical models of cathodic protection described in this report, the assumption was made that E_{Zn} was constant throughout the cathodic protection process. The analysis of the Zn-concrete interface presented in this appendix does not shed much light on the validity of that assumption, since the reactions discussed don't appear to be those that poise the Zn electrode. Further work would be required to establish the set of reactions that *do* poise the Zn electrode, and the effects of mass transfer and charge transfer polarization at the Zn-concrete interface during cathodic protection. However, it is noteworthy that, if the cathodic protection system is controlled by the three-electrode potentiostat described in Section 3.2, potential drops across the Zn-concrete interface are irrelevant for control of cathodic protection (but may still play a role in power consumption).

Table B.1 Composition of Portland Cement[27]

Oxide	Common Name	Composition (weight %)	Molecular Weight (g/mol)
Cao	lime	63.0	56
SiO_2	silica	22.0	60
Al_2O_3	alumina	6.0	102
Fe_2O_3	ferric oxide	2.5	160
MgO	magnesia	2.6	40
K_2O	alkali	0.6	94
Na_2O	alkali	0.3	62
SO_3	sulfur trioxide	2.0	80
	TOTAL	99.0	

Table B.2 Composition of Concrete

Component	Composition (lb/yd^3)
cement	564
aggregate	2100
sand	1115
water	270

Table B.3 Elemental Composition of Concrete

Oxide	Common Name	Composition[a] (mol/L_{total})[b]	Composition[a] $(mol/L_{pore\ water})$[c]
CaO	lime	3.7643	29.046
SiO_2	silica[d]	12.2519	94.537
Al_2O_3	alumina	0.1968	1.519
Fe_2O_3	ferric oxide	0.0523	0.403
MgO	magnesia	0.2175	1.678
K_2O	alkali	0.0214	0.165
Na_2O	alkali	0.0162	0.125
SO_3	sulfur trioxide	0.0837	0.645

[a] The number of digits should not be interpreted as the precision with which the quantity is known. The sand is treated as if it were 100% silica, and the aggregate is treated as though it were inert.

[b] Computed from Columns 3 and 4 of Table B.1 and Row 1 of Table B.2; "total" refers to total volume of concrete.

[c] Computed from Column 3 of Table B.3 with porosity = 0.27 and pore saturation = 48%.

[d] The sand is approximated as 100% silica sand.

Table B.4 Equilibrium Model of Concrete[a]

A. Solid Phases

Wollastonite	$CaSiO_3$
Ca-nontronite	$CaFe_{12}Al_2(SiO_3)_{22}(H_2O)_6$
Leonhardite	$Ca_2Al_4(SiO_3)_8(H_2O)_7$
Diopside	$CaMg(SiO3)_2$
Microcline	$KAl(SiO_3)_2SiO_2$
Quartz	SiO_2
Gypsum	$CaSO_4$

B. Solution Chemistry (pH = 10.35, concentrations in mM)

Anions

SO_4^{2-}	70.7
$NaSO_4^-$	65.4
KSO_4^-	22.4
$H_3SiO_4^-$	0.3
OH^-	0.2
Total Charge	**-230.0**

Cations

Na^+	184.6
K^+	44.8
Ca^{2+}	0.2
Total Charge	**+229.8**

C. Zinc Chemistry

Solid Phase

Zinc Silicate	$ZnSiO_3$

Solution Species (concentrations in picomole)

Zn^{2+}	0.0173
$Zn(OH)^+$	109
$Zn(SO_4)_2^{2-}$	307
Total Soluble Zn(II)	**416**

[a]   Composition of concrete given in Table B.3, Column 4; thermodynamic data from the MINTEQA1 database[28].

<u>Appendix C</u>

<u>COMPUTER CODE FOR ONE-DIMENSIONAL MODEL</u>

```basic
PROGRAM$ = "\bc7\concrete\ctmts7.bas" + " " + DATE$ + " " + TIME$

'PROGRAM written in Microsoft Basic Ver. 7.1
'Locke and Siman electrode kinetics, 0.2% NaCl, Figures 3 and 4
'Webb regression of Locke and Siman data
'Wranglen CuCuSO4 vs SHE
'Farid 2-D physical parameters
'Single-Table output
'solves for Icorr, Ecorr
'computes CO2s at a given Eprot (set to give E-Ecorr = -100 mV)
'computes "Instant off" E-Ecorr
'revised constants 8/1/94
'added spectator H2 8/1/94 : question about CsH2>??????
'calculate Einstant off for various O2 levels

DEFDBL A-Z
OUTFILE$ = "c:out.tmp"
OPEN OUTFILE$ FOR OUTPUT AS #6
    GOSUB GetConstants
    GOSUB PrintParameters
 'corrosion potential
    GOSUB DetermineEcorr
    CASE$ = "Corrosion Potential"
    GOSUB TABLEOUT
 'protection criterion
    CO2s = .04135# / .2606# * CO2b
    GOSUB DetermineIofCO2s
    CASE$ = "Protection"
    GOSUB TABLEOUT
 'instant off
    GOSUB InstantOff
    CASE$ = "Instant OFF"
    GOSUB TABLEOUT
 'systematic table of results for plotting
    GOSUB OUT1X
    FOR Q = 1 TO 30 STEP 2
        GOSUB SetE
        GOSUB DetermineI
        GOSUB OUT1
    NEXT Q
    PRINT #6, CHR$(12)
CLOSE #6
SHELL "QE " + OUTFILE$
END

CalcPolar decay:
    E = Ecorr + Eprot
    GOSUB DetermineI
    GOSUB InstantOff
    Edepol = E - Ecorr
RETURN

GetConstants:
'parameter values
    rho = 138#:             'ohm m
    kOx = .0000001# * 33#:   'm/s
    H = 33#                  '----
    CO2b = 8.6# / 33#:       'mol/m3
    IOO2 = .00000077#:       'A/m2
    EO2 = .509#:             'V vs SHE
    bO2 = .18#:              'V
    IOFe = .000071#:         'A/m2
    EFe = -.44#:             'V vs SHE
    bFe = .41#:              'V
    CH2s = .000000001#       'mol/m3
    IOH2 = .012#             'A/m2
    EH2 = -.739#             'V
    bH2 = .15#               'V
    EZn = -.358#:            'V vs SHE
    nO2 = 4#:                '-----
    F = 96485#:              'C/mol
    delta = .0254#:          'm
    nFe = 2#:                '-----
'ancillary values
```

```
    DensityFe = 7860#:         'kg/m3
    MolarMassFe = .055847#:    'kg/mol
    speryr = 31536000#:        's/yr
    mpermil = .0000254#:       'm/mil
    mpermm = .001#:            'm/mm
RETURN
PrintParameters:
    F1$ = "\              \  ##.######^^^^  \                              \"
    F2$ = "\              \  ######.######  \                              \"
    PRINT #6, PROGRAM$
    PRINT #6,
    PRINT #6, USING F2$; "rho "; rho; "ohm m"
    PRINT #6, USING F1$; "kOx"; kOx; "m/s (for concentrations in water)"
    PRINT #6, USING F2$; "H"; H; "----"
    PRINT #6, USING F2$; "CO2b"; CO2b; "mol/m3 (for concentration in water)"
    PRINT #6, USING F1$; "IOO2"; IOO2; "A/m2"
    PRINT #6, USING F2$; "EO2 "; EO2; "V vs SHE"
    PRINT #6, USING F2$; "bO2"; bO2; "V"
    PRINT #6, USING F1$; "IOFe"; IOFe; "A/m2"
    PRINT #6, USING F2$; "EFe"; EFe; "V vs SHE"
    PRINT #6, USING F2$; "bFE"; bFe; "V"
    PRINT #6, USING F1$; "CH2s"; CH2s; "mol/m3"
    PRINT #6, USING F1$; "IOH2"; IOH2; "A/m2"
    PRINT #6, USING F2$; "EH2"; EH2; "V"
    PRINT #6, USING F2$; "bH2"; bH2; "V"
    PRINT #6, USING F2$; "EZn"; EZn; "V vs SHE"
    PRINT #6, USING F2$; "nO2"; nO2; "-----"
    PRINT #6, USING F2$; "F"; F; "C/mol"
    PRINT #6, USING F2$; "delta"; delta; "m"
    PRINT #6, USING F2$; "nFe"; nFe; "-----"
    PRINT #6, CHR$(12)
RETURN

InstantOff:
    E = (LOG(IOO2 / IOFe * CO2s / CO2b) / 2.3# + (EO2 / bO2 + EFe / bFe)) / (1 / bO2 + 1 / bFe)
    Ilc = nO2 * F * kOx * CO2b
    IhatO2 = IOO2 * EXP(-2.3# * (E - EO2) / bO2)
    IO2 = CO2s / CO2b * IhatO2
    IFe = -IOFe * EXP(2.3# * (E - EFe) / bFe)
    IH2 = -CH2s * IOH2 * EXP(-2.3# * (E - EH2) / bH2)
    I = IO2 + IFe
'Kirchhoff
    IRs = I * rho * delta
    Eappl = E - IRs - EZn
    eta = E - Ecorr
'Check
    CO2s = CO2b * IO2 / IhatO2
    IO2x = IOO2 * CO2s / CO2b * EXP(-2.3# * (E - EO2) / bO2)
'Corrosion Rate
    JFe = IFe / (nFe * F): 'mol/m2/s  = mol/(m2 s)
    Jmass = JFe * MolarMassFe
    CorrVel = JFe * (MolarMassFe / DensityFe):  'm/s
    CorrVelx = CorrVel * speryr / mpermil: 'mil/yr
    CorrVely = CorrVel * speryr / mpermm: 'mm/yr
RETURN

SetE:
    Eapplx = INT(10 * (Ecorr - EZn)) / 10 - (Q - 1) * .1#: ID$ = "Eappl = " + STR$((Q - 1) * 100) + " mV"
    GOSUB DetermineEfromEapplx
RETURN


DetermineI:
    Ilc = nO2 * F * kOx * CO2b
    IhatO2 = IOO2 * EXP(-2.3# * (E - EO2) / bO2)
    IO2 = IhatO2 / (1# + IhatO2 / Ilc)
    IFe = -IOFe * EXP(2.3# * (E - EFe) / bFe)
    IH2 = -CH2s * IOH2 * EXP(-2.3# * (E - EH2) / bH2)
    I = IO2 + IFe
'Kirchhoff
    IRs = I * rho * delta
    Eappl = E - IRs - EZn
    eta = E - Ecorr
'Check
```

```
        CO2s = CO2b * IO2 / IhatO2
        IO2x = IOO2 * CO2s / CO2b * EXP(-2.3# * (E - EO2) / bO2)
'Corrosion Rate
        JFe = IFe / (nFe * F): 'mol/m2/s  = mol/(m2 s)
        Jmass = JFe * MolarMassFe
        CorrVel = JFe * (MolarMassFe / DensityFe):  'm/s
        CorrVelx = CorrVel * speryr / mpermil: 'mil/yr
        CorrVely = CorrVel * speryr / mpermm: 'mm/yr
RETURN

DetermineIofCO2s:
        Ilc = nO2 * F * kOx * CO2b
        IO2 = nO2 * F * kOx * (CO2b - CO2s)
        E = EO2 - bO2 / 2.3# * (LOG(IO2 / IOO2 * CO2b / CO2s))

        IhatO2 = IOO2 * EXP(-2.3# * (E - EO2) / bO2)
        'IO2 = IhatO2 / (1# + IhatO2 / Ilc)
        IO2x = IOO2 * CO2s / CO2b * EXP(-2.3# * (E - EO2) / bO2)
        IFe = -IOFe * EXP(2.3# * (E - EFe) / bFe)
        IH2 = -CH2s * IOH2 * EXP(-2.3# * (E - EH2) / bH2)
        I = IO2 + IFe
'Kirchhoff
        IRs = I * rho * delta
        Eappl = E - IRs - EZn
        eta = E - Ecorr
'Check
        CO2s = CO2b * IO2 / IhatO2
        IO2x = IOO2 * CO2s / CO2b * EXP(-2.3# * (E - EO2) / bO2)
'Corrosion Rate
        JFe = IFe / (nFe * F): 'mol/m2/s  = mol/(m2 s)
        Jmass = JFe * MolarMassFe
        CorrVel = JFe * (MolarMassFe / DensityFe):  'm/s
        CorrVelx = CorrVel * speryr / mpermil: 'mil/yr
        CorrVely = CorrVel * speryr / mpermm: 'mm/yr
RETURN


OUT1X:
        PRINT #6, PROGRAM$
        PRINT #6,
        IF I = 0 THEN I = 1D-99
        F1$ = "Eappl    I              log I     E       IRs    IFe      log IFe  log corr vel"
        F2$ = "  V      A/m2           A/m2      V       V      A/m2     A/m2      mil/yr"
        F3$ = "##.###   ##.##^^^^   ###.##   ##.###   ##.###  ##.##^^^^   ###.##    ###.##"
        PRINT #6,
        PRINT #6, F1$
        PRINT #6, F2$
        PRINT #6,
RETURN

OUT1:
        PRINT #6, USING F3$; Eappl; I; LOG(ABS(I)) / LOG(10); E; IRs; IFe; LOG(ABS(IFe)) / LOG(10);
LOG(ABS(CorrVelx)) / LOG(10)
RETURN

DetermineEprotfromEdepolgoal:
        Edepolgoal = -.1#
        Eprot = -.7#
        GOSUB CalcPolar decay
        Y = Edepol - Edepolgoal
        SELECT CASE Y
            CASE IS > 0
                Epos = Eprot
                Ypos = Y
                WHILE Y >= 0
                    Eprot = Eprot - .1#
                    GOSUB CalcPolar decay
                    Y = Edepol - Edepolgoal
                WEND
                Eneg = Eprot
                Yneg = Y
            CASE IS < 0
                Eneg = Eprot
                Yneg = Y
```

```
                    WHILE Y <= 0
                        Eprot = Eprot + .1#
                        GOSUB CalcPolar decay
                        Y = Edepol - Edepolgoal
                    WEND
                    Epos = Eprot
                    Ypos = Y
            CASE IS = 0
        END SELECT
        'PRINT USING "##.###"; Epos; Ypos; Eneg; Yneg; Eprot
        DO WHILE ABS(Edepol - Edepolgoal) > .00000000000001#
            Eprot = Eneg - (Epos - Eneg) / (Ypos - Yneg) * Yneg
            GOSUB CalcPolar decay
            Y = Edepol - Edepolgoal
            SELECT CASE Y
                CASE IS > 0
                    Epos = Eprot
                    Ypos = Y
                CASE IS < 0
                    Eneg = Eprot
                    Yneg = Y
                CASE IS = 0
                    EXIT DO
            END SELECT
        'PRINT USING "##.###"; Epos; Eapplpos; Eneg; Eapplneg; Eapplx
        LOOP
        'PRINT USING "##.###"; Epos; Eapplpos; Eneg; Eapplneg; Eapplx
RETURN

DetermineEfromEapplx:
        E = Eapplx + EZn
        GOSUB DetermineI
        Y = Eappl - Eapplx
        SELECT CASE Y
            CASE IS > 0
                Epos = E
                Ypos = Y
                WHILE Y >= 0
                    E = E - .1#
                    GOSUB DetermineI
                    Y = Eappl - Eapplx
                WEND
                Eneg = E
                Yneg = Y
            CASE IS < 0
                Eneg = E
                Yneg = Y
                WHILE Y <= 0
                    E = E + .1#
                    GOSUB DetermineI
                    Y = Eappl - Eapplx
                WEND
                Epos = E
                Ypos = Y
            CASE IS = 0
        END SELECT
        'PRINT USING "##.###"; Epos; Ypos; Eneg; Yneg; Eapplx
        DO WHILE ABS(Eappl - Eapplx) > (ABS(E) + ABS(EZn) + ABS(IRs)) * .00000000000001#
            E = Eneg - (Epos - Eneg) / (Ypos - Yneg) * Yneg
            GOSUB DetermineI
            Y = Eappl - Eapplx
            SELECT CASE Y
                CASE IS > 0
                    Epos = E
                    Ypos = Y
                CASE IS < 0
                    Eneg = E
                    Yneg = Y
                CASE IS = 0
                    EXIT DO
            END SELECT
        'PRINT USING "##.###"; Epos; Eapplpos; Eneg; Eapplneg; Eapplx
        LOOP
        'PRINT USING "##.###"; Epos; Eapplpos; Eneg; Eapplneg; Eapplx
```

```
RETURN

DetermineEcorr:
        E = 0
        I = 0
        WHILE I >= 0
            E = E + .1#
            GOSUB DetermineI
        WEND
        Ineg = I
        Eneg = E
        E = 0
        I = 0
        WHILE I <= 0
            E = E - .1#
            GOSUB DetermineI
        WEND
        Ipos = I
        Epos = E
        DO WHILE ABS(I) > (ABS(IO2) + ABS(IFe)) * .00000000000001#
            E = Eneg - (Epos - Eneg) / (Ipos - Ineg) * Ineg
            GOSUB DetermineI
            SELECT CASE I
                CASE IS > 0
                    Epos = E
                    Ipos = I
                CASE IS < 0
                    Eneg = E
                    Ineg = I
                CASE IS = 0
                    EXIT DO
            END SELECT
            'PRINT USING "##.#######^^^^   ##.###^^^^   ##.###^^^^ ##.###^^^^"; E; I; IO2; IFe
        LOOP
     Ecorr = E
RETURN

TABLEOUT:
F1$ = "\                     \  ##.###^^^^"
PRINT #6, PROGRAM$
PRINT #6,
PRINT #6, CASE$ + " - All units SI (m, s, V, A, ohm, C, mol)"
PRINT #6,
PRINT #6, USING F1$; "IhatO2"; IhatO2
PRINT #6, USING F1$; "IO2"; IO2
PRINT #6, USING F1$; "IFe"; IFe
PRINT #6, USING F1$; "IH2"; IH2
PRINT #6, USING F1$; "I "; I
PRINT #6, USING F1$; "Ilc"; Ilc
PRINT #6, USING F1$; "IO2/Ilc "; IO2 / Ilc
PRINT #6, USING F1$; "CO2s"; CO2s
PRINT #6, USING F1$; "CO2b"; CO2b
PRINT #6,
PRINT #6, USING F1$; "Eappl"; Eappl
PRINT #6, USING F1$; "E"; E
PRINT #6, USING F1$; "EZn"; EZn
PRINT #6, USING F1$; "IRs"; IRs
PRINT #6,
PRINT #6, USING F1$; "E-Ecorr"; E - Ecorr
PRINT #6, USING F1$; "E-EFe"; E - EFe
PRINT #6, USING F1$; "E-EO2"; E - EO2
PRINT #6, USING F1$; "Ecorr"; Ecorr
PRINT #6,
PRINT #6, USING F1$; "JFe"; JFe
PRINT #6, USING F1$; "Jmass"; Jmass
PRINT #6, USING F1$; "CorrVel"; CorrVel
PRINT #6, USING F1$; "CorrVel mil/yr"; CorrVelx
PRINT #6, USING F1$; "CorrVel mm/yr"; CorrVely
PRINT #6,

PRINT #6, USING F1$; "Chk IO2"; CO2s / CO2b * IOO2 * EXP(-2.3# * (E - EO2) / bO2)
PRINT #6, USING F1$; "Chk IFe"; -IOFe * EXP(2.3# * (E - EFe) / bFe)
PRINT #6, USING F1$; "Chk Ict"; CO2s / CO2b * IOO2 * EXP(-2.3# * (E - EO2) / bO2) - IOFe * EXP(2.3# * (E -
EFe) / bFe)
```

C-5

```
PRINT #6, USING F1$; "Chk Imt"; nO2 * F * kOx * (CO2b - CO2s)
PRINT #6, USING F1$; "Chk Kirchhoff"; Eappl - E + EZn + IRs

PRINT #6, CHR$(12)
RETURN
```

Appendix D

E-log i PLOTS
OF THE ONE-DIMENSIONAL SYSTEM

D-1 GRAPHICAL METHODOLOGY

The goal of this section is to present a graphical representation of all the processes occurring in the 1 dimensional model. This is accomplished through extension of an Evan's diagram. First the basic Evan's diagram for the corrosion of reinforcing steel is introduced in the context of the model parameters discussed in Section 3.2. This formulation is then extended to other processes considered in the model.

The equilibrium potential, E^{eq}, is a measure of the energy of each half reaction in the absence of a net current. At the equilibrium potential, the current of the cathodic half reaction is equal and opposite the corresponding anodic half reaction resulting in no net reaction and no net current. The absolute value of the current density of each half reaction at equilibrium is termed the exchange current density, i^0 (A/m^2). The equilibrium potentials and exchange current densities for reactions 3-1 and 3-2 are shown schematically in the Evan's diagram in Figure D-1.
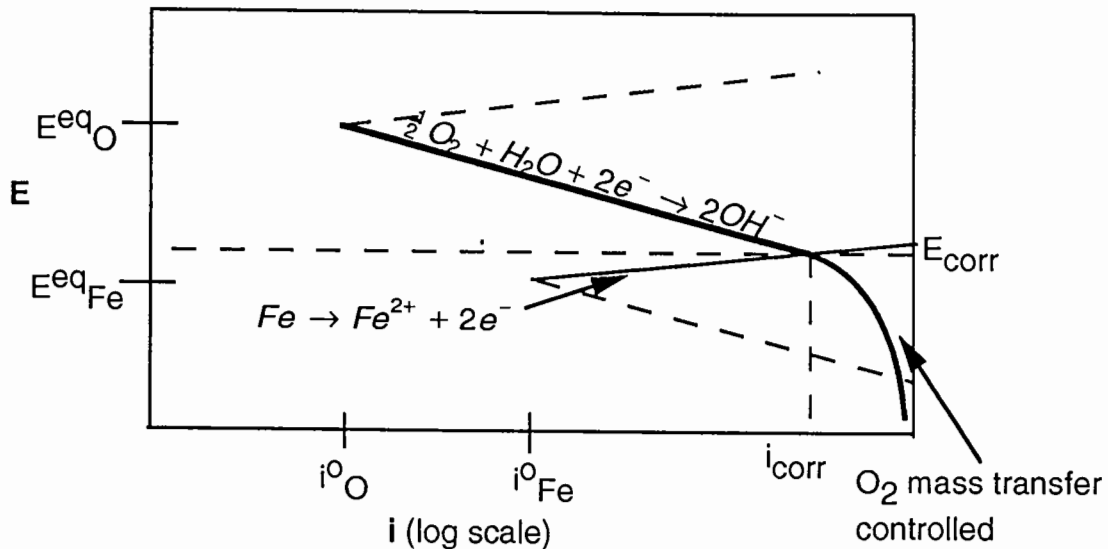

Figure D-1 Schematic Evan's Diagram of Corrosion of Reinforced Steel.

As Figure D-1 shows, when a corrosion current begins to flow, the electrodes depart from their equilibrium potential; the cathodic half cell becomes more negative and the anodic more positive. This phenomenon is termed polarization. **In the case of a single activated process,** the change in potential with respect to the log of the current gives a straight line at large current densities, with a Tafel slope proportional to the activation energy.

In actively corroding systems both reactions depicted in Figure D-1 can occur at the Fe-concrete interface. In other words there are two "oxidation-reduction cells" which coexist. In microcorrosion, the corrosion current will increase until the potential of both processes are identical. This defines the "mixed" potential that the system obtained at steady-state. This potential is termed the corrosion potential of the iron, E_{corr}; the rate of corrosion is proportional to the corrosion current, i_{corr}. As Figure D-1 shows, a more negative system (corrosion) potential coincides with a slower corrosion rate. Cathodic protection then can be thought of as a means to make the system potential negative enough so that corrosion proceeds at a negligible rate. Similarly, one method of monitoring the performance of cathodic protection is through the system potential.

If one of the reactant species becomes depleted, for example, oxygen, then the corrosion rate becomes limited by the availability of that species. This is termed mass transfer control.

The model for corrosion of reinforcing steel is presented by an Evan's diagram in Figure D-2. The values of "intercept," i.e. the (i^0, E^{eq}) pair, and the slope are presented in Table 3.1 and are discussed in Section 3.2.5.
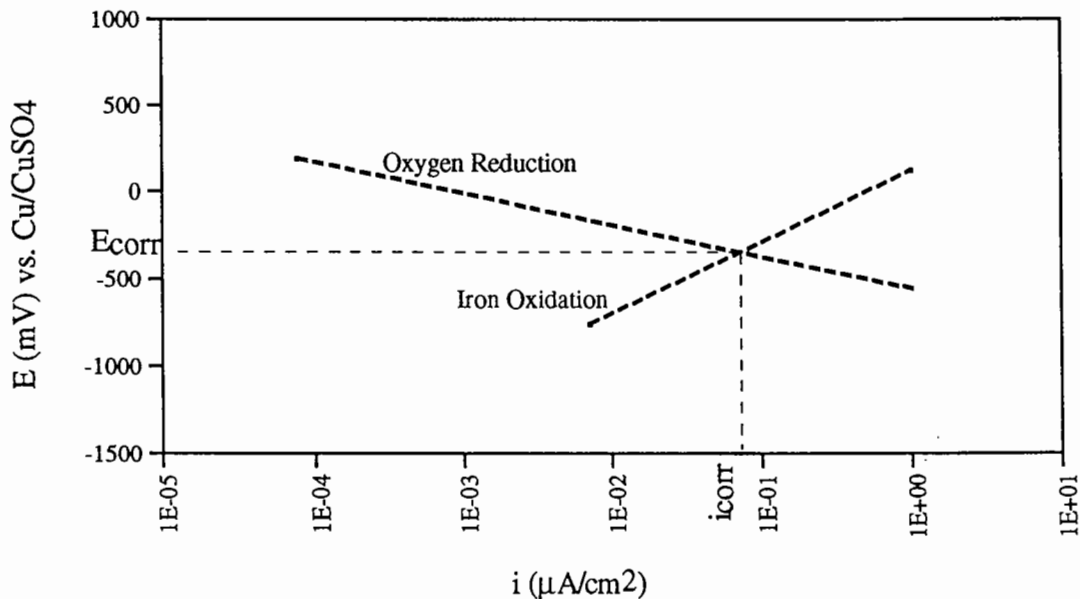

Figure D-2 Evan's Diagram for Corrosion of Reinforcing Steel with Base Case Parameters.

When the system is connected to a sprayed zinc anode for cathodic protection, the electrochemical circuit shown in Figure 3.3 is formed. In this case, an additional anodic reaction "competes" with iron in supplying electrons for the reduction reaction. Since the zinc potential is assumed to be constant in the model, the effect of the CP anode can be included on a similar diagram to those above. In constructing such a plot it is useful to consider all the electrochemical processes occurring in the electrolyte adjacent to the iron. The effect of the zinc anode on the potential at the iron includes an ohmic drop which increases with current density. Current density is defined with respect to the area of the iron electrode. Such a plot can be constructed using either ϕ_{Fe} or E_{Fe} as the ordinate. In the plots that follow ϕ_{Fe} is chosen. As a Kirchhoff's Law analysis of Figure 3.3 shows, these values are related according to: $\phi_{Fe} = E_{Fe} - E_{appl}$.

A ϕ_{Fe} - log i plot of a galvanically connected zinc anode ($E_{appl} = 0$) for the base case is shown in Figure D-3. In this diagram, one reduction process is balanced by two competing oxidation processes. Zinc oxidation is corrected by the ohmic drop across the concrete electrolyte. To compare the relative effect of each oxidation processes, the current densities at a given potential are simply added. This forms the curve labeled "combined oxidation." It is clear that the oxidation of zinc is the dominant process as this curve is nearly identical to the "combined oxidation" curve which sums the current densities for both oxidation processes. Steady state is reached when the combined oxidation current density equals the reduction current density. This occurs at $i_O = 2 \ \mu A/cm^2$ and $\phi_{Fe} = E_{Fe} = -610$ mV vs. Cu/CuSO$_4$. Figure D-3 also shows the value for $i_{Fe} = 0.017 \ \mu A/cm^2$. These values are consistent with those generated by the computer program in Appendix C.
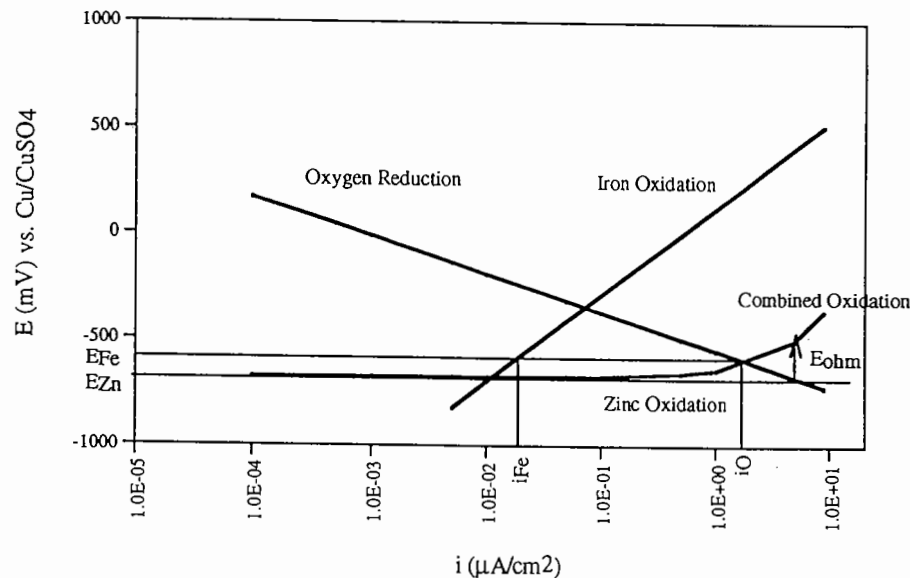

Figure D-3 E-log i Plot for the Base Case at an Applied Potential of 0 Volt.

D-3

A graphical solution (ϕ_{Fe} - log i) to the model for the base case with an applied potential of -1 V is shown in Figure D-4. All oxidation and reduction processes are shown individually. In addition to those processes discussed above, reduction processes include mass transfer limitations (as labeled by the limiting current and calculated according to equation 3-11) and hydrogen evolution. The sum of these processes is labeled "combined reduction," and represents all processes which consume electrons. The oxidation processes again include zinc oxidation and iron oxidation. Since the zinc electrode is separated from the iron by the concrete electrolyte, the ohmic potential drop, E_{ohm}, is also included in the "combined oxidation" curve. The zinc oxidation curve is separated from the other polarization curves by the magnitude of the applied potential. All values are consistent with the equivalent circuit of Figure 3.3. The solution to the 1-dimensional model occurs at the potential and current density where the combined oxidation curve crosses the combined reduction curve and the number of electrons produced equal the number consumed. This occurs at a potential of E_{Fe} - E_{appl} which is separated from E_{Zn} by E_{ohm}. The value for current density is 22 $\mu A/cm^2$ Fe (0.92 $\mu A/cm^2$ Zn) and E_{Fe} is - 800 mV vs. Cu/CuSO$_4$ (E_{Fe} - E_{appl} = 200 mV). Since the curves cross at a potential more positive than the equilibrium potential for hydrogen evolution, this reaction has a negligible effect.

D-2 HYDROGEN EVOLUTION

Plots as shown in Figure D-4 can be useful in parametric studies of the cathodic protection system. For example, the onset of hydrogen evolution can be studied. Figure D-5 a,b,c shows E-logi plots for 60 % PS at thicknesses of 12, 25, and 50 mm. In each case, the hydrogen evolution process just begins to contribute to the "combined reduction" curve at steady-state. From these data, the applied potential for the onset of hydrogen evolution decreases from -2.5 V to -1 V as the cover thickness increases from 12.7 to 50.8mm. This trend is due to the greater availability of oxygen at lower cover thicknesses.

Figure 3.8 plots the maximum applied potential before hydrogen evolution begins as a function of pore saturation for three different cover thicknesses. Due to the approximations discussed above as well as uncertainty in the input parameters, caution is urged in using the quantitative results; however, it is qualitatively accurate. As the cover thickness increases, the maximum applied potential decreases, since the limiting current density decreases. In dry concrete, hydrogen evolution is unlikely. On the other hand care should be taken when applying cathodic protection to wet concrete. This analysis is extremely sensitive to the equilibrium potential of hydrogen evolution. As can be seen through the Nernst equation, a decrease in pH increases the likelihood of hydrogen evolution. For example for a pH of 7 the maximum potential for a pore saturation of 60% and a concrete cover of 12 mm. decreases from 2.5 V to less than 1 V.

D-4
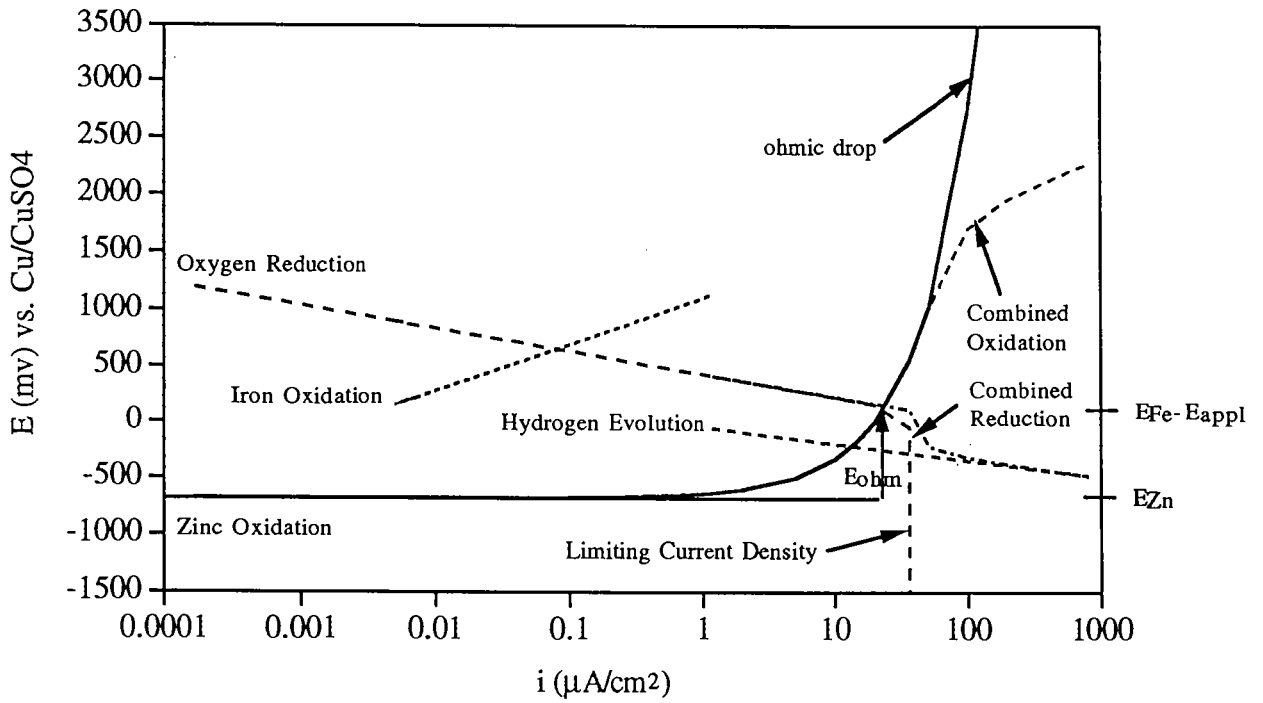
Figure D-4 E-log i Plot for the Base Case at an Applied Potential of -1 Volt.

60% PS, t=0.5 in.
Eappl = -2500 mV
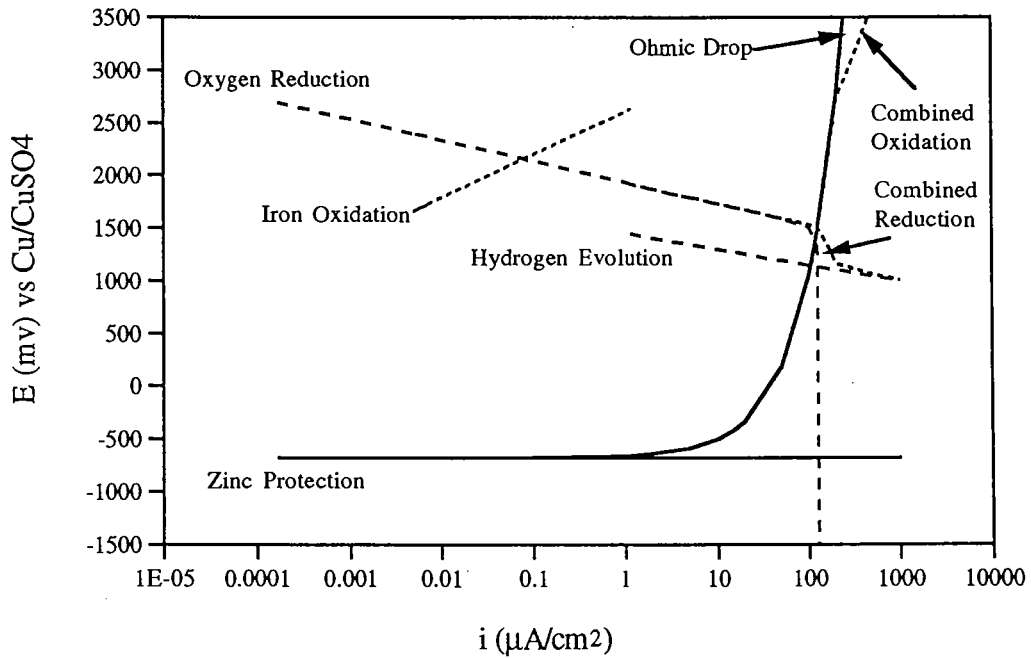
Figure D-5a E-logi Plot Depicting the Onset of Hydrogen Evolution at 60% PS and a Cover Thickness of 12 mm.

D-5

60% PS, t=1.0 in.
Eappl = -1500 mV
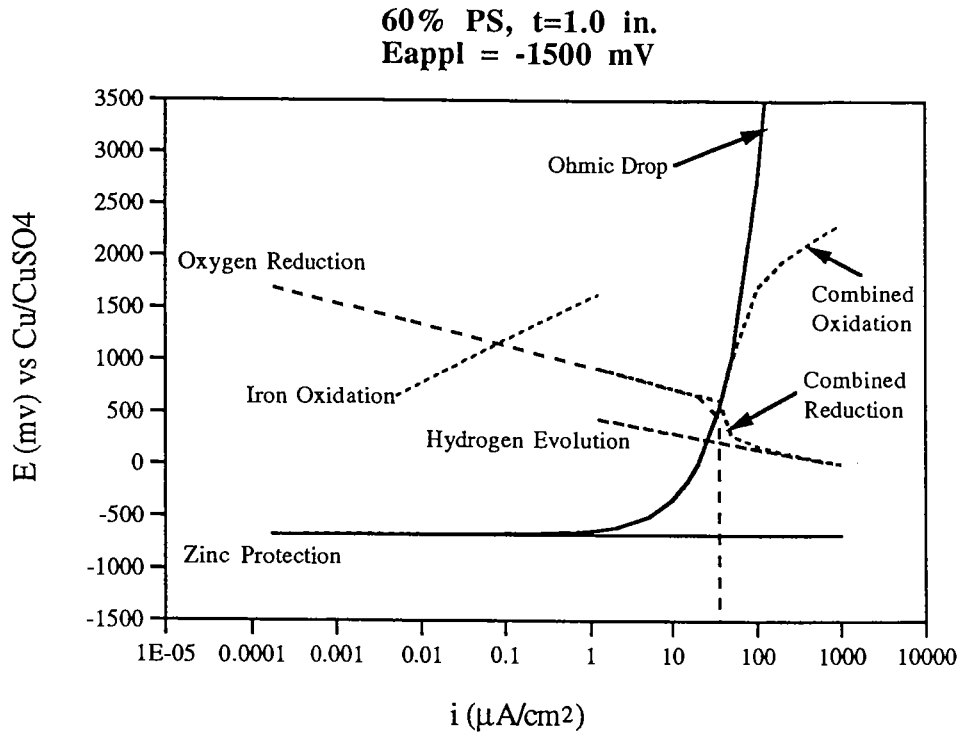
Figure D-5b E-logi Plot Depicting the Onset of Hydrogen Evolution at 60% PS and a Cover Thickness of 25 mm.

60% PS, t=2.0 in.
Eappl = -1000 mV
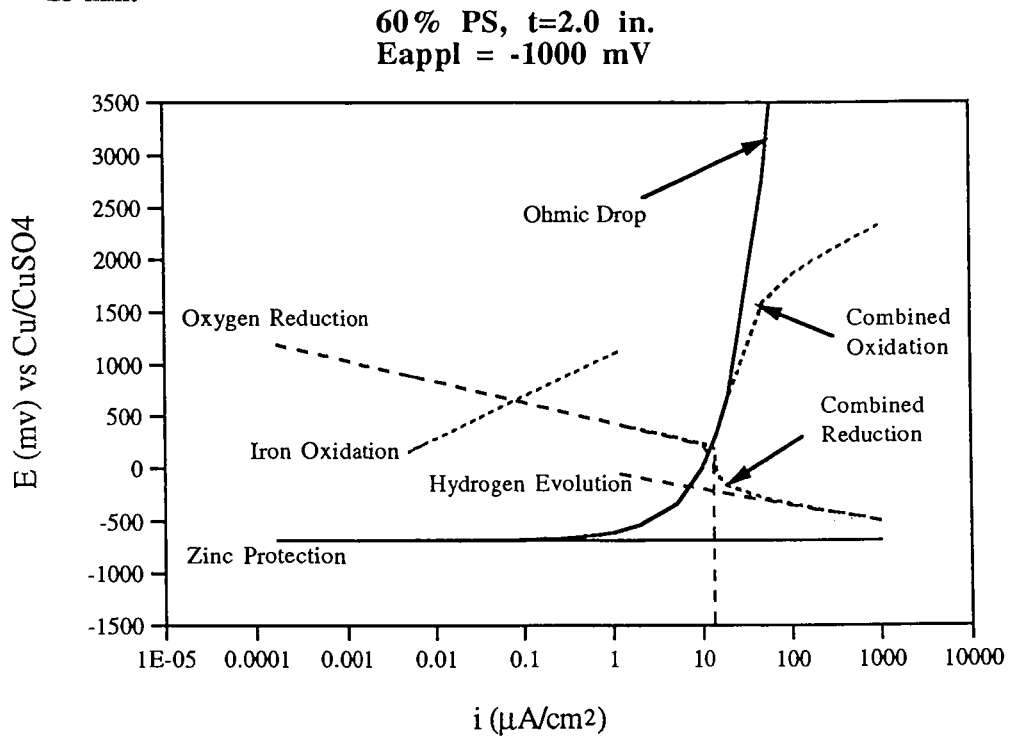
Figure D-5c E-logi Plot Depicting the Onset of Hydrogen Evolution at 60% PS and a Cover Thickness of 50.8mm.

D-6

Appendix E

COMPUTER CODE
FOR TWO-DIMENSIONAL MODEL

```fortran
C       The program 'PROTECT' finds potential distribution in 2 dimensional
C       geometry.
C       PROGRAM written in Fortran Ver.
        IMPLICIT REAL*8 (A-H,O-Z)
        REAL*8 IDOTFE
        Dimension E(0:200,0:200)
        ITMAX=200000
        EMAX=1.0E-15
C
C       EZN:zinc potential (Cu/CuSO4)
        EZN=-0.678
C
C       NX and NY:number of intervals in the X and Y directions respectively
        NX=40
        NY=20
        NPX=NX+1
        NPY=NY+1
C
C       A:conductivity in the bulk of concrete
        A=0.007441
        B=0.00
C
C       XL and YL:lengths in the X and Y directions respectively; FEX:width of
C       the iron in the X direction
        XL=0.0635
        YL=0.0254
        FEX=0.00635
        DELTX=XL/NX
        DELTY=YL/NY
C
C       HENRY:Henry's constant
        HENRY=33.064
C
C       W:overrelaxation factor
        W=1.3
C
C       IDOTFE:oxygen reduction exchange current density; DEFF:oxygen mass
C       transfer
C       coefficient; BULKCONC:oxygen concentration in the bulk; BC:inverse of
C       Tafel
C       slope for oxygen reduction; ENUMBER:equivalent number of electron
C       moles per 1 mole of oxygen; EEQ:equilibrium potential of oxygen
C       reduction
        IDOTFE=7.7E-7
        DEFF=1.09E-7
        BULKCONC=8.5
        BC=0.18
        ENUMBER=4.0
        EEQ=0.189
C
C       F and FARAD:fundamental constants
        F=38.9
        FARAD=96485.0
        KMAX=100
        EEE=0.001
C
C       CURNTLIM:limiting current density
        CURNTLIM=ENUMBER*FARAD*DEFF*BULKCONC
C
C       XIOX:iron oxidation exchange current density; EOFE:equilibrium potential
C       of iron oxidation; BA:inverse of Tafel slope for iron oxidation
        XIOX=7.1E-5
        EOFE=-0.76
        BA=0.41
C
C       EAPL:applied potential
        EAPL=0.0
C
C       determine the node where the iron edge is located
                X=0.0
                DO 211 I=1,NPX
                IF (ABS(X-FEX).LE.0.00001) THEN
                IFE=I
                PRINT*,IFE
```

```
              ENDIF
              X=X+DELTX
211           CONTINUE
C
C       potential values are stored in an output file: OUT.DAT
        OPEN  (UNIT=3,FILE='OUT.DAT',STATUS='UNKNOWN')
C
C       zinc potential is constant
        DO 1 I=1,NPX
        E(I,1)=-EZN
1       CONTINUE
C
C       EE:maximum error; IT:number of iteration
        EE=0.0
        IT=0
C
C       guess an initial value for the unknown potentials
        DO 4 J=2,NPY
        DO 3 I=1,NPX
        E(I,J)=0.6
3       CONTINUE
4       CONTINUE
C       start iteration
9       IF(INT(IT/100).EQ.FLOAT(IT/100.0)) THEN
        PRINT*,EE,IT
        ENDIF
        EE=0.0
        IT=IT+1
        DO 15 J=2,NY
        I=1
        E(I-1,J)=E(I+1,J)
        CALL INTERIOR(E,I,J,A,B,DELTX,DELTY,EE,W)
        I=I+1
14      IF (I.NE.NPX) THEN
        CALL INTERIOR(E,I,J,A,B,DELTX,DELTY,EE,W)
        I=I+1
        GO TO 14
        ENDIF
        E(I+1,J)=E(I-1,J)
        CALL INTERIOR(E,I,J,A,B,DELTX,DELTY,EE,W)
15      CONTINUE
C
C       go to the level where rebar is located
        J=NPY
        I=1
16      IF (I.NE.NPX) THEN
        IF (I.GT.IFE) THEN
        E(I,J+1)=E(I,J-1)
        CALL INTERIOR(E,I,J,A,B,DELTX,DELTY,EE,W)
        ELSE
                IF(I.EQ.1) THEN
                EHOLD=E(I,J)
                E(I-1,J)=E(I+1,J)
                CALL SUCCESS (E,I,J,IDOTFE,DELTX,DELTY,BC,KMAX,EEE,EEQ,
+                             A,B,CURNTLIM,EAPL,XIOX,EOFE,BA)
                ENEW=E(I,J)
                E(I,J)=EHOLD*(1-W)+W*ENEW
                ERROR=ABS((E(I,J)-EHOLD)/E(I,J))
                IF(EE.LT.ERROR) EE=ERROR
                ELSE
                EHOLD=E(I,J)
                CALL SUCCESS (E,I,J,IDOTFE,DELTX,DELTY,BC,KMAX,EEE,EEQ,
+                             A,B,CURNTLIM,EAPL,XIOX,EOFE,BA)
                ENEW=E(I,J)
                E(I,J)=EHOLD*(1-W)+W*ENEW
                ERROR=ABS((E(I,J)-EHOLD)/E(I,J))
                IF(EE.LT.ERROR) EE=ERROR
                ENDIF
        ENDIF
        I=I+1
        GO TO 16
        ELSE
        E(I+1,J)=E(I-1,J)
        E(I,J+1)=E(I,J-1)
```

```fortran
            CALL INTERIOR(E,I,J,A,B,DELTX,DELTY,EE,W)
            ENDIF
            IF (EE.LE.EMAX) THEN
            PRINT*,EE,IT
            X=0.0
                    DO 21 I=1,NPX
                    WRITE(3,*)I,X
                    WRITE (3,25) (E(I,J), J=1,NPY)
                    X=X+DELTX
                    WRITE(3,*)
21          CONTINUE
            J=NPY
            SUM=0.0
            DO 99 I=1,IFE
            SUM=SUM+E(I,J)
99          CONTINUE
            AVG=SUM/IFE
            WRITE (3,91) AVG,IFE,J,E(IFE,J)
            WRITE (3,*)
C
C           calculate oxygen concentration at the center of iron, OXGCENT
            XNUMCNT=CURNTLIM*IDOTFE*EXP(-2.3*(EAPL-E(1,J)-EEQ)/BC)
            DENMCNT=CURNTLIM+IDOTFE*EXP(-2.3*(EAPL-E(1,J)-EEQ)/BC)
            CURCNT=XNUMCNT/DENMCNT
            OXGCENT=(BULKCONC - CURCNT/(ENUMBER * FARAD*DEFF))/
     +                      HENRY
C
C           calculate oxygen concentration at the edge of iron, OXGEDG
            XNUMEDG=CURNTLIM*IDOTFE*EXP(-2.3*(EAPL-E(IFE,J)-EEQ)/BC)
            DENMEDG=CURNTLIM+IDOTFE*EXP(-2.3*(EAPL-E(IFE,J)-EEQ)/BC)
            CUREDG=XNUMEDG/DENMEDG
            OXGEDG=(BULKCONC-CUREDG/(ENUMBER*FARAD*DEFF))/HENRY
            WRITE(3,*)
            WRITE(3,*)'OXGCENT',OXGCENT,'  OXGEDG',OXGEDG
C
C           determine the net current, CURT, through Ohm's law
            CURT=0.0
            DO 55 J=2,NPY
            I=1
            CURT=(E(I,J)-E(I,J-1))*(DELTX/2.0)
            DO 45 I=2,NX
            CURT=CURT+(E(I,J)-E(I,J-1))*DELTX
45          CONTINUE
            I=NPX
            CURT=CURT+(E(I,J)-E(I,J-1))*(DELTX/2.0)
            CURT=(-A/DELTY)*CURT
            WRITE(3,*)J,CURT
            CURT=0.0
55          CONTINUE
            GO TO 100
            ENDIF
            IF (IT.LE.ITMAX) THEN
            GO TO 9
            ENDIF
            PRINT*,'NO CONVERGENCE'
C
C           format statements
25          FORMAT(6(e12.5,1X))
91          FORMAT(2X,'AVG = ',E12.5,10X,'E(',I2,',',I2,')=',E12.5)
C
100         END
C
C
C           subroutine INTERIOR determines potential values in bulk of concrete
C
            SUBROUTINE INTERIOR(E,I,J,A,B,DELTX,DELTY,EE,W)
            IMPLICIT REAL*8 (A-H,O-Z)
            DIMENSION E(0:200,0:200)
            XKAPPA=A+B*(J-1)*DELTY
            DERKAPPA=B
            DX=DELTX**2.0
            DY=DELTY**2.0
            EHOLD=E(I,J)
            ENEW=(2.0*XKAPPA*DY*(E(I+1,J)+E(I-1,J))
```

E-3

```fortran
     +      +((2.0*XKAPPA+DERKAPPA*DELTY)*E(I,J+1)+(2.0*XKAPPA
     +      -DERKAPPA*DELTY)*E(I,J-1))*DX)/
     +      (4.0*XKAPPA*(DX+DY))
            E(I,J)=EHOLD*(1-W)+W*ENEW
            ERROR=ABS((E(I,J)-EHOLD)/E(I,J))
            IF(EE.LT.ERROR) EE=ERROR
            RETURN
            END

C       subroutine SUCCESS and function FUNC determine potential values at
C       the rebar
C
        SUBROUTINE SUCCESS (E,I,J,IDOTFE,DELTX,DELTY,
     +  BC,KMAX,EEE,EEQ,A,B,CURNTLIM,EAPL,XIOX,EOFE,BA)
        IMPLICIT REAL*8 (A-H,O-Z)
        REAL*8 IDOTFE
        DIMENSION E(0:200,0:200)
        XKAPPA=A+B*(J-1)*DELTY
        DERKAPPA=B
        COEFF1=2.0*XKAPPA+DERKAPPA*DELTY
        DX=DELTX**2.0
        DY=DELTY**2.0
        DENOMIN=4.0*XKAPPA*(DX+DY)
        X1=-5.0
        X2=5.0
        XACC=1.0E-15
        FMID=FUNC(CURNTLIM,IDOTFE,EAPL,X2,EEQ,BC,XKAPPA,DY,E,I,J
     +       ,COEFF1,DELTY,DX,DENOMIN,XIOX,EOFE,BA)
        F=FUNC(CURNTLIM,IDOTFE,EAPL,X1,EEQ,BC,XKAPPA,DY,E,I,J
     +  ,COEFF1,DELTY,DX,DENOMIN,XIOX,EOFE,BA)
        IF(F*FMID.GE.0.) PAUSE 'ROOT MUST BE BRACKETED IN RTBIS'
        IF(F.LT.0.) THEN
        RTBIS=X1
        DDX=X2-X1
        ELSE
        RTBIS=X2
        DDX=X1-X2
        ENDIF
        DO 10 KK=1,KMAX
        DDX=DDX*0.5
        XMID=RTBIS+DDX
        FMID = FUNC (CURNTLIM, IDOTFE, EAPL, XMID, EEQ, BC, XKAPPA,
     +  DY,E,I,J,COEFF1,DELTY,DX,DENOMIN,XIOX,EOFE,BA)
        IF(FMID.LE.0.) RTBIS=XMID
        IF(ABS(DDX).LT.XACC.OR.FMID.EQ.0.) GO TO 11
10          CONTINUE
        PRINT*,'NO CONVERGENCE IN BISECT'
        GO TO 2
11      E(I,J)=RTBIS
        FF=FUNC(CURNTLIM,IDOTFE,EAPL,RTBIS,EEQ,BC,XKAPPA,DY,E,I,J
     +  ,COEFF1,DELTY,DX,DENOMIN,XIOX,EOFE,BA)
        IF(FF.GT.EEE) THEN
        PRINT*,'ASSIMPTOTE'
        ENDIF
        RETURN
        END

        FUNCTION FUNC (CURNTLIM , IDOTFE, EAPL, AA, EEQ, BC, XKAPPA,
     +  DY, E,I,J,COEFF1,DELTY,DX,DENOMIN,XIOX,EOFE,BA)
        IMPLICIT REAL*8 (A-H,O-Z)
        REAL*8 IDOTFE
        DIMENSION E(0:200,0:200)
        XNUM=CURNTLIM*IDOTFE*EXP(-2.3*(EAPL-AA-EEQ)/BC)
        DENM=CURNTLIM+IDOTFE*EXP(-2.3*(EAPL-AA-EEQ)/BC)
        ANODE=XIOX*EXP(2.3*(EAPL-AA-EOFE)/BA)
        BOUND=XNUM/DENM-ANODE
        FUNC=AA-(2.0*XKAPPA*DY*(E(I+1,J)+E(I-1,J))+(COEFF1*(-2.0*DELTY/
     +  XKAPPA*BOUND)+4.0*XKAPPA*E(I,J-1))*DX)/DENOMIN
        RETURN
        END
```